SYNTHETIC AND ELECTROCHEMICAL STUDIES OF NOVEL IRON NITROSYL COMPLEXES

Dedicated to my Dad,

who always believed in me

SYNTHETIC AND ELECTROCHEMICAL STUDIES OF NOVEL IRON NITROSYL COMPLEXES

By

NADA REGINATO, B.Sc.

A Thesis

Submitted to the School of Graduate Studies

in Partial Fulfillment of the Requirements

for the Degree

Master of Science

McMaster University

August 1999

MASTER OF SCIENCE (1999) McMASTER UNIVERSITY

(Chemistry) Hamilton, Ontario

TITLE: SYNTHETIC AND ELECTROCHEMICAL STUDIES OF NOVEL IRON NITROSYL COMPLEXES

AUTHOR: Nada Reginato, B.Sc. (McMaster Univeristy)

SUPERVISORS: Professor L. Li and

Professor M. J. McGlinchey

NUMBER OF PAGES: xiv, 113

ABSTRACT

Dinitrosyliron complexes have gained importance as a result of their biological and chemical relevance. Their biological significance stems from the roles exhibited by nitric oxide, including its ability to regulate blood pressure, to act as a biological messenger and because of its involvement in memory storage. Other functions that these dinitrosyliron-based complexes have displayed include their ability to transfer molecular oxygen to alkenes or phosphines, and its use in the polymerization of olefins. One area not yet extended to iron dinitrosyl complexes involves the synthesis of polymeric materials containing a conjugated backbone in the polymer. Thus, the next logical approach was to apply this idea, while investigating their potential to demonstrate unique properties such as optical, redox, and/or conducting behaviour exemplified by other inorganic and organometallic polymeric species. Hence, reactions involving $Fe(NO)_2(CO)_2$ and bidentate diphosphine ligands, bis(diphenylphosphino)methane (DPPM), trans-1,2-bis(diphenylphosphino)ethylene (t-DPPEN), 1,1'-bis(diphenylphosphino)ferrocene (FcP_2), bis(diphenylphosphino)acetylene (DPPA) and 1,4-bis(diphenylphosphino)benzene (DPPB) have been investigated. Three types of compounds arose from these reactions: the monometallic system $Fe(DPPM)(NO)_2(CO)$ **9**, linear dimetallic molecules of the type $Fe_2(\mu\text{-}L)(NO)_4(CO)_2$ (L = $PPh_2CH_2PPh_2$ **10**, $PPh_2C{\equiv}CPPh_2$ **11**, $PPh_2(p\text{-}C_6H_4)PPh_2$ **12**, $PPh_2CH{=}CHPPh_2$ **13**, and $PPh_2((C_5H_4)_2\text{-}Fe)PPh_2$ **14**), and cyclic dimetallic species of the type $Fe_2(\mu\text{-}L)(NO)_4$ (L = $PPh_2(p\text{-}$

$C_6H_4)PPh_2$ **15**, $PPh_2CH_2PPh_2$ **16**, and $PPh_2C{\equiv}CPPh_2$ **17**). These systems were isolated and characterized by the use of NMR and IR spectroscopy. The structures of compounds **10**, **11**, **16** and **17** were also determined by X-ray crystallography. The linear dimetallic compounds, **11**, **13** and **14**, were treated with tetracyanoethylene (TCNE) to afford compounds of the type $Fe_2(\mu\text{-}L)(NO)_4(TCNE)_2$ (L = $PPh_2C{\equiv}CPPh_2$ **18** and $PPh_2((C_5H_4)_2\text{-}Fe)PPh_2$ **19**) and $[(TCNE)(NO)_2Fe(\mu\text{-}L)[Fe(NO)_2(CO)]$ (L = $PPh_2CH{=}CHPPh_2$ **20**). These TCNE adducts were probed by means of cyclic voltammetry to investigate their potential redox properties; only compound **18** revealed communication between the two iron centres.

Dinitrosyldicarbonyliron, $Fe(NO)_2(CO)_2$ and other four-coordinate dinitrosyliron systems have been extensively examined in terms of nucleophilic substitution, including the effects of both hard and soft bases. These findings prompted us to ask whether electrophiles attack dinitrosyliron complexes. Hence, $Fe(NO)_2(CO)_2$ **1**, and also the phosphine complexes $Fe(NO)_2(CO)(PPh_3)$ **21**, and $Fe(NO)_2(PPh_3)_2$ **22**, have been treated with a variety of electrophiles (HCl, $SiMe_3Cl$, $Et_3O^+SbCl_6^-$, trifluoroacetic acid (TFA) and trifluoromethanesulfonic acid (TFSA)) to probe the nucleophilic character of the iron centres. Moreover, another approach involved examining the nucleophilic nature of the iron nitrosyl salts, $[PPN^+][Fe(CO)_3(NO)^-]$, **24** and $[N(Bu)_4^+][Fe(CO)_3(NO)^-]$, **25**.

ACKNOWLEDGEMENTS

I wish to express my sincere gratitude to my supervisors Dr. L. Li and Dr. M. J. McGlinchey for their guidance and support throughout the course of my graduate career. They provided an enjoyable approach to research along with their ideas, patience and understanding.

I would also like to thank Dr. Don Hughes and Brian Sayer in the NMR facility for the assistance and advice, as well as George Timmins for his help and training. Thanks also to Dr. Jim Britten for his help in obtaining several crystal structures. Along with answering many of the questions I had and taking the time to demonstrate how crystallography works. Along with Dr. Jim Britten, I would like to thank Mark Stradiotto for all his time, help and advice with X-ray crystallography. I would like to thank the ladies in the Chemistry Department office for their help, kindness and generosity.

To everyone with whom I worked with in ABB 206, Chris McCrory, Guodong Zheng, Roger Liu and Michael Urschey, thanks for all your advice. To everyone in ABB 357, Mark Stradiotto, Pippa Lock, Stacey Brydges, John Kaldis and Hari Gupta, for welcoming me into their lab halfway through my Masters, and for their kindness, advice and friendship.

I would like to thank others who have made McMaster a memorable experience. I would like to thank Nadine, Darren and Paul of ABB 358 for letting me use their lab. I would like to thank Nadine for being such a great friend and how could I forget our excursions for hot chocolate and whip cream in the winter and who could live without

DQ in the summer. Also, the polymer lab group, Randy and Jeff (Buck), for their friendship and times at the Phoenix. I would like to thank all members of the IR Sox baseball and 200 Toes of Fury soccer teams for their team spirit and believing that winning isn't always everything, it's the skills and fun we all had that matter.

Finally, a special thanks goes out to my Mom, my sister Lisa and my brother Marco for their constant support, patience and belief in me. Their constant encouragement and faith in me got me to where I am today.

TABLE OF CONTENTS

LIST OF SCHEMES

LIST OF TABLES

LIST OF COMPOUNDS

$[Fe(DPPM)(NO)_2(CO)]$, **9**

$[Fe_2(\mu\text{-}DPPM)(NO)_4(CO)_2]$, **10**

$[Fe_2(\mu\text{-}DPPA)(NO)_4(CO)_2]$, **11**

$[Fe_2(\mu\text{-}DPPB)(NO)_4(CO)_2]$, **12**

$[Fe_2(\mu\text{-}t\text{-}DPPEN)(NO)_4(CO)_2]$, **13**

$[Fe_2(\mu\text{-}FcP_2)(NO)_4(CO)_2]$, **14**

$[Fe_2(\mu\text{-}DPPB)_2(NO)_4]$, **15**

$[Fe_2(\mu\text{-}DPPM)_2(NO)_4]$, **16**

$[Fe_2(\mu\text{-}DPPA)_2(NO)_4]$, **17**

$[Fe_2(\mu\text{-}DPPM)(NO)_4(TCNE)_2]$, **18**

$[Fe_2(\mu\text{-}FcP_2)(NO)_4(TCNE)_2]$, **19**

$[Fe(NO)_2(TCNE)](\mu\text{-}t\text{-}DPPEN)[Fe(NO)_2(CO)]$, **20**

CHAPTER 1

INTRODUCTION

1.1 Nitric Oxide

Nitric oxide, NO, is a thermally persistent paramagnetic molecule. It is a colourless, monomeric gas that is thermodynamically unstable ($\Delta G° = 86.57$ kJ/mol, $\Delta S° = 217.32$ kJ/mol K) with respect to N_2 and O_2.[1] The molecular orbital diagram of NO (Figure 1-1) shows that the unpaired electron is located in a π^* antibonding orbital.

The simplest reactions of NO are oxidation and reduction, the former generating NO^+ and the latter giving rise to NO^-. The *nitrosonium cation*, (NO^+) is isoelectronic with CO, while the *nitroside anion*, (NO^-) is isoelectronic with O_2. A comparison of the N-O bond lengths and infrared stretching frequencies for NO^+, NO and NO^- appears as Table 1.

Table 1. Bond Lengths and IR Stretching Frequencies for NO^+, NO and NO^-.

	NO^+	NO	NO^-
N-O distance (Å)	1.06	1.15	1.26
ν_{NO} (cm^{-1})	2377	1875	1470
Ref.	2	3	3

Figure 1-1. Molecular Orbital Diagram of NO.

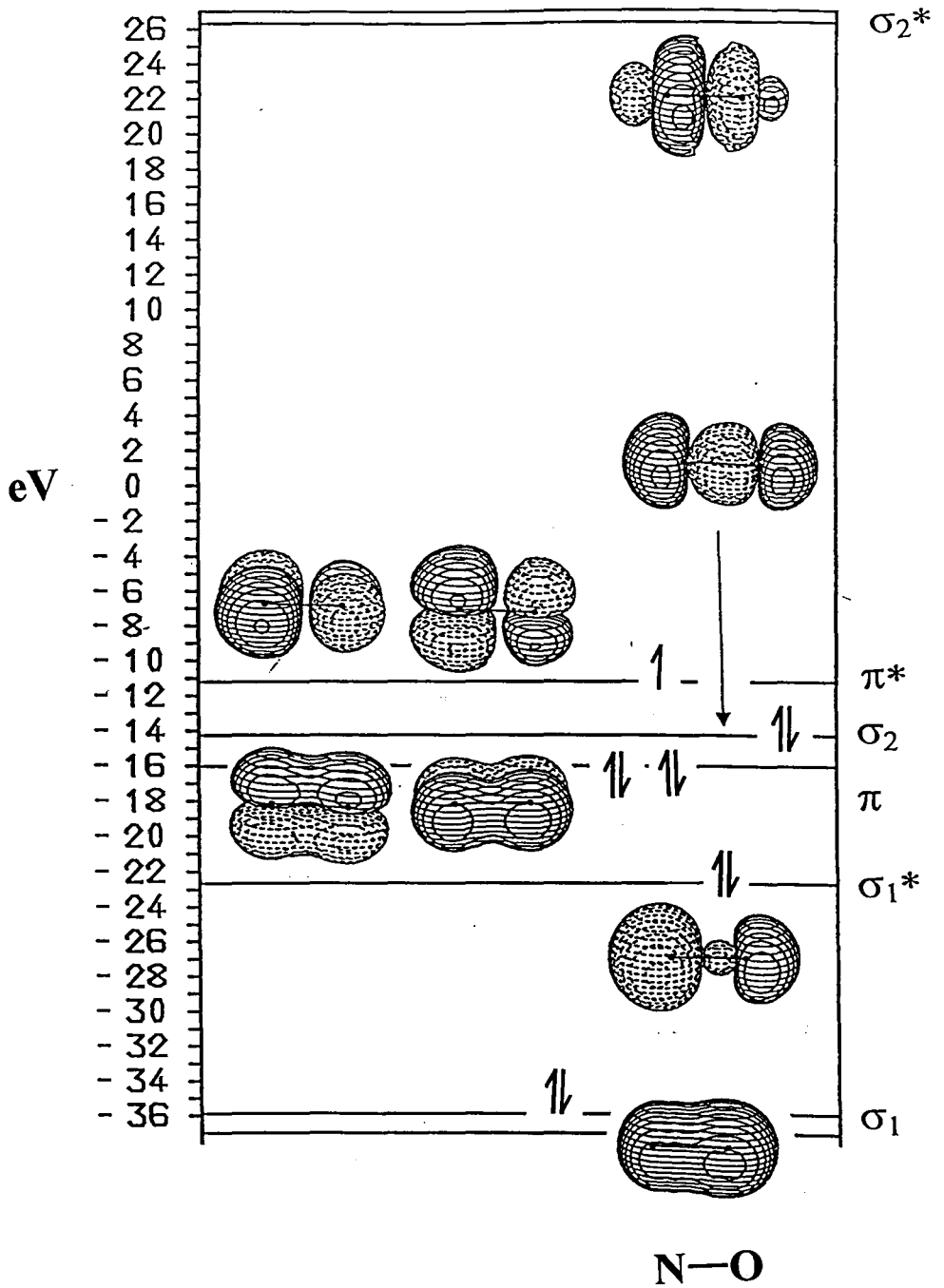

The chemistry and biology of nitric oxide have been the subjects of intense investigation. Previously this diatomic molecule had been associated primarily with its toxic effects. Up until a decade ago, NO was linked as an environmental pollutant found in cigarette smoke and smog; it was also associated with ozone depletion, a suspected carcinogen and a precursor of acid rain. Despite this, numerous investigations have led to the direct identification of nitric oxide as the molecule that regulates blood pressure, acts as a biological messenger and is an immune system cytotoxic agent. NO is also involved in memory storage, as well as a variety of other roles that are still being explored.[2] Nitric oxide's emerging biological and chemical importance has led to its nomination as "Molecule of the Year" in 1992.[3] It has also been suggested that nitric oxide is the body's natural defense against some cancers.[4] An editorial in the *Journal of Cardiothoracic and Vascular Anaesthesia* has discussed the potential of nitric oxide in the medical field by posing the question "Has it progressed from the Molecule of the Year to Wonder Drug of the Decade?"[5] In 1998, the Nobel Prize in medicine and physiology was awarded to Robert F. Furchgott, Louis J. Ignarro and Ferid Murad for their discoveries concerning nitric oxide as a signaling molecule in the cardiovascular system. The importance of nitric oxide has created and expanded interest in the chemistry of iron nitrosyl complexes, and has also resulted in tremendous advances in transition-metal-mediated processes.

1.2 Nitrosyl Structure and Bonding

The bonding of NO to a metal centre *via* the nitrogen atom gives rise to a nitrosyl

linkage, most commonly in the form, M-NO. The other type of bonding that can occur is through the oxygen atom of nitric oxide giving rise to an isonitrosyl linkage, M-ON. The bonding in transition metal nitrosyl and carbonyl complexes can be described in terms of two contributions: (1) a σ component arising from the donation of electron density from the carbon or nitrogen atom of the carbonyl and/or nitrosyl ligand to the metal and (2) a π component involving back-donation of electron density from an occupied metal d-orbital into the vacant antibonding orbital of the ligand (NO or CO).

The bonding of nitrosyls to metals is similar to that of metal carbonyls. Nonetheless, there are some differences in the nature of the electron distribution in the M-NO and M-CO links. These differences can be attributed to the nitrogen atom of the nitrosyl being more electronegative than the carbon atom of the carbonyl. NO is a better π-acceptor than CO, despite that it is usually considered a weak σ-donor. One major distinction is that the M-N bond is usually strong and the N-O bond is relatively weak in the M-NO grouping. This is opposite to the M-CO link, where the M-C bond is relatively weak and C-O bond is strong. The M-NO unit has a more equal electron-density distribution as opposed to the M-CO unit where there is more charge density on the carbon atom than on the oxygen atom.

The bonding between metal nitrosyl complexes can also be described in terms of oxidation states or the Valence Bond Theory.[6] Firstly, the bonding of the M-NO unit in metal nitrosyl complexes will be considered by using the oxidation state approach by assigning formal oxidation states to the metal and the nitrosyl ligand. The donation of an

electron from NO to the metal forms NO^+, with a linear geometry. However, the acceptance of an electron from the metal results in the formation of NO^- with a bent geometry. Coordination of nitric oxide as NO^+ to a metal center involves a net donation of three electrons from NO to the metal, whereas the coordination of NO as NO^- involves a net donation of only one electron to the metal. This method of classifying the bonding of metal nitrosyl complexes by oxidation states is less useful, since it gives rise to unrealistic formal oxidation states. For example, the iron atom in $Fe(NO)_2(CO)_2$ would have a formal oxidation state of -2.

The second approach involves valence bond theory in which the linear bonding mode previously denoted as NO^+ is considered to be sp hybridized at both the N and O atoms. On the other hand, the bonding of NO as NO^- is viewed as being sp^2 hybridized at both the N and O atoms. For a more quantitative picture, molecular orbital calculations are more commonly used.

1.3 Four-coordinate Iron Dinitrosyl Complexes

1.3.1 Iron Dinitrosyl Dicarbonyl, $Fe(NO)_2(CO)_2$

Mond and Wallis were the first to observe the formation of a volatile iron nitrosyl carbonyl, $Fe(NO)_2(CO)_2$, **1**.[7] The isolation of this compound was achieved by Hieber in 1932 from the reaction of a solution of $Fe_3(CO)_{12}$ in $Fe(CO)_5$ with NO at 95 °C. However, yields were low due to decomposition at this temperature, and it was difficult to purify.[8] Other methods have been established, but also resulted in a low yield of the

compound. The best method of preparation commenced from a solution of MeOH with Na, $Fe(CO)_5$ and $NaNO_2$ producing the $Fe(CO)_3(NO)^-$ intermediate; and further reaction with $NaNO_2$, H_2O and dry CO_2 yields **1**.[9] $Fe(NO)_2(CO)_2$ is a red liquid and decomposes at 50 °C. It is insoluble in water but soluble in organic solvents and readily oxidized by air. The compound is stored under nitrogen at temperatures below 0 °C, and protected from light to avoid decomposition. It is known to completely decompose to Fe_2O_3, CO, N_2O and N_2 upon heating between 50 to 100 °C. Aqueous NaOH also decomposes **1** to $Fe(OH)_3$, CO_3^{2-}, N_2 and NH_3.[8, 10]

Infrared spectroscopy of **1** in the liquid state reveals two nitrosyl stretching frequencies at 1810 and 1766 cm^{-1} and two carbonyl stretching frequencies at 2090 and 2040 cm^{-1} attributable to the symmetric and asymmetric stretches, respectively. $Fe(NO)_2(CO)_2$ is diamagnetic and is characterized by a ^{13}C NMR singlet at 207 ppm.[11] In 1937, Brockway and Anderson utilized electron diffraction to determine the bond lengths of the isoelectronic molecules, $Fe(NO)_2(CO)_2$ and $Co(CO)_3(NO)$. It was shown that **1** adopts a tetrahedral geometry with the following bond lengths: Fe-N (1.77 Å), Fe-C (1.84 Å), N-O (1.12 Å) and C-O (1.15 Å).[12]

$Fe(NO)_2(CO)_2$ undergoes substitution reactions, losing CO exclusively, to give products with the expected distorted tetrahedral geometry. It has been demonstrated that aromatic phosphines replace two carbonyl groups in both $Fe(NO)_2(CO)_2$ and $Co(CO)_3(NO)$, analogous to the behaviour of $Ni(CO)_4$.[13] In contrast, tertiary aromatic arsines and stibines only replace one carbonyl group. The iron derivatives are less stable

than the Ni and Co analogues.[14]

1.3.2 Kinetic Studies

It is generally known that monomeric binary metal carbonyls such as $Ni(CO)_4$ react by a dissociative mechanism, as shown in Equation 1.[15]

$$\underset{\text{18-electron}}{M(CO)_n} \xrightarrow[\text{slow}]{-CO} \underset{\text{16-electron}}{M(CO)_{n-1}} \xrightarrow[\text{fast}]{+L} \underset{\text{18-electron}}{M(CO)_{n-1}L} \qquad (1)$$

However, $Fe(NO)_2(CO)_2$[20] and $Co(CO)_3(NO)$[16] were found to react by an associative mechanism. This was an astonishing result since $Ni(CO)_4$, $Fe(NO)_2(CO)_2$ and $Co(CO)_3(NO)$ are all members of an isoelectronic and isostructural series. This behaviour is attributed to the localizing of a pair of electrons on the nitrogen atom in the transition state to vacate a metal orbital of low energy for nucleophilic attack, as shown in Equation 2.[15] This concept was concocted prior to the theory of the 18-electron rule[17] and X-ray structures of bent nitrosyls.[18]

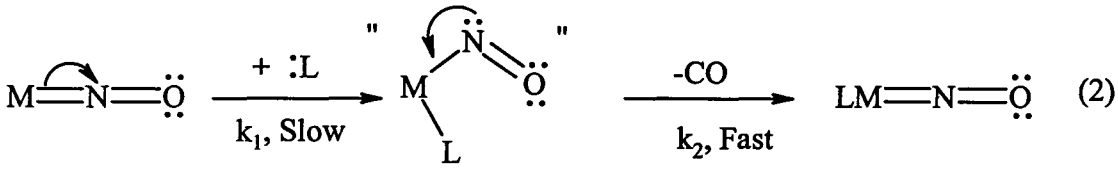

(2)

The associative S_N2 type mechanism for ligand substitution reactions is common for metal nitrosyl carbonyls, while metal carbonyls primarily undergo a dissociative S_N1 type mechanism. Most of the research was concentrated on $Mn(NO)(CO)_4$, $Fe(NO)_2(CO)_2$ and

$Co(CO)_3(NO)$.[19]

Basolo and co-workers were the first to use kinetic studies to quantify the nucleophilic strengths of various entering ligands in the $M(NO)_x(CO)_{4-x}$ complexes. These substitution reactions yielded a second-order rate expression, rate = $k_2[Fe(NO)_2(CO)_2][L]$, that is dependent on the nature and concentration of the coordinating phosphine ligand. Thus, the substitution occurs *via* an associative mechanism as seen in Equation 3.[20]

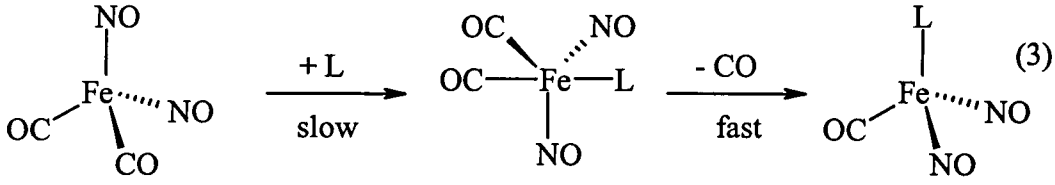

(3)

The kinetic data concerning the first step of the carbonyl substitution of $Fe(NO)_2(CO)_2$ were obtained from the following reaction:

$$Fe(NO)_2(CO)_2 + L \rightarrow Fe(NO)_2(CO)L + CO \quad (4)$$

where L = phosphines, phosphites, or triphenylarsine. This study was performed as a further investigation of the kinetic behaviour of the members of the pseudo-tetracarbonylnickel series.

The five-coordinate species is assumed to be the active intermediate since stable compounds of this type are known. It was suggested that the intermediate is a trigonal bipyramid since there is precedence for such structures containing π-bonding ligands including $Fe(CO)_5$, $Mn(NO)(CO)_2[(C_6H_5)_3P]_2$, $Rh[(C_6H_5)_3P]_3(CO)(H)$ and $[Pt(SnCl_3)_5]^3$.[20]

Since the substitution reactions of $Fe(NO)_2(CO)_2$ are second-order, it is possible to determine the nucleophilic strengths of various reagents toward the substrate. Three important properties of the reagent that may determine the nucleophilic strength are basicity, polarizability, and π-bonding ability. It was observed that, as basicity increases, so does the rate of the reaction. This behaviour has also been demonstrated for the following compounds: $Co(NO)(CO)_3$, $Mn(NO)(CO)_4$, $(C_5H_5)Rh(CO)_2$ and trans-$[Pt(py)_2Cl_2]$.[20] Nucleophilic strength of various reagents towards the substrate may be largely determined by polarizability instead of basicity. Since the iron in $Fe(NO)_2(CO)_2$ is in a very low oxidation state, formally Fe(-2), it is considered a Lewis acid because it can localize a pair of electrons on the nitrogen atom of the nitrosyl and thus it can react more rapidly with a Lewis base.

When Morris and Basolo investigated the reactions of $Fe(NO)_2(CO)_2$ with both soft and hard bases, they proposed two mechanisms for the hard bases and one for soft bases. For soft bases, the reaction occurs by substitution involving nucleophilic attack by the entering ligand on the metal atom (Equation 4). One of the proposals is that $Fe(NO)_2(CO)_2$ has a second electrophilic center that is hard, i.e., the carbon atom of a carbonyl or the nitrogen of a nitrosyl.[21] They suggested that this second electrophilic center would be the carbon atom due to the fact that the attack at the nitrogen atom would increase electron density in the system and enhance the metal-carbon π–bonding, which would retard the substitution.[21] Their proposed mechanism, whereby the hard base attacks the electrophilic carbon in the rate determining step (I), is shown in Equation 5. Structure

(I) is stabilized by a resonance hybrid **(II),** or by the delocalization of the negative charge on the iron onto other nitrosyl and carbonyl groups bonded to the iron.[21] Hence, the leaving CO group has been destabilized (i.e. the CO attacked by the base) and can be quickly displaced by the ligand, L, to generate the product $Fe(NO)_2(CO)L$[21]

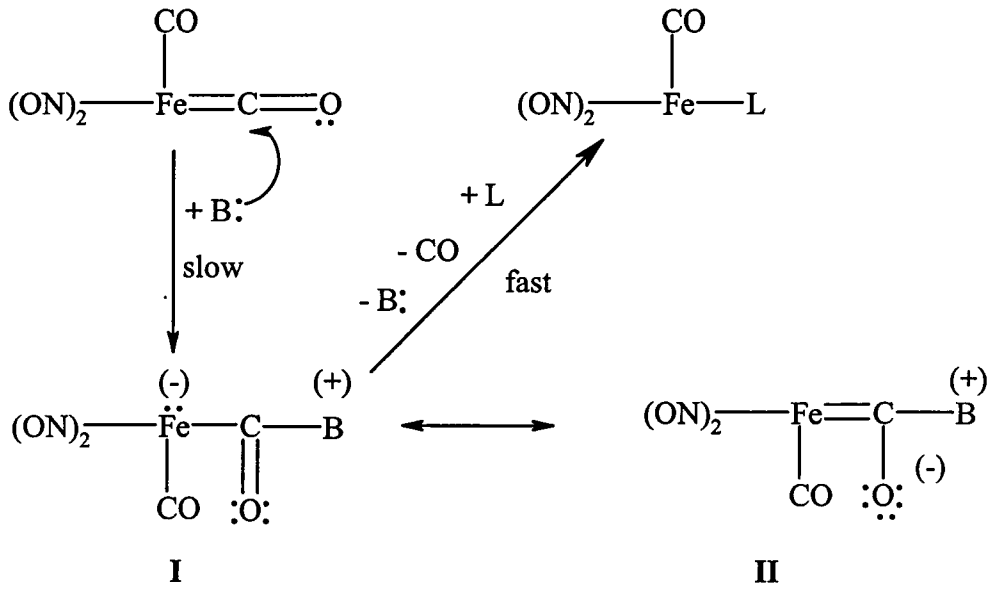

(5)

The second mechanism involves the attack of the hard base on the soft metal atom as illustrated in Equation 6. The rate-determining step is the attack of the solvent molecule on the metal forming a four-coordinate intermediate.[21] In the first step, the equilibrium lies almost completely to the left, while the final step involves the fast displacement of the solvent by ligand L.[21]

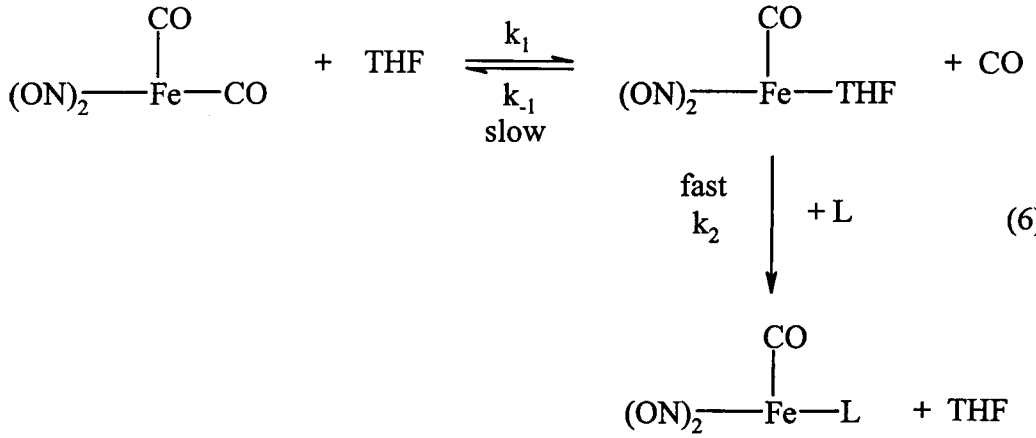

Lewis bases are known to displace a carbonyl ligand in $Fe(NO)_2(CO)_2$ to afford $Fe(NO)_2(CO)_{2-n}(L)_n$ derivatives and, as well, many compounds of the form $Fe(NO)_2(L)_n$ have been reported in the literature. The following sections briefly review the chemistry of iron dinitrosyl compounds, illustrating its importance, even though this field has not been thoroughly researched.

1.4 Other Substitution Reactions

The replacement of one carbonyl by a phosphorus ligand occurs at room temperature in 12 hours; however, the substitution of the second carbonyl with another phosphorus ligand requires heating at 85 °C for 48 hours. The reactions of $Fe(NO)_2(CO)_2$ with Lewis bases such as phosphines, phosphites and diphosphines have been thoroughly examined.

During the first step of the scheme below, one of the two carbonyls in $Fe(NO)_2(CO)_2$ was substituted by a phosphorus ligand. The second step involved the substitution of the remaining carbonyl with TCNE. Replacement of the first carbonyl requires stirring overnight at room temperature. Replacement of the second carbonyl

with TCNE occurs by stirring at room temperature for three hours. This fast reaction is believed to occur *via* a process entitled the Electron Transfer Autocatalysis Mechanism, which involves a 17-electron paramagnetic intermediate.[22]

Scheme 1-1. Electron Transfer Autocatalysis Mechanism.

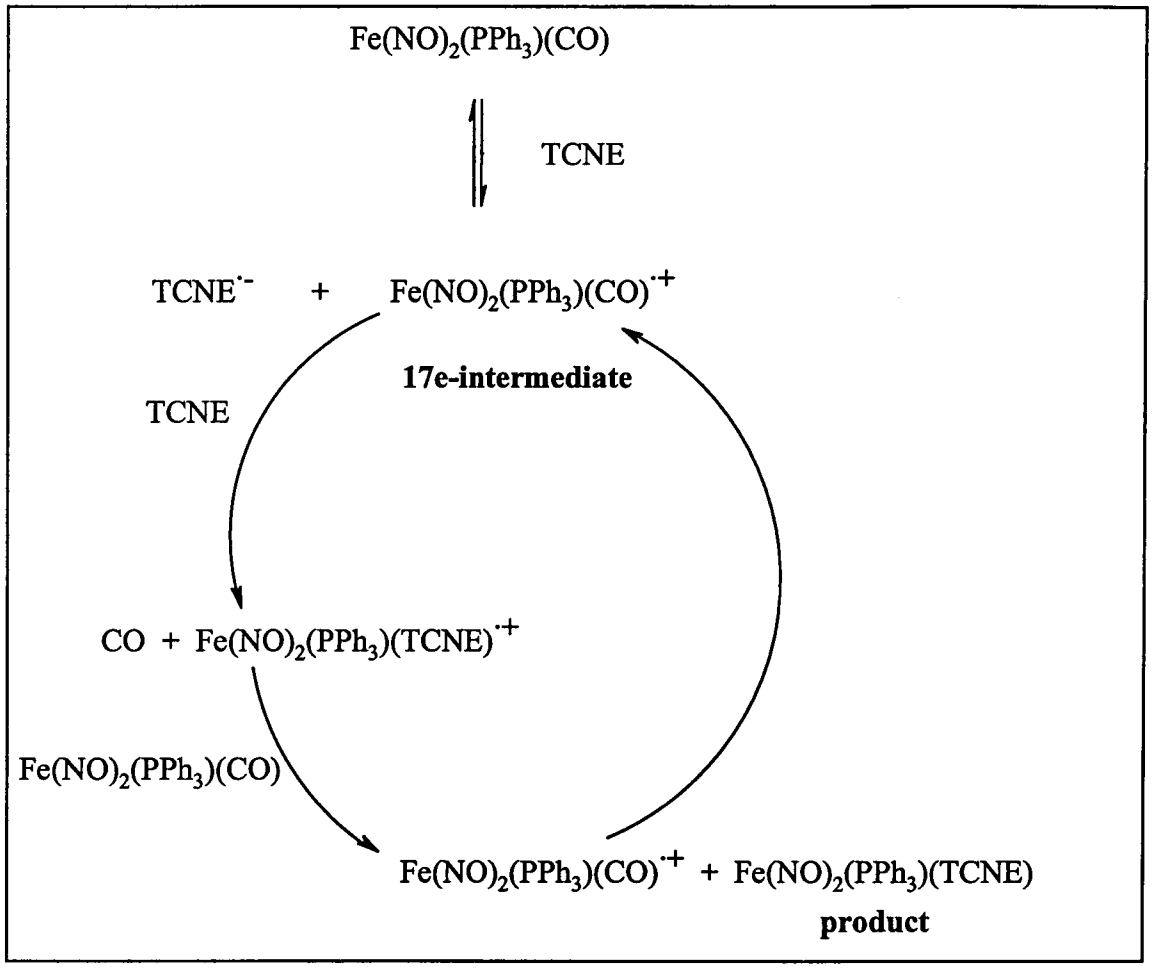

1.5 Olefin Complexes

1.5.1 Photosubstitution

UV photolysis of $Fe(NO)_2(CO)_2$ dissolved in liquid Xe doped with 1-butene

yields $Fe(NO)_2(CO)(\eta^2\text{-}1\text{-butene})$ and $Fe(NO)_2(\eta^2\text{-}1\text{-butene})_2$.[23] A similar reaction occurs with 1,3-butadiene giving rise to $Fe(NO)_2(CO)(\eta^2\text{-}C_4H_6)$ and $Fe(NO)_2(\eta^4\text{-}C_4H_6)$.[24] It was observed that the reactions with 1,3-butadiene are more complicated than with 1-butene, because both $\eta^4\text{-}C_4H_6$ and $\eta^2\text{-}C_4H_6$ complexation occurs with the former.[23] However, the $\eta^4\text{-}C_4H_6$ complexes are thermally more reactive than $\eta^2\text{-}C_4H_6$.

In comparison, the reaction of $Co(CO)_3(NO)$ with 1-butene gives rise to a significant difference between Fe and Co. The Co compound yielded only the monosubstituted product, $Co(CO)_2(NO)$(1-butene); while $Fe(NO)_2(CO)_2$ gave both the mono- and disubstituted products. In the case involving 1,3-butadiene, the Ni analogue, $Ni(CO)_4$, forms only $Ni(CO)_3(\eta^2\text{-}C_4H_6)$, which is thermally less stable than the compounds of Fe and Co.[24] Both Fe and Co compounds give rise to $\eta^2\text{-}C_4H_6$ complexes: $Fe(NO)_2(CO)(\eta^2\text{-}C_4H_6)$ and $Co(NO)(CO)_2(\eta^2\text{-}C_4H_6)$. The most interesting observation was that $Co(NO)(CO)_3$ forms the $\eta^4\text{-}C_4H_6$ complex, $Co(NO)(CO)(\eta^4\text{-}C_4H_6)$, under conditions that do not normally produce disubstituted $Co(NO)(CO)(L)_2$.[24] However, the disubstituted Co complex was not formed in the presence of 1-butene. The formation of iron and cobalt $\eta^4\text{-}C_4H_6$ complexes proceed from an $\eta^2\text{-}C_4H_6$ complex to the $\eta^4\text{-}C_4H_6$ complex *via* a dissociative mechanism, as shown below.

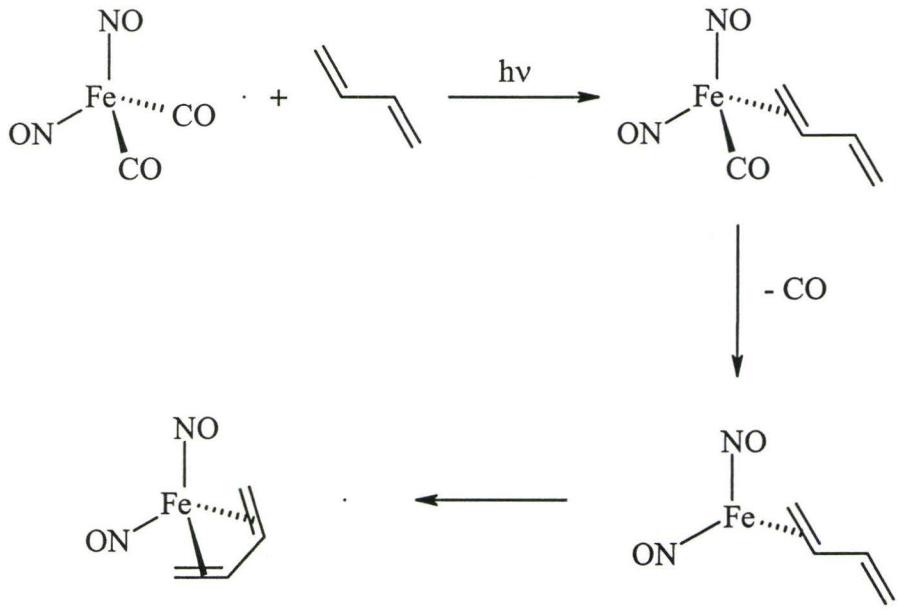

(7)

The possible mechanism for catalytic dimerization of butadiene involves $Fe(NO)_2(\eta^2\text{-}C_4H_6)(\eta^4\text{-}C_4H_6)$ as the active intermediate, where one NO is linear and the other is bent.[24]

1.5.2 Other Olefin Complexes

The reactions of $[Fe(\eta^3\text{-}C_3H_4X)(CO)_2(NO)]$ with trialkylphosphines have been studied by Cardaci[25] in order to isolate the intermediates resulting from nucleophilic attack on the allylic ligand. $[Fe(\eta^3\text{-}C_3H_4X)(CO)_2(NO)]$ was prepared from a reaction of $Na[Fe(CO)_3NO]$ with the required halide in diethyl ether solution. The reaction of the phosphine with $[Fe(\eta^3\text{-}C_3H_4X)(CO)_2(NO)]$ results in the formation of a σ-allylic complex $[Fe(\sigma\text{-}C_3H_4X)(CO)_2(NO)L]$ which, by chelation of the allylic group, forms the complex $[Fe(\eta^3\text{-}C_3H_4X)(CO)(NO)L$.[25] The reaction scheme is shown below.

Scheme 1-2. The Reaction Scheme for $[Fe(\eta^3\text{-}C_3H_5)(CO)_2(NO)$ with PR_3 and L (L = PR_3, $P(OR)_3$, or PPh_3; R = Me, Et, Bu^n, or C_6H_{11}).

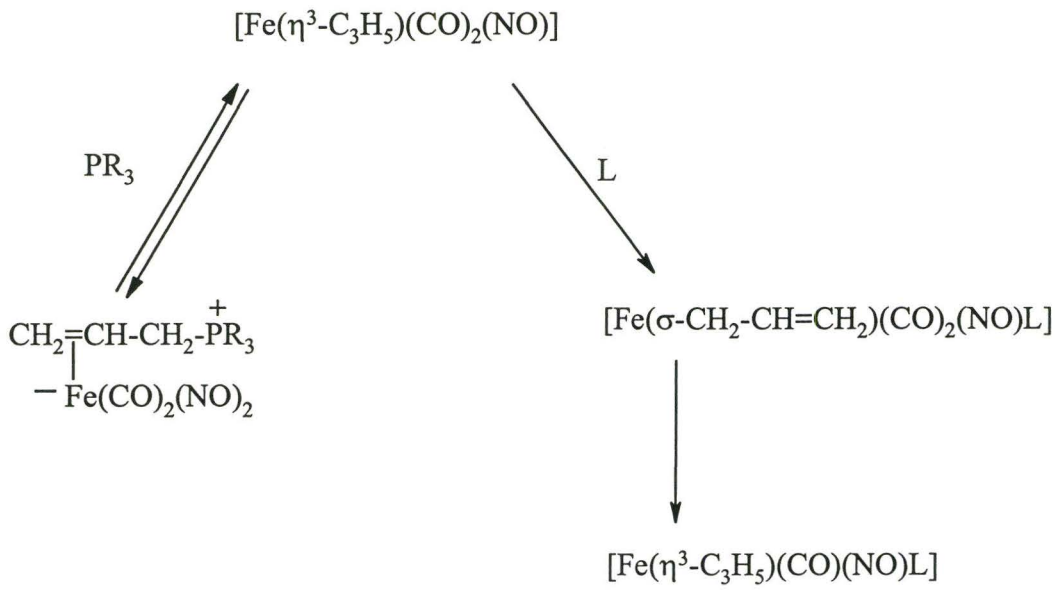

Thus, the reactivity of $(\eta^3\text{-}CH_2{=}CHCH_2)Fe(NO)L_2$ compounds (L = CO, CNMe, PR_3) with neutral nucleophiles can occur through two processes. The use of very basic phosphine ligands results in the formation of a zwitterionic adduct *via* the attack of the basic phosphine at the terminus of the allyl ligand.[26] On the other hand, less basic phosphines or phosphites give rise to the substitution of only carbonyl ligands.[26] The general mechanism illustrated in Scheme 1-2, involves the initial coordination of a Lewis base (L) to form a five-coordinate compound, which may then undergo allyl-L coupling or CO loss to give the observed product. In addition, carbonyl insertion occasionally occurs into the Fe-(η^1-allyl) bond to yield a but-3-enoyl complex.[25]

The reaction of $(\eta^3$-allyl)Fe(NO)(CO)L with NO^+ gives rise to the cationic

dinitrosyl complex $[(\eta^3\text{-allyl})Fe(NO)_2L]^+$, which exhibits fluxionality at room temperature attributable to slow allyl rotation. Treatment of these dinitrosyl allyl cations with nucleophiles mainly results in the loss of the allyl ligand. This property has been thoroughly studied in allylic alkylations of Fe- and Ru-complexed cyclopentadienyl or cyclooctatetraene groups;[27] however, further discussion of this chemistry is not warranted.

1.6 Catalysis

In the past few years, the 14 electron species "$Fe(NO)_2$" has been of interest, since it is the active fragment present in the catalytic cyclodimerization of 1,3-dienes. Reports of the activity of this "$Fe(NO)_2$" species dates back to as early as 1968.[29] Since then, Tkatchenko and Janes have conducted several detailed investigations. In 1977 Tkatchenko revealed that the metathetical reactions of $Na[Fe(CO)_3NO]$ with metal halides such as $[M(NO)_2X]_2$ where M = Fe, Co; X = Cl, Br, I are the active catalysts for the selective dimerization of butadiene to 4-vinylcyclohexene.[28] However, for $Fe(NO)_2(CO)_2$ and $Fe(\eta^3\text{-}C_3H_5)(CO)_2(NO)$ the only product observed was 4-vinylcyclohexene, which was generated through a dissociative pathway with butadiene. In the thermal and photochemical dimerization of butadiene to 4-vinylcyclohexene, both processes gave rise to identical product distributions, suggesting that there is a common intermediate, thereby ruling out the possibility of a diradical pathway.[29] A diradical pathway was proposed for the photosensitized dimerizations of butadiene and isoprene,

where 1,2-disubstituted cyclobutanes are the major products.

Numerous studies have demonstrated that "$Fe(NO)_2$" is the active catalyst and that carbon monoxide compresses catalysis. "$Fe(NO)_2$" precursors can be synthesized to generate catalysts by a variety of methods:[6]

(i) the electrochemical reduction of $FeCl_3$ in the presence of NO,

(ii) the electrochemical reduction of $[Fe(NO)_2X]_2$ where X = Cl or I, or

(iii) the reaction of $[Fe(NO)_2Cl]_2$ with either $Ni(COD)_2$, (COD = 1,5-cyclooctadiene), zerovalent metal carbonyls, or even bare metals.

However, not all iron dinitrosyl compounds can be "$Fe(NO)_2$" precursors, for instance $Fe(NO)_2(PPh_3)_2$ is not a catalyst because it does not easily lose its PPh_3 ligands.

Despite the fact that the "$Fe(NO)_2$" moiety has been labeled a catalytic species, its interaction with dienes was not established until 1987, when Gadd *et al.* characterized several nitrosyl compounds of both Fe and Co by low temperature infrared spectroscopy.[24] Both chemical and electrochemical electron transfer to $[Fe(NO)_2Cl]_2$ in THF of norbornadiene, butadiene and isoprene led to the same active complex, "$Fe(NO)_2$".[30]

Further studies have been performed using DAD (1,4-diaza-1,3-diene, R-N=CR'-CR'=N-R) as the ligand, which were in agreement with the "$Fe(NO)_2$" fragment being the catalytically active species in the cyclodimerization of 1,3-dienes.[31]

$$Fe(NO)_2(CO)_2 + DAD \xrightarrow{-2CO} [(DAD)Fe(NO)_2] \qquad (8)$$

Experimental results along with bonding descriptions indicate that $[(DAD)Fe(NO)_2]$ will

most likely dissociate to the $Fe(NO)_2$ fragment and the DAD ligand upon thermal treatment.[31] In spite of the proposed π-bound olefin as the intermediate in iron dinitrosyl complexes in catalytic processes, most of these complexes have been characterized only by the use of *in situ* methods such as EPR and IR spectroscopy. It was not until 1994 that the first stable compound of "$Fe(NO)_2$" π-bonded to TCNE, $Fe(NO)_2(PPh_3)(\eta^2\text{-TCNE})$ was isolated and characterized. The details of this reaction were previously discussed (Section 1.4). Catalytic routes to dimerizations of dienes have been extensively studied because thermal dimerization of dienes is, in general, an inefficient process.

1.7 Electrophilic Additions

Reactions of metal nitrosyls with electrophiles such as protons may bind to the oxygen atom of the bound nitrosyl group forming NOH species.[6] Haymore *at al.*[32] have reported the formation of trifluoroacetohydroxamate(-2) ligand, $CF_3(CO):NO$, by attack of trifluoroacetic acid on $Os(NO)_2(PPh_3)_2$ giving rise to $Os\{ON:C(O)CF_3\}(O_2CCF_3)(NO)(PPh_3)_2$, **2**.

Figure 1-2. Crystal Structure of $Os\{ON:C(O)CF_3\}(O_2CCF_3)(NO)(PPh_3)_2$, **2**.

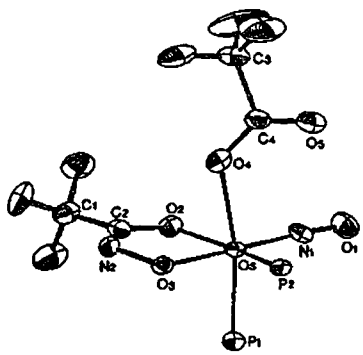

However, the main focus was the electrophilic attack on the nitrogen atom of the MNO moiety. Such attack occurs when the MNO group is sufficiently electron rich. Electrophilic addition by protons usually occurs with bent nitrosyls since the nitrogen is formally sp^2 hybridized and possesses a lone pair of electrons.[6] Dinitrosyl complexes may also undergo electrophilic attack at the nitrogen atom(s) if the $M(NO)_2$ group is sufficiently electron rich.[33]

$$Re(NO)_2(PPh_3)_2(I) + HCl \rightarrow Re(NO)(HNO)(PPh_3)_2Cl(I) \qquad (9)$$

The infrared spectrum of $Re(NO)(HNO)(PPh_3)_2Cl(I)$ revealed two stretching frequencies for NO at 1380 and 1745 cm^{-1}, in which the former stretching frequency is attributed to the HNO ligand.[33] The assignment of HNO in this Re complex is consistent with the value for $Os(CO)(HNO)(PPh_3)_2Cl_2$. Infrared spectroscopy, elemental composition and/or melting points have been solely used to characterize the protonation of nitrosyl complexes. In 1979, Wilson and Ibers[34] provided sufficient evidence for the existence of the coordinated HNO ligand by isolating and obtaining a crystal structure of $Os(CO)(HNO)(PPh_3)_2Cl_2$, **3**. The bond distances and angles for the coordinated HNO ligand are H-N = 0.94 (11) Å, N-O = 1.193 (7) Å and H-N-O = 99.(7)° which are in close agreement with the free HNO molecule, 1.026 Å, 1.211 Å and 108.5°, respectively.[35]

Figure 1-3. Crystal Structure of $Os(CO)(HNO)(PPh_3)_2Cl_2$, **3**.

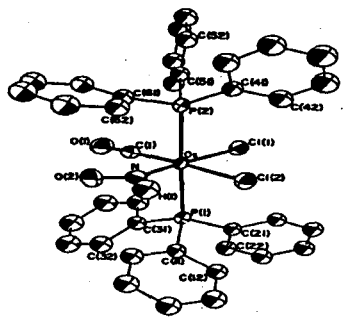

To further confirm the assignment, solution spectroscopic techniques were performed. The ^{1}H NMR spectrum of **3** showed a singlet at 21.2 ppm for the HNO proton, which is consistent with metal-formyl complexes.[34] In addition, the spectrum of the ^{15}N-labeled **3** complex gave rise to a doublet that was further split into a triplet attributable to virtual coupling of the proton to two equivalent phosphorus nuclei.[34]

Furthermore, interconversions of the bound NO to η^2-bound HNOH, H_2NOH and H_2NO ligands have also been observed for Mo,[36] Ir[37] and Os[38] complexes.

$$Ir(NO)(PPh_3)_3 + 3HCl \rightarrow Ir(H_2NOH)(PPh_3)_2Cl_3 + PPh_3 \quad (10)$$

$$Os(NO)_2(PPh_3)_2 + 2HCl \rightarrow Os(NHOH)(NO)(PPh_3)_2Cl_2 \quad (11)$$

$$(s\text{-}s)Mo(NO)_2 + 1/2N_2H_4 \rightarrow (s\text{-}s)Mo(NO)(H_2NO) \quad (12)$$

where s-s = 2,2'-(ethylenedithio)dibenzenethiolate.

The formation of $Ir(H_2NOH)(PPh_3)_2Cl_3$ in Equation 10 was confirmed by infrared spectroscopy, since the absorptions were not attributed to NO or Ir-H but instead to NH, OH and Ir-Cl. The chemistry involving electrophilic attack on the nitrosyl is limited and has not been thoroughly investigated. To the best of our knowledge, electrophilic attack on nitrosyls has not yet been reported for iron nitrosyl complexes.

1.8 Chemistry of $Fe(CO)_3(NO)^-$ anion

Several forms of the anion have been synthesized with a variety of counterions, such as sodium, potassium, bis(triphenylphosphine)iminium, and tetrabutylammonium cations. The tricarbonylnitrosyliron(-1) anion is the intermediate generated from the

synthesis of $Fe(NO)_2(CO)_2$. Several studies have been conducted in order to develop an improved method of introducing the NO ligand into a complex. The first method described earlier by Hieber and Beutner[9] utilizes nitrite in a basic media giving rise to $Na[Fe(CO)_3(NO)]$. The reaction proceeds as follows:

$$Fe(CO)_5 + NaNO_2 + NaOCH_3 \rightarrow Na[Fe(CO)_3(NO)] + CO + Na(CH_3OCO_2).$$

This type of chemistry has not been extended to other metal carbonyls to produce analogous products to $[Fe(CO)_3(NO)]^-$. It was not until 1983, that Stevens and Gladfelter[38] improved the preparation of several nitrosyl carbonyl complexes including $[Fe(CO)_3(NO)]^-$ by their reactions with bis(triphenylphosphine)nitrogen (+1) nitrite, $PPN(NO_2)$. The reason for choosing the PPN cation was due to the ease of preparation of $PPN(NO_2)$ in pure crystalline form, its solubility in water, and its non-hygroscopic nature. The reaction of $Fe(CO)_5$ in THF with $PPN(NO_2)$ produces a slurry which dissolves and becomes a clear yellow solution within 30 minutes. There are no side reactions and the final product is air-stable giving rise to an 87% yield. This synthesis is less complicated and time consuming compared to the method described by Hieber. The reaction involving the use of $PPN(NO_2)$ to convert monomeric carbonyl complexes into nitrosyl-containing products is:

$$Fe(CO)_5 + PPN(NO_2) \rightarrow [PPN^+][Fe(CO)_3(NO)^-] + CO + CO_2. \qquad (14)$$

Two reaction pathways have been proposed for the formation of $[PPN^+][Fe(CO)_3(NO)^-]$ (Scheme 1-3), which are similar to the formation of $[PPN^+][Cr(CO)_4(NO)^-]$. Kinetic experiments have demonstrated that the reaction is first order in both the reactants and not

inhibited by CO, thus eliminating the possibility of a simple dissociative substitution of NO_2^- for CO, in the formation of the intermediate $[Fe(CO)_4(NO_2)]^-$.[38] Hence, the most reasonable rate-determining state has been suggested as the nucleophilic attack of NO_2^- on the coordinated carbon monoxide. This suggestion is analogous to the reaction of $Fe(CO)_5$ and various other metal carbonyls with OH^- or OCH_3^-. Path A involves the dissociation of CO to form the unsaturated species **4**, which can add nitrite to produce **6**. Loss of CO_2 after an oxygen atom transfer to a carbonyl carbon gives the observed product. Path A involves anion-catalyzed substitution, similar to that proposed by Morris and Basolo, with regards to the effect of anions on the phosphine substitution of $Fe(NO)_2(CO)_2$ and $Co(NO)(CO)_3$. Conversely, path B involves initial attack of a carbonyl carbon by nitrite, forming an acylnitrite intermediate, **3**. This would be followed by the loss of CO and migration of the NO ligand onto the metal center, **5**. The final product is obtained from the loss of CO_2. Stabilization of the intermediate **4** *via* chelation of the acyl nitrile ligand will produce **8**. Thus, the results are consistent with path B.

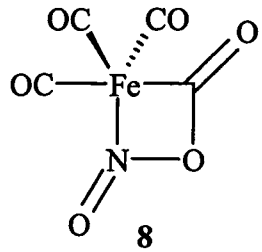

8

Scheme 1-3. Two Plausible Reaction Mechanisms for the Formation of $[PPN^+][Fe(CO)_3(NO)^-]$

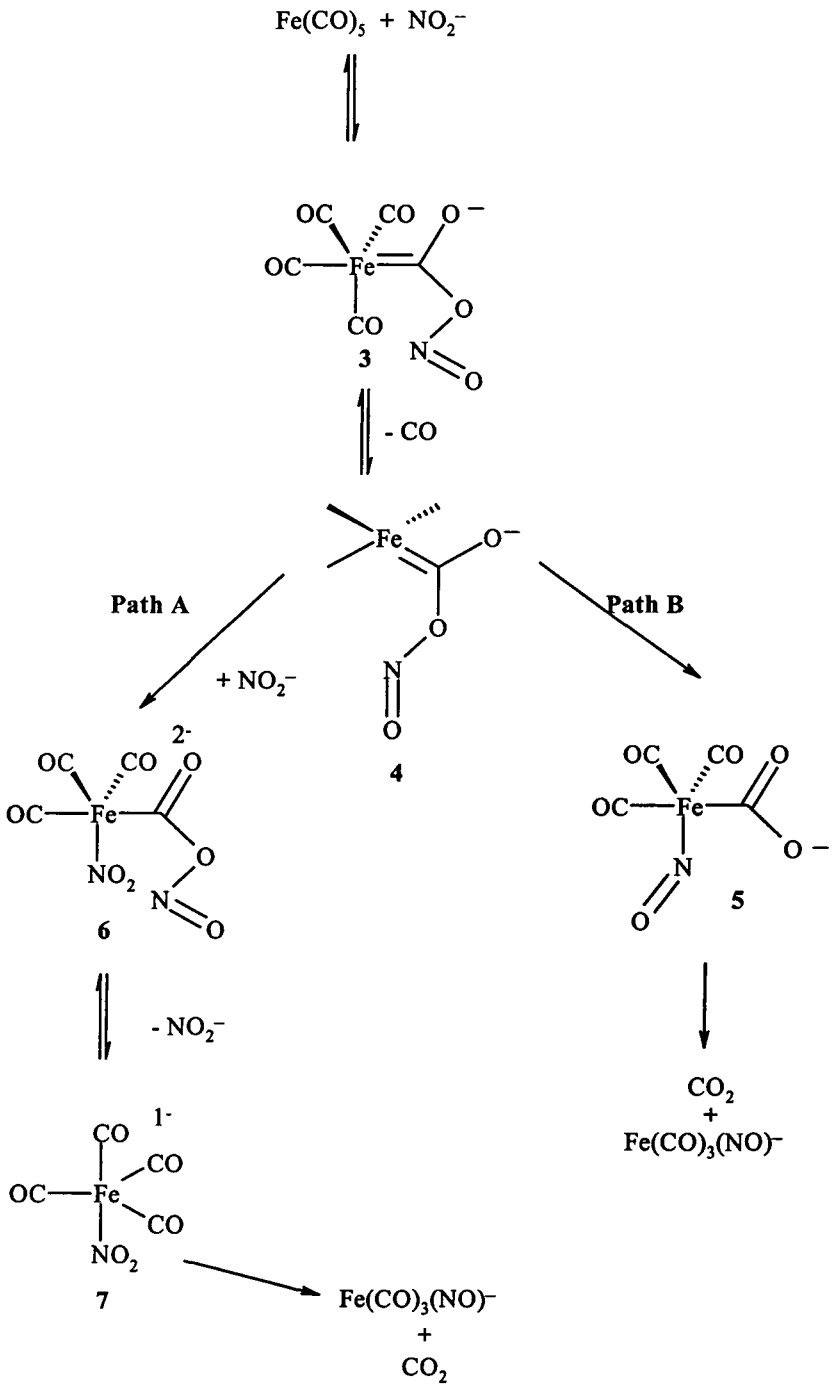

The anion has been used to synthesize a variety of compounds. For instance, the protonation of the sodium salt yielded a very unstable hydride species.[9] However, the protonation with trifluoroacetic acid of the sodium salt, $[Fe(CO)_3(NO)^-][Na^+]$ in ether and in the presence of excess triphenylphosphine, yielded the iron nitrosyl hydride $FeH(CO)(NO)(P(C_6H_5)_3)_2$, which was crystallized.[39] Prior to this iron nitrosyl hydride complex, only two other crystal structures of pentacoordinated nitrosyl hydrides had been isolated, $RuH(NO)(P(C_6H_5)_3)_3$[40] and $[IrH(CO)(NO)(P(C_6H_5)_3)_2^+]$.[41] In comparison to the carbonyl hydrides reported, only a limited number of nitrosyl hydrides have been reported. The sodium salt reacted with group 4 halides to produce such compounds as $[Fe(CO)_3(NO)SnEt_3]$ and $[Fe(CO)_3(NO)GeCl_3]$ which were characterized solely by infrared spectroscopy.[42] The reaction of the anion with $Hg(CN)_2$ led to $[Fe(CO)_3(NO)]_2Hg$, and the addition of tris(dimethylamino)phosphine (Tdp) yielded $[(Tdp)Fe(CO)_2(NO)][Fe(CO)_3(NO)]$ and $(Tdp)_2Fe(NO)_2$ depending on the reaction conditions.[43] Note that these studies were primarily conducted in the late 60's and early 70's, in which the structures of many of the compounds were deduced by use of infrared spectroscopy and melting points. However, the chemistry of the anion has not been thoroughly investigated since these early reports.

CHAPTER 2

DINITROSYLIRON COMPLEXES CONTAINING BIS(PHOSPHINE) BRIDGING LIGANDS, AND THEIR COORDINATION WITH TCNE

2.1 Background

Dinitrosyliron-based complexes have displayed a variety of functions, including the ability to transfer molecular oxygen to alkenes or phosphines,[44,45] and the polymerization of olefins.[24,46] As previously mentioned in Section 1.6, $Fe(NO)_2(CO)_2$ catalyses the polymerization of butadiene, styrene and isoprene, however, the mechanism is unknown. In 1987 Gadd *et al.* proposed that the dimerization of butadiene might occur via a 5-coordinate intermediate, $Fe(NO)_2(\eta^2\text{-}C_4H_6)(\eta^4\text{-}C_4H_6)$, which is very unstable even at the low temperature of -50 °C.[24] It was not until 1994, that the first crystallographically characterized $Fe(NO)_2(PPh_3)(TCNE)$ containing a π-bound olefinic ligand was reported.[22] As an extension of this research, Li *et al.* have reported on the molecular dynamics, electrochemical behaviour and structural characterization of other analogous $Fe(NO)_2(PR_3)(TCNE)$ complexes.

Furthermore, the reactivity of these $Fe(NO)_2$-containing bidentate phosphines with the TCNE ligand was of interest. This investigation was triggered by the possibility of the formation of conductive links between redox-active metal centres and conjugated bidentate phosphine ligands. Organometallic and inorganic polymers have attracted

considerable interest because of their potential to exhibit unique properties, difficult or otherwise inconceivable with conventional organic polymers. Transition metal-containing polymer materials with an extended conjugation in the polymer backbone have the potential to possess optical, redox and conducting behaviour.[47] Our primary goal was to extend these ideas to generate polymeric materials containing dinitrosyliron units in the backbone connected by a bidentate phosphine ligand. By altering the spacer group in the diphosphines, the property of the polymeric species could be easily changed. This chapter investigates and discusses both the preliminary series of the compounds possessing the $(NO)_2FeP{\sim}PFe(NO)_2$ structural motif along with its reactivity with TCNE in order to probe their electrochemical behaviour.

2.2 Results and Discussion

As a probe for electrochemical studies and to extend their coordination chemistry,[48,49h] bis(diphenylphosphino)methane (DPPM), trans-1,2-bis(diphenylphosphino)ethylene (t-DPPEN), bis(diphenylphosphino)acetylene (DPPA), 1,4-bis(diphenylphosphino)benzene (DPPB) and 1,1'-bis(diphenylphosphino)ferrocene (FcP_2), were selected to bridge $Fe(NO)_2$ centers in model compound studies. The selected bidentate phosphines along with other related compounds have been known to function as phosphorus σ-donor bridges between metal centres in coordination and organometallic compounds, which in principle give rise to either dimeric[49] or polymeric[50] species. By utilizing the diphosphine ligands, the metal-containing polymeric complex may be investigated with regards to its

spectroscopic properties. However, despite the wide spread use of the rigid phosphorus-containing ligands, DPPA and DPPB, their coordination to polymetallic centres remains relatively undeveloped. In principle, by choosing saturated (DPPM) and unsaturated (t-DPPEN, DPPA, DPPB and FcP_2) bis(phosphine) ligands, a probe for the effectiveness of using a phosphine bridging unit on the electronic properties of the transition metal complex and related polymeric material should be provided. One possibility of both the linear and cyclic dimetallic species (molecules **A** and **B**) was their use as monomers in organometallic polymerization reactions. For instance, the linear compounds containing two reactive terminal Fe(CO) units could be used in the preparation of heteropolymetallic polymers by the addition of a difunctional (and possibly metal-containing) ligand. This concept has been demonstrated by Puddephatt and co-workers by linking gold centres with a DPPB ligand[50a], while Wright and co-workers[49j] have prepared polymers containing both backbone rhodium atoms and pendant chromium fragments. Furthermore, the cyclic species, $[Fe_2(\mu\text{-}P)_2(NO)_4]$ could serve as a single-source precursor to organometallic polymers *via* ring-opening polymerization processes.[47a]

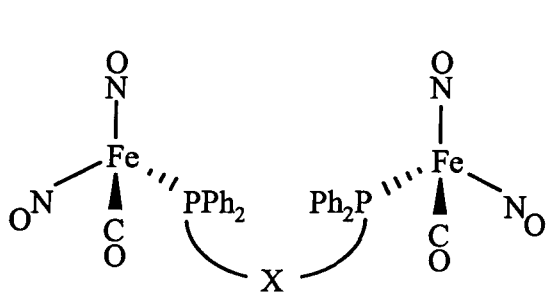

A

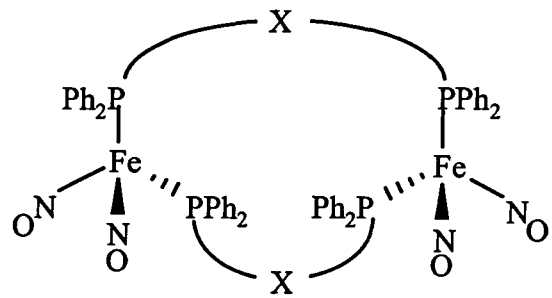

B

2.2.1 Syntheses and Reactions

Linear and cyclic dimetallic compounds were synthesized by treatment of $Fe(NO)_2(CO)_2$ with the aforementioned series of bidentate phosphine ligands. The syntheses of the dimetallic linear iron nitrosyl complexes **9-14** were adapted from a similar synthetic technique utilized in the preparation of $Fe(NO)_2(CO)(PPh_3)$,[22] and were monitored by IR and ^1H, ^{13}C and ^{31}P NMR spectroscopy. The general synthesis of the linear dimetallic complexes **9-14** is depicted in Scheme 2-1.

Scheme 2-1. Generalized Synthetic Pathway for Compounds **9** to **14**.

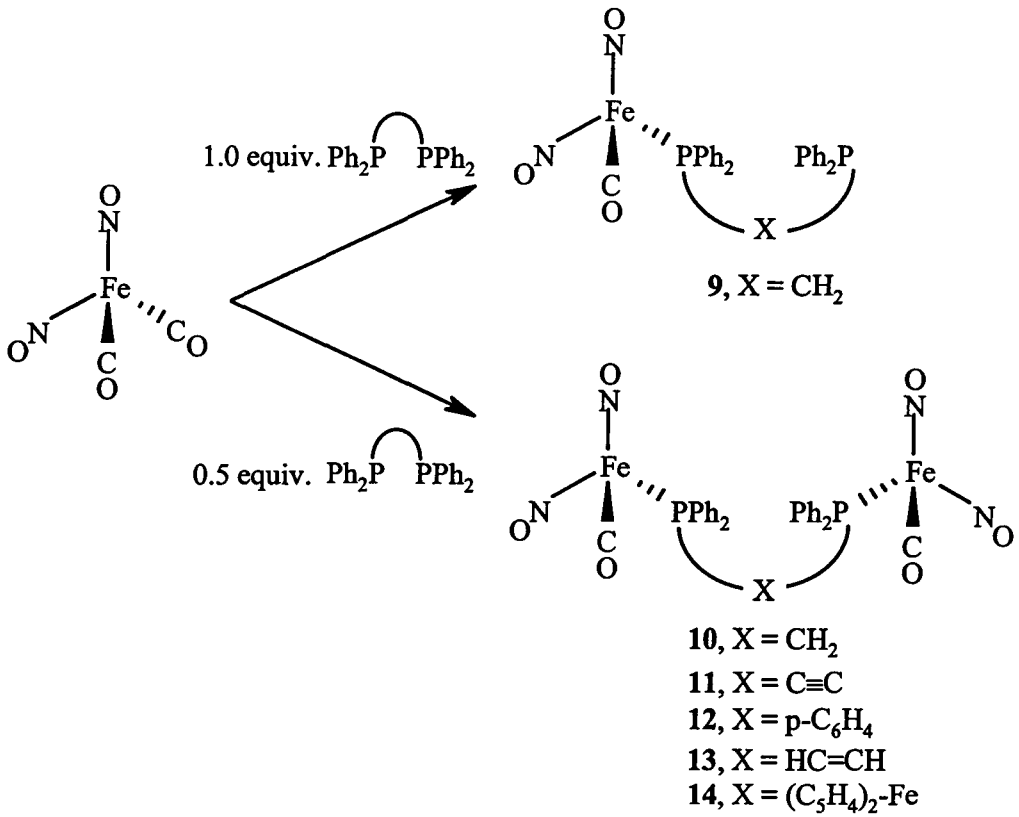

Application of heat to compounds **9** or **10**, afforded the cyclic compound **16**, while heating compound **11** formed the cyclic compound **17** (Scheme 2-2).

Scheme 2-2. Preparation of Compounds **16** and **17**.

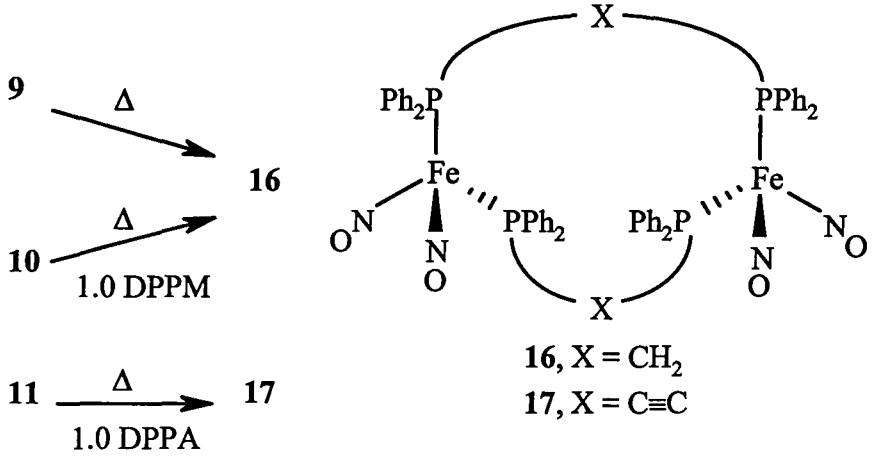

The reaction of $Fe(NO)_2(CO)_2$ with the DPPB ligand in a 2:1 ratio produced the cyclic DPPB compound, **15**. The formation of a cyclic compound containing a DPPB derivative at room temperature was achieved by Hogarth and co-workers from the reaction of cis-$[Mo(CO)_4(pip)_2]$ in CH_2Cl_2 with equimolar amounts of DPFB (1,4-bis(diphenylphosphino)-2,5-difluorobenzene) and DPPA.[49h]

In solution, compounds **9-17** are air sensitive and undergo complete decomposition after several hours even when stored in a degassed solution under nitrogen. Solid samples stored at ambient temperatures under an atmosphere of nitrogen also undergo decomposition, albeit more slowly. Braunstein *et al.* have previously observed the formation of both **9** and **16** as side products in the process of preparing Pt-Fe

clusters,[51] while Atkinson and co-workers, in examining the reaction between [$Fe_2(\mu$-$I)_2(NO)_4$] and DPPM, were able to isolate compound **16** as the corresponding tetrahydrofuran-solvated complex.[52] However, in both cases, no X-ray crystallographic data were provided.

The compounds with the formula [$Fe_2(\mu$-$X)(NO)_4(CO)_2$] where X = DPPA, t-DPPEN and FcP_2, were allowed to react with TCNE to afford complexes [$Fe_2(\mu$-$X)(NO)_4(TCNE)_2$] where X = DPPA, **18**, and FcP_2, **19**, and [$Fe(NO)_2(TCNE)$](μ-X)[$Fe(NO)_2(CO)$] for X = t-DPPEN, **20**. The TCNE adducts were characterized by IR, ^{13}C and ^{31}P NMR spectroscopy, as well as electrochemistry. Similar to the linear and cyclic dimetallic compounds, the TCNE adducts showed similar decomposition in solution and solid states. The rapid decomposition of complexes **9-20** can be rationalized in terms of a nucleophile-induced disproportionation reaction as observed in the reaction of $[Fe(CO)_3(PPh_3)_2]^+$ and pyridine[53], and in the conversion of $Fe(NO)_2(PPh_3)_2^+$ to $Fe(NO)_2(PPh_3)_2$.[52] As previously mentioned in Section 1.4, carbonyl substitution reactions are typically slow. However, the substitution of a carbonyl by TCNE is completed in 1-3 hours at room temperature as observed in the synthesis of $Fe(NO)_2(PPh_3)(\eta^2$-TCNE)[22] and $Fe(NO)_2[P(OMe)_3(\eta^2$-TCNE).[60] A 17-Electron Transfer Autocatalysis Mechanism has been suggested as the reason for the rate of enhancement. In 1996 Atkinson and co-workers showed that two types of four-coordinate iron dinitrosyl complex [$Fe(NO)_2L_2$] and [$Fe(NO)_2LX$] (X = Cl or I), are also interconvertible through a 17-electron redox system. As a result, they were able to synthesize complexes of the

series $[Fe(NO)_2(PR_3)_2]$ in the presence of reducing agents within a few minutes.

Figure 2-1. Molecular Orbital Illustration of The TCNE σ- and π-Bonding to the Metal (a) TCNE σ-bond and (b) TCNE π-bond.

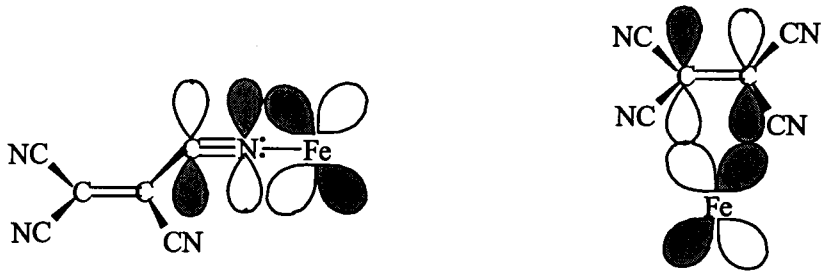

(a) (b)

2.2.2 IR Spectroscopy

The formation of compounds **9-20** was readily monitored by the use of infrared spectroscopy, as the substitution of a carbonyl for a phosphine is accompanied by the loss of signals attributable to carbonyl vibrations. The MNO moiety is expected to exhibit three types of vibrations: ν_{NO}, ν_{MN} stretches and ν_{MNO} bend; however, only the ν_{NO} has been identified in most cases in the vibrational spectra of metal nitrosyl complexes.[6] The assignment of ν_{NO} in metal polynitrosyl complexes follow a similar pattern established for metal carbonyl compounds. In the case of nitrosyl-carbonyl compounds, the distinction between nitrosyl and carbonyl vibrational frequencies can be deduced from the fact that ν_{NO} bands are typically a little broader than those of ν_{CO}. Generally for metal nitrosyl complexes, the N–O stretching frequency is observed as an intense and

characteristic band in the region of 1550-1950 cm^{-1}, which is primarily associated with monodentate nitrosyl groups. Considering the nitrosonium coordination model, where the free NO^+ cation has a stretching frequency of 2250 cm^{-1}, coordination with a metal atom would lower the ν_{NO}. The magnitude of difference between the free and coordinated NO is dependent on the nature of the metal atom and the degree of σ- and π-bonding involved. A decrease in the nitrosyl vibration is a result of the increased backdonation of electron density from the filled metal d-orbital into the π^* orbital of the NO group, which weakens the N–O bond. Conversely, a net donation of electron density from the NO group to the metal center results in a stronger N–O bond and thus, a higher ν_{NO}. Typically, bent M–N–O groups have stretching frequencies that lie within the region of 1510-1700 cm^{-1}, while linear M–N–O groups are in the region of 1550-1950 cm^{-1}.[54] Infrared spectroscopy is the most widely used technique for the characterization of metal nitrosyl complexes, however, it cannot be solely used to identify the mode of linkage of the NO moiety to the metal center.

The infrared spectrum of the starting material, $Fe(NO)_2(CO)_2$, exhibits two nitrosyl stretches and two carbonyl stretches. Upon replacement of one carbonyl moiety by one phosphine of a bis(phosphine) ligand, the remaining CO absorbs in the region of 1993-2014 cm^{-1}. The phosphorus donor increases electron density at the iron center, which in turn enhances the back-bonding from the filled d-orbitals on the metal to the vacant antibonding orbitals of the nitrosyl, resulting in a weakening of the N≡O bond. As a result the nitrosyl stretches shift to lower wavenumbers in the region of 1707-1777 cm^{-1}.

The replacement of the second carbonyl group by another bis(phosphine) ligand gave rise to the cyclic iron nitrosyl complexes. The cyclic DPPM-based complex, **16**, exhibits four distinct IR absorptions in both the solid and solution states, presumably arising from the interaction of the $Fe(NO)_2$ centres, as has been observed in similar cyclic systems.[55] The CH_2Cl_2 solution spectra of **16** match previously reported values.[52] The bridged complexes $[\{Fe(\mu\text{-dmpz})(NO)_2\}_2]$[55] (dmpz = 3,5-dimethylpyrazolyl) and $[\{Ni(\mu\text{-dppm})(CO)_2\}_2]$[56] have also shown four absorptions for nitrosyl and carbonyl bands respectively. This phenomenon appears to be dependent on ring size, as the related ten-membered ring compound, **17**, displays only two nitrosyl stretching signals in both the solid and liquid states. Based on the observed IR frequencies, the nitrosyl groups are best described as linear NO^+ fragments (*vide infra*).[57] Occasionally, the ν_{NO} is seen as a shoulder in the infrared spectrum, and may arise from solid state effects.

Conversely, the replacement of the second carbonyl group by TCNE gives rise to a peak at ~2222 cm^{-1}, attributable to nitrile functionalities. In contrast to the phosphine ligand's donor properties to the iron centre, the electron-withdrawing effect of TCNE reduces the back-bonding which in turn strengthens the nitrosyl bond. This results in a shift of the two nitrosyl signals to higher frequencies ranging from 1769 to 1845 cm^{-1}.

Generally, ferrocene reacts with TCNE to form charge transfer complexes of the type $(\eta^5\text{-}C_5Me_5)_2Fe^+(TCNE)^-$, in which the cyano stretching frequency appears unchanged from free TCNE.[58] However, the σ-bound TCNE (Figure 2-1(a)) shows multiple CN absorptions owing to the effective local C_s symmetry of the coordinated

TCNE.[59] The observation of one broad cyano stretching frequency in the IR spectrum of **18**, **19**, and **20** confirms that TCNE is π-bonded to the iron. The observation of only one strong cyano stretching frequency in other π-bonded TCNE complexes have been reported for $Fe(NO)_2[P(OMe)_3](\eta^2$-TCNE) ($\nu_{C\equiv N}$ = 2230 cm^{-1}),[22] $Fe(NO)_2(PPh_3)(\eta^2$-TCNE) ($\nu_{C\equiv N}$ = 2224 cm^{-1}),[60] $W(CO)_5(\eta^2$-TCNE) ($\nu_{C\equiv N}$ = 2190 cm^{-1}),[58] $(PR_3)_2Pt(\eta^2$-TCNE) ($\nu_{C\equiv N}$ = 2222 cm^{-1}), $Rh(PPh_3)(CO)Cl(\eta^2$-TCNE) ($\nu_{C\equiv N}$ = 2230 cm^{-1}),[61] $Cr(CO)_5(\eta^2$-TCNE) ($\nu_{C\equiv N}$ = 2203 cm^{-1}).[62] Dinitrosyliron bis(phosphine) compounds previously synthesized by our group have also exhibited one stretching frequency for the cyano moiety for **22**, **23** and **24** (where DPPE = 1,2-bis(diphenylphosphino)ethane).[63] The π-bonded TCNE complexes (Figure 2-1(b)) revealed cyano stretching frequencies shifted to lower wavenumbers in comparison with stretching frequencies for free TCNE (2256 and 2220 cm^{-1}). This result may be explained by the efficient back-donation from the filled metal d-orbitals on the iron into the vacant π^* orbital of TCNE, thus weakening the C≡N bond. Table 2 lists the stretching frequencies for complexes **9-20**.

Table 2. Infrared Frequencies for Complexes **3-15**.

Complex	ν_{CO} (cm^{-1})	ν_{NO} (cm^{-1})	ν_{CN} (cm^{-1})	Ref.* *
$Fe(NO)_2(CO)_2$, **1**	2090	1810		
	2040	1766		
[Fe(DPPM)$(NO)_2$(CO)], **9**	2014	1765		
	1993	1721		
[Fe_2(μ-DPPM)$(NO)_4(CO)_2$], **10**	2005	1760		
		1719 (shoulder)		
		1702		
[Fe_2(μ-DPPA)$(NO)_4(CO)_2$], **11**	2004	1777		
		1735		
[Fe_2(μ-DPPB)$(NO)_4(CO)_2$], **12**	2009	1760		
	1999	1707		
[Fe_2(μ-t-DPPEN)$(NO)_4(CO)_2$], **13**	2009	1765		
		1724		
[Fe_2(μ-FcP_2)$(NO)_4(CO)_2$], **14**	2004	1758		
		1708		
[Fe_2(μ-DPPE)$(NO)_4(CO)_2$], **21**	1997	1756		65
		1716		
[Fe_2(μ-DPPB)$_2(NO)_4$], **15**		1677		
		1721		
[Fe_2(μ-DPPM)$_2(NO)_4$], **16**		1733		
		1721		
		1687		
		1668		
[Fe_2(μ-DPPA)$_2(NO)_4$], **17**		1723		
		1679		
[Fe_2(μ-DPPA)$(NO)_4(TCNE)_2$], **18**		1837	2224	
		1789		
[Fe_2(μ-FcP_2)$(NO)_4(TCNE)_2$], **19**		1831	2222	
		1789	2160 (shoulder)	
[Fe_2(μ-DPPM)$(NO)_4(TCNE)_2$], **22**		1829	2230	65
		1781		
[Fe_2(μ-DPPE)$(NO)_4(TCNE)_2$], **23**		1840	2226	65
		1779		
[$Fe(NO)_2$(TCNE)](μ-t-DPPEN)[$Fe(NO)_2$(CO)], **20**	2017	1845	2220	
		1769		
		1726		
[$Fe(NO)_2$(TCNE)](μ-DPPM)[$Fe(NO)_2$(CO)], **24**	2015	1827	2229	65
		1789 (shoulder)		
		1777		
		1716		
[$Fe(NO)_2$(TCNE)](μ-DPPE)[$Fe(NO)_2$(CO)], **25**	1997	1839	2227	65
		1778		
		1756		
		1711		

* The values listed are those in which the sample was prepared as a KBr pellet.
** All compounds were characterized in this thesis, unless otherwise stated.

2.2.3 NMR Spectroscopy

Compounds **9-20** were identified by the use of ^{1}H, ^{13}C and ^{31}P nuclear magnetic resonance spectroscopy. For the singly-complexed bis(phosphine), **9**, two ^{31}P-^{31}P coupled phosphorus NMR resonances were observed, with chemical shift values being consistent with the presence of complexed (48 ppm) and uncomplexed (-25 ppm) diphenylphosphine units. Conversely, each of the symmetrical dimetallic compounds (**10-15**) exhibit a single ^{31}P NMR resonance, consistent with a doubly iron-complexed bis(phosphine). However, the spectrum of **14** gave rise to two singlets, owing to a mixture of products. In accord with the infrared spectrum of **14**, the two products have been identified as $[Fe_2(\mu\text{-}FcP_2)(NO)_4(CO)_2]$, **14** and $[Fe(FcP)_2(NO)_2]$, **14a**, with ^{31}P NMR signals at 48.4 and 57.7 ppm, respectively. The values for **14a** are consistent with the literature values[64] and experimental data, where **14a** was the sole product synthesized. The ^{13}C NMR signals attributed to the phenyl carbons in **10** appear as triplets (with the exception of the *para*-carbon) suggesting the presence of "virtual" coupling in this system.[65] Interestingly, this phenomenon is not observed in the ^{13}C NMR spectra of compounds **11-14**, likely owing to the increased length of the coupling path in these molecules.

TCNE adducts, **18-20**, were sufficiently stable in CD_2Cl_2 in a vacuum-sealed NMR tube to obtain ^{13}C and ^{31}P NMR spectra. The former were recorded at room temperature at 75 MHz. The ^{13}C phenyl resonances were found to appear as overlapping peaks in the region of ~128 to 136 ppm. The four cyano carbons in the symmetrical

TCNE adduct **18**, appeared in pairs at 113.0 ppm, doublet, J_{CP} = 53 Hz and 118.0 ppm, doublet, J_{CP} = 34 Hz. The symmetrical TCNE adduct **19**, revealed two singlets at 113.1 and 108.4 ppm, assigned to the cyano carbons. Despite overnight collection of NMR data, the cyano peaks were relatively weak. The four cyano carbons in the unsymmetrical t-DPPEN TCNE adduct gave rise to a singlet at 112.6 ppm. The ethylene carbons of t-DPPEN appeared as a triplet at 137.2 ppm with a carbon-phosphorus coupling of 15.2 Hz. Only complexes **18** and **20** revealed a very weak peak at 25-30 ppm attributable to the ethylene carbons of TCNE. The low intensity of the aforementioned peaks may be attributable to its relatively long relaxation time. As a result of the coordination of TCNE to the iron centre, the ethylene carbons are significantly shielded compared to those of free TCNE (112.6 ppm). This phenomenon was observed in the ^{13}C NMR for both $Fe(NO)_2(PPh_3)(\eta^2\text{-TCNE})$[22] and both $Fe(NO)_2[P(OMe)_3](\eta^2\text{-TCNE})$.[60] These chemical shifts are generally indicative of an sp^3 saturated carbon rather than an unsaturated carbon. A similar effect was observed in $Pt(PPh_3)_2(\eta^2\text{-}CH_3CF{=}CF_2)$ where the ^{19}F NMR spectrum revealed a geminal $^2J_{FF}$ coupling constant of 200 Hz, which is typically observed for saturated fluorocarbon systems.[66] This trend was also reported for the Rh complex of $(C_5H_5)Rh(\eta^2\text{-}C_2F_4)(\eta^2\text{-}C_2H_4)$.[67]

The ^{31}P spectrum of **18** revealed a singlet at 24.7 ppm, which is consistent with the two phosphorus nuclei having the same chemical environment since the molecule is symmetrical. However, the ^{31}P spectrum of **19** shows two singlets at 25.7 and 41.4 ppm; these signals may be a result of a mixture of products: $[Fe(FcP_2)(NO)_4(TCNE)_2]$, **19** and

19a, respectively. There is also a mixture of products evident from the ^{31}P spectrum of **20**. The two sets of doublets at 55.0 and 37.0 ppm were assigned to the two inequivalent phosphorus nuclei, while the singlet at 38.0 ppm may be attributed to the formation of $[Fe(NO)_2(TCNE)]_2(\mu$-t-DPPEN). The peak at 37.0 ppm corresponds to the ~$PFe(NO)_2$ fragment bound to the TCNE ligand. This effect is attributable to the strong π-acceptor abilities of the TCNE fragment resulting in less electron density around the iron atom which, in turn, causes the corresponding phosphorus atom to be less shielded relative to the phosphorus atom bound to the iron atom containing the carbonyl ligand. Thus, the phosphorus chemical shift appears at a higher field. In the case, where both carbonyl groups are substituted by TCNE fragments, the two phosphorus atoms become equivalent and the observation of only one phosphorus signal appears at a lower frequency. These results are consistent with previous findings for the dinitrosyliron complexes containing the bis(phosphines), DPPM and DPPE.[63]

Table 3. ^{31}P NMR Chemical Shifts of Compounds **9-21, 23** and **25.**

Complex	^{31}P (ppm)	Ref.**
$[Fe(DPPM)(NO)_2(CO)]$, **9**	-25.0 48.0	
$[Fe_2(\mu\text{-DPPM})(NO)_4(CO)_2]$, **10**	45.6	
$[Fe_2(\mu\text{-DPPA})(NO)_4(CO)_2]$, **11**	33.1	
$[Fe_2(\mu\text{-DPPB})(NO)_4(CO)_2]$, **12**	57.1	
$[Fe_2(\mu\text{-t-DPPEN})(NO)_4(CO)_2]$, **13**	52.6	
$[Fe_2(\mu\text{-FcP}_2)(NO)_4(CO)_2]$, **14**	48.4	
$[Fe_2(\mu\text{-DPPE})(NO)_4(CO)_2]$, **21**	55.8	65
$[Fe_2(\mu\text{-DPPB})_2(NO)_4]$, **15**	80.2	
$[Fe_2(\mu\text{-DPPM})_2(NO)_4]$, **16**	43.5	
$[Fe_2(\mu\text{-DPPA})_2(NO)_4]$, **17**	38.6	
$[Fe_2(\mu\text{-DPPA})(NO)_4(TCNE)_2]$, **18**	24.7	
$[Fe_2(\mu\text{-FcP}_2)(NO)_4(TCNE)_2]$, **19**	41.4	
$[Fe_2(\mu\text{-DPPE})(NO)_4(TCNE)_2]$, **23**	42.4	65
$[Fe(NO)_2(TCNE)](\mu$-t-DPPEN$)[Fe(NO)_2(CO)]$, **20**	37.0 55.0	
$[Fe(NO)_2(TCNE)](\mu$-DPPE$)[Fe(NO)_2(CO)]$, **25**	42.0 54.8	65

** All compounds were characterized in this thesis, unless otherwise stated.

2.2.4 X-Ray Crystallography

The crystal structures of **10**, **11**, **16** and **17•CH_2Cl_2** were determined by the use of suitable single crystals mounted on glass fibers. Crystallographic collection and refinement parameters, and selected bond lengths and angles may be found in Tables 4 and 5. Both compounds **10** and **11** crystallized in the space group $P(\bar{1})$ and have a triclinic unit cell. The structures are shown in Figures 2-2 and 2-3, respectively.

Figure 2-2. The X-ray structure of [Fe_2(μ-DPPM)$(NO)_4(CO)_2$], **10**, showing the atomic numbering scheme. Anisotropic thermal displacement ellipsoids are shown at the 30% probability level.

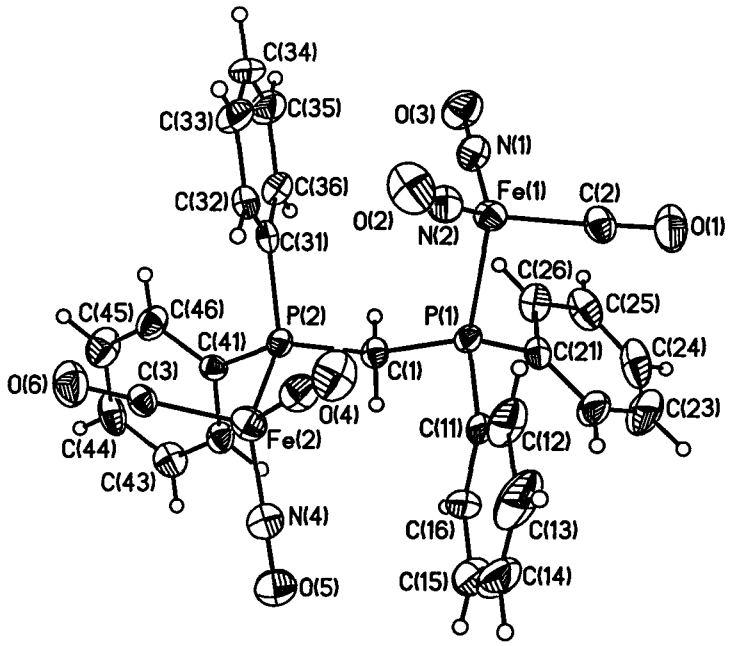

Figure 2-3. The X-ray structure of $[Fe_2(\mu\text{-DPPA})(NO)_4(CO)_2]$, **11**, showing the atomic numbering scheme. Anisotropic thermal displacement ellipsoids are shown at the 30% probability level.

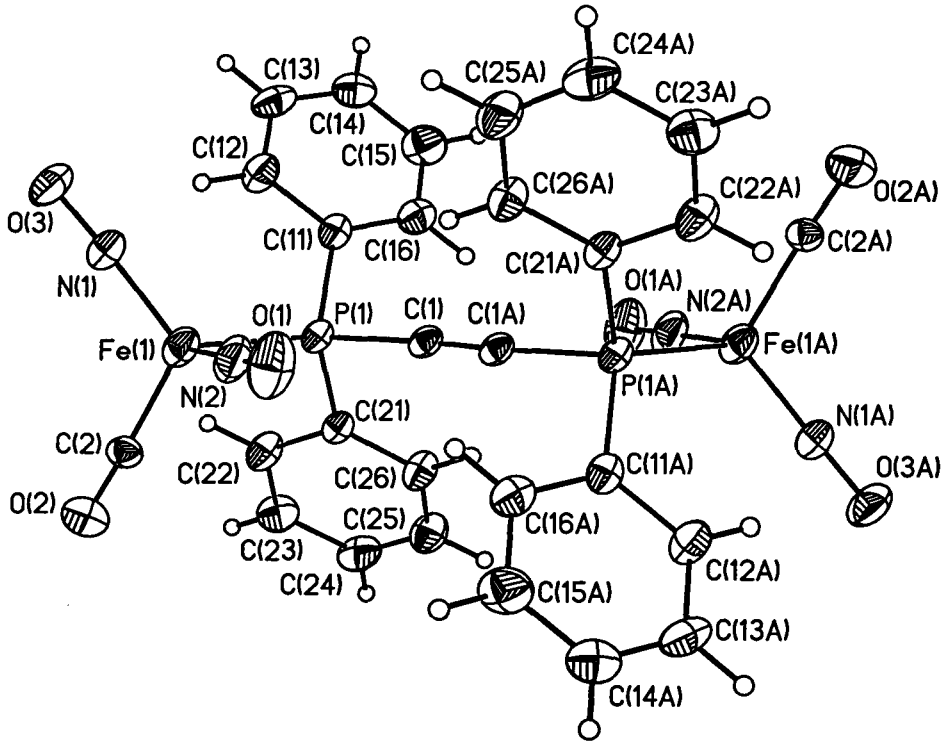

Both cyclic compounds **16** and **17** crystallized in the space group $P2_1/c$ and have monoclinic unit cells. The structures are shown in Figures 2-4 and 2-5, respectively.

Figure 2-4. The X-ray structure of $[Fe_2(\mu\text{-DPPM})_2(NO)_4]$, **16**, showing the atomic numbering scheme. Anisotropic thermal displacement ellipsoids are shown at the 30% probability level.

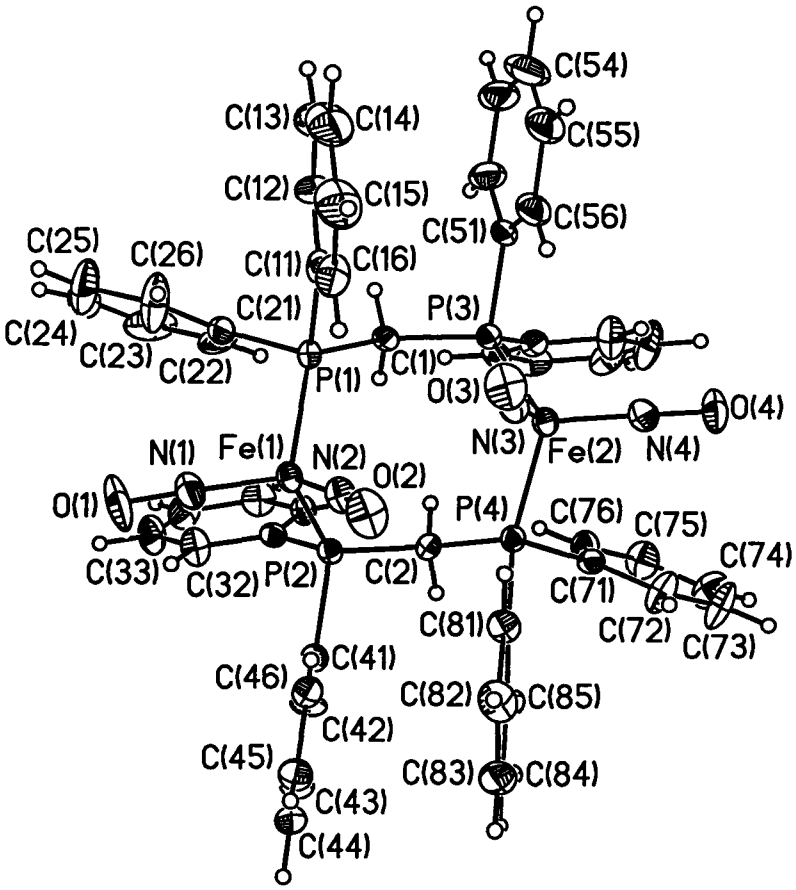

Figure 2-5. The X-ray structure of $[Fe_2(\mu\text{-DPPA})_2(NO)_4]\bullet CH_2Cl_2$, **17•$CH_2Cl_2$**, with thermal displacement ellipsoids shown at the 30% probability level. For clarity, hydrogen atoms and the dichloromethane solvate have been omitted, and only the most highly populated components of the disordered phenyl rings are shown.

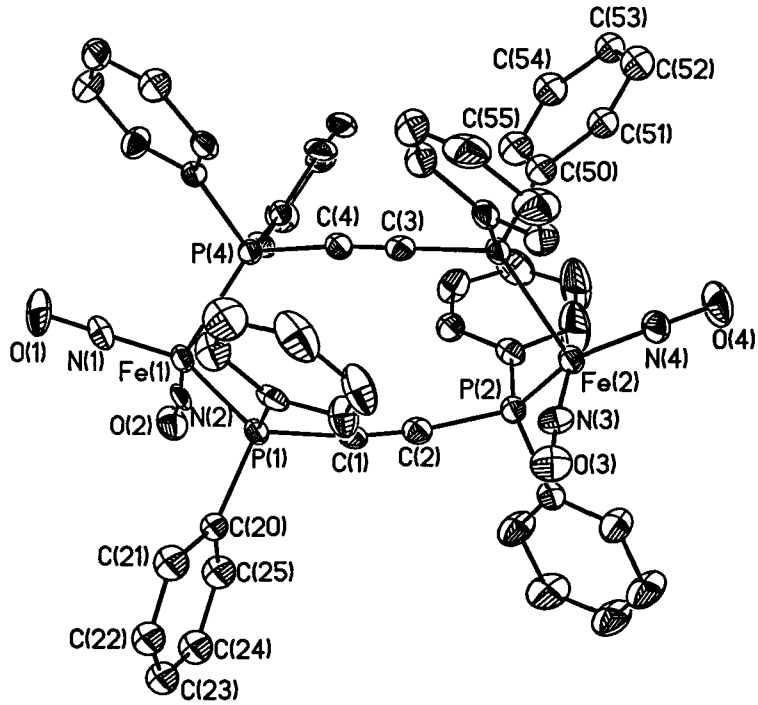

The iron centres in all four of the crystallographically characterized compounds, **10**, **11**, **16**, and **17**, exhibit distorted tetrahedral geometries. Several other dinitrosyliron complexes have been reported to possess distorted tetrahedral geometries.[22,57,60] The iron-iron distances in both the linear (**10** and **11**) and cyclic (**16** and **17**) compounds are all

significantly longer than the related distances found in other structurally characterized $[Fe(NO)_2]_2$ compounds which possess a metal-metal bond.[68] Despite the range in N-Fe-N angles (115.6(4)° to 126.5(4)°), all eight of the $Fe(NO)_2$ units in the aforementioned molecules exhibit "*attracto*" conformations (N-Fe-N > O-Fe-O). These are considered having "*attracto*" conformations because the N-M-N bond angle is less than 130° and the two oxygen atoms bend towards each other.[6] "*Attracto*" conformations are generally favored for first row transition-metal dinitrosyls containing good π-acceptor ligands. The observation of contracted Fe-N distances (~1.64 to ~1.73 Å) and lengthened N-O bonds (~1.16 to ~1.20 Å) in **10**, **11**, **16**, and **17** indicates significant iron-nitrosyl multiple bond character in these species, arising from the appreciable back-donation of the iron fragment into the π* orbital on the nitrosyl ligand. These structural data, in addition to the observation of nearly linear Fe-N-O linkages, support the infrared spectroscopic results and suggest that the NO units in these molecules function as three-electron donors.

The two cyclic complexes, **10** and **11**, are only similar in that the $Fe(NO)_2$ moiety is linked by diphosphine ligands. The structure of **16** shows two $[Fe(NO)_2]$ moieties linked by two DPPM bridges, thereby giving an 8-membered ring. Conversely, **17** is a 10-membered ring composed of two $[Fe(NO)_2]$ groups linked by two DPPA ligands. Both of these cyclic complexes reveal their own distinctive properties dependent on their ring size and bridging diphosphine ligand. The 8-membered ring of **16** folds over to one side bringing the two $[Fe(NO)_2]$ groups to the same side. However, the cyclic dppa complex, **17**, behaves quite differently, instead of folding over, the 10-membered ring

appears to be severely twisted to form a totally asymmetrical structure which has the $[Fe(NO)_2]$ groups on opposite sides.

Despite the numerous examples containing the DPPA ligand, crystallographic data for compounds containing the $Fe(NO)_2$(DPPA) fragment or just the DPPA ligand are limited. As far back as 1969, Carty *et. al.* reported the structure of $[\{CpFe(CO)(\mu\text{-}CO)\}_2(\mu\text{-DPPA})]$,[49f] while in the last decade, the structures of $[\{CpMn(CO)_2\}_2(\mu\text{-DPPA})]$,[48e] $[\{Os_3(CO)_{11}\}_2(\mu\text{-DPPA})]$,[48d] $[PdPtCl_4(\mu\text{-DPPA})_2]$,[69] $Mo_2(\mu\text{-DPPA})_2(CO)_8$ and $Mo_2(\mu\text{-DPPA})_3(CO)_6$[70] were published. In light of the handful of crystallographic structures reported, a more detailed discussion of the solid state geometries of **11** and **17** is given. The "*anti*" orientation of the $Fe(NO)_2$ groups, along with the presence of a crystallographic inversion center, results in an interesting solid state molecular geometry for **11**, in which ten of the non-hydrogen atoms (O(1), N(2), Fe(1), P(1), C(1), C(1A), P(1A), Fe(1A), N(2A) and O(1A)) are essentially co-planar (mean deviation from the plane ~0.32 Å). The non-linear nature of the P-C≡C fragment in **11** (P(1)-C(1)-C(1A) 172.9(8)°) parallels other crystallographically characterized compounds of the type L_nM-DPPA-ML_n,[48] and presumably arises due to steric congestion in the vicinity of the triple bond. Interestingly, such steric demands do not result in the lengthening of the alkyne bonds in either **11** (1.21(1) Å) or **17** (C(1)-C(2) 1.198(4) Å, C(3)-C(4) 1.20(1) Å), which remain essentially unchanged relative to free DPPA.

Thus, the overall molecular structure of the cyclic DPPA compound, **17**, can be described as a severely twisted ten-membered ring, a geometry which is strikingly similar

to that of $Mo_2(\mu\text{-DPPA})_2(CO)_8$,[70] but different from the nearly planar structure found for $PdPtCl_4(DPPA)_2$.[69] The puckering of the ring framework in **17** gives rise to a "bow-tie" orientation of the alkyne units, in which these fragments are twisted by approximately 49° with respect to one another (Figure 2-6). As was observed for **11**, the two P-C≡C-P units in **17** exhibit concave bowing; however, one P-C≡C-P fragment is only slightly bent (P(3)-C(3)-C(4) 173.9(9)°, P(4)-C(4)-C(3) 175.5(9)°), while the other exhibits more pronounced asymmetric bending (P(1)-C(1)-C(2) 170.8(9)°, P(2)-C(2)-C(1) 165.8(9)°). Upon viewing the structure of **17** down the Fe-Fe vector, it is evident that the DPPA ligands can be classified as "*anti*" (P(1)-C(1)-C(2)-P(2)) and "*syn*" (P(3)-C(3)-C(4)-P(4)), with the former experiencing greater strain, and subsequently more pronounced deviation from linearity, than the latter. It is interesting to note that although $Mo_2(\mu\text{-DPPA})_2(CO)_8$ possesses similarly "*syn*" and "*anti*"-oriented DPPA ligands, a correlation between the degree of non-linearity of the DPPA ligands and their relative orientation does not exist in this molybdenum-based system.

Figure 2-6. Views of the crystallographically determined structure of $[Fe_2(\mu\text{-DPPA})_2(NO)_4]\bullet CH_2Cl_2$, **17•$CH_2Cl_2$**: **(I)** highlighting the "bow-tie" orientation of the alkyne units, and **(II)** down the Fe(1)-Fe(2) vector (For clarity, only the ipso-phenyl carbons are shown).

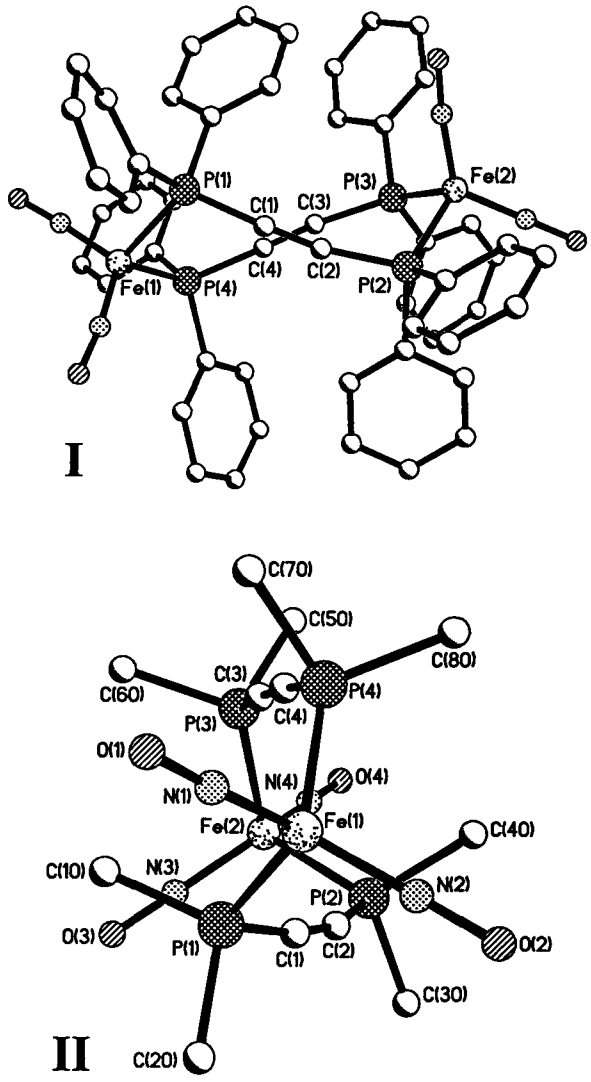

Table 4. Crystallographic Collection and Refinement Parameters for **10**, **11**, **16** and **17**• CH_2Cl_2.

	10	**11**	**16**	**17**• CH_2Cl_2
Empirical formula	$C_{27}H_{22}P_2N_4Fe_2O_6$	$C_{28}H_{20}P_2N_4Fe_2O_6$	$C_{50}H_{44}P_4N_4Fe_2O_4$	$C_{53}H_{42}P_4N_4Fe_2O_4Cl_2$
Molecular Weight	672.13	682.12	1000.47	1105.39
Description	red needle	dark red plate	dark red prism	dark red prism
Size, mm^3	0.42 x 0.09 x 0.03	0.3 x 0.16 x 0.08	0.25 x 0.15 x 0.14	0.28 x 0.25 x 0.12
Temperature, K	213(2)	213(2)	213(2)	213(2)
Crystal system	triclinic	triclinic	monoclinic	monoclinic
Space group	$P(\bar{1})$	$P(\bar{1})$	$P2_1/c$	$P2_1/c$
a, Å	8.3037(1)	8.714(23)	21.2512(1)	21.3908(2)
b, Å	10.9324(3)	9.539(28)	12.3414(1)	13.8839(1)
c, Å	17.6037(2)	9.959(25)	22.2870(2)	17.8203(2)
α, deg.	78.43(2)	114.52(8)	90.000	90.000
β, deg.	77.318(1)	96.13(16)	112.49(1)	101.463(1)
γ, deg.	82.198(2)	97.76(12)	90.000	90.000
Volume, $Å^3$	1520.35(5)	734.1(34)	5400.69(7)	5186.84(8)
Z	2	1	4	4
Calcd Dens., g/cm^3	1.468	1.543	1.230	1.416
Scan Mode	ω-scans	ω-scans	ω-scans	ω-scans
F(000)	684	346	2064	2264
Abs. Coef., mm^{-1}	1.105	1.145	0.698	0.834
θ-range, deg.	1.20 to 22.50	2.29 to 27.34	1.04 to 22.50	0.97 to 22.50
Index ranges	$-10 \le h \le 10$	$-11 \le h \le 11$	$-27 \le h \le 27$	$-27 \le h \le 27$
	$-13 \le k \le 13$	$-12 \le k \le 12$	$-16 \le k \le 16$	$-17 \le k \le 17$
	$-21 \le l \le 21$	$-12 \le l \le 12$	$-28 \le l \le 20$	$-22 \le l \le 22$
No. Diffr. Refl.	11146	5231	31207	28244
No. Refl. Total	3892	2673	6976	6769
Data / restr. / param.	3851 / 0 / 370	2673 / 0 / 190	6922 / 0 / 577	6763 / 12 / 656
GOF on F^2 (all)	1.011	0.938	1.120	1.017
Final R ($I>2\sigma(I)$)	R1 = 0.0658;	R1 = 0.0772;	R1 = 0.0885;	R1 = 0.1134;
	wR2 = 0.1162	wR2 = 0.1810	wR2 = 0.2818	wR2 = 0.2865
R indices (all data)	R1 = 0.1384;	R1 = 0.1462;	R1 = 0.1201	R1 = 0.1451
	wR2 = 0.1466	wR2 = 0.2146	wR2 = 0.3163	wR2 = 0.3264
Trans., (max., min.)	0.9098, 0.79139	0.8722, 0.1802	0.8944, 0.6976	0.8577, 0.2080
Largest diff. Peak, $e/Å^3$	0.338	0.971	2.932	2.605
Largest diff. Hole, $e/Å^3$	-0.302	-0.405	-0.444	-1.606

Table 5. Selected Bond Lengths [Å] and Angles [deg.] for **10, 11, 16** and **17• C H_2Cl_2.**

	10	**11**	**16**	**17• CH_2Cl_2**
Fe-Fe	5.21	7.60	4.35	7.01
Fe(1)-N(1)	1.693(8)	1.680(7)	1.643(9)	1.66(1)
Fe(1)-N(2)	1.654(6)	1.73(1)	1.644(8)	1.65(1)
Fe(2)-N(3)	1.675(8)	--------	1.668(9)	1.67(1)
Fe(2)-N(4)	1.705(8)	--------	1.644(9)	1.646(9)
N(1)-O	1.171(8)	1.169(7)	1.19(1)	1.19(1)
N(2)-O	1.175(6)	1.164(9)	1.20(1)	1.19(1)
N(3)-O	1.182(8)	--------	1.18(1)	1.16(1)
N(4)-O	1.163(8)	--------	1.19(1)	1.20(1)
Fe(1)-N(1)-O	177.8(7)	175.9(6)	174(1)	176.2(8)
Fe(1)-N(2)-O	174.8(7)	178.1(7)	168.9(8)	172.9(7)
Fe(2)-N(3)-O	175.0(7)	--------	166.6(8)	174.5(9)
Fe(2)-N(4)-O	177.1(8)	--------	177.1(9)	179.6(8)
N(1)-Fe(1)-N(2)	122.1(8)	115.6(4)	117.0(4)	120.5(4)
N(3)-Fe(2)-N(4)	118.1(9)	--------	116.8(4)	126.5(4)
O-Fe(1)-O	119.9	114.1	109.6	116.4
O-Fe(2)-O	116.2	--------	110.3	124.3

* nitrosyl oxygen atoms

2.2.5 Electrochemical Studies

The formation of dinitrosyliron compounds with ferrocene, ethylene, or acetylene phosphine linkages and an η^2-bound TCNE ligand, led us to test the hypothesis of conducting behaviour through electrochemical studies. Cyclic voltammograms of the complexes **14a** and **18-20** were recorded in CH_2Cl_2 containing a 0.1 M electrolyte at a scan rate of 300 mVs^{-1} and the data are listed in Table 6. All the compounds, except $[Fe(FcP)_2(NO)_2]$, **14a**, revealed a potential, E°, at approximately 1.33 V, assigned to the ferrocene reference with a one-electron reduction. The compound $[Fe_2(\mu\text{-DPPA})(NO)_4(TCNE)_2]$, **18**, showed three chemically reversible reduction processes at approximately -0.77, -0.80 and -1.28 V. The potentials at -0.77 V and -0.80 V can be clearly assigned to the two iron centres interacting with each other through the acetylene bridge with a separation of ~0.12 V, as seen in Figure 2-7. Hence, **18** exhibits conducting behaviour as a result of the two metal centres joined with a conjugated bidentate phosphine ligand, DPPA and the strong electron-withdrawing group, TCNE. The last reduction peak at -1.28 V is consistent with the reduction of $TCNE^-$ to $TCNE^{2-}$, which is also evident in the cyclic voltammograms of $[Fe_2(\mu\text{-}FcP_2)(NO)_4(TCNE)_2]$, **19** and $[Fe(NO)_2(TCNE)](\mu\text{-t-DPPEN})[Fe(NO)_2(CO)]$, **20**. It has been observed by Hörsken *et. al.* that the coordination of TCNE to $Fe(NO)_2(PR_3)(CO)$ complexes leads to a negative shift in potentials, in comparison to free TCNE. In addition, the uncoordinated TCNE compound, $Fe(NO)_2(PR_3)(CO)$ gave rise to positive values. The results reveal that the back-bonding from the iron centre to the TCNE ligand is stronger than the characteristic

covalent bond arising from σ-donation by the TCNE ligand. The iron becomes easier to reduce as a result of the back-donation to the TCNE ligand, giving the iron atom a partial positive charge.

On the other hand, **19** exhibits three reduction peaks at potentials of approximately -0.10, -0.92 and -1.33 V. The potential at -0.10 V corresponds to the reduction of ferrocene in the compound, while the potential at -0.92 V is attributed to the reduction of the entire compound. To ensure there was no effect on the outcome of the cyclic voltammogram of **19** due to a mixture of products, **14a** was also examined by cyclic voltammetry. The voltammogram revealed a large peak in the ferrocene region, possibly owing to the reduction of ferrocene in the compound. Compound **20** gave rise to potentials at approximate values of -0.16, -0.88 and -1.25 V, similar to the values seen for $[Fe(NO)_2(TCNE)](\mu\text{-DPPE})[Fe(NO)_2(CO)]$, **25**. The potential at -0.16 corresponded to the reduction of TCNE to $TCNE^-$. This reduction is attributed to the presence of excess TCNE within the solid, confirming that a second TCNE ligand could not be added to **20** in order to produce a symmetrical compound. The reduction at -0.88 V corresponds to the reduction of the entire compound, as a result of the instability of the anion, its decomposition caused the liberation of $TCNE^-$. Since TCNE is a strong electron-withdrawing group, its coordination to one of the iron centres in $Fe_2(\mu\text{-DPPA})(NO)_4(CO)_2$ causes the iron centre to become slightly positively charged and, hence it becomes more difficult to add another TCNE. In order for a second TCNE to coordinate to the other iron centre, the compound must be reduced. Thus, the t-DPPEN

ligand does not exhibit any conducting behaviour because it cannot compensate for the slightly positive charge rendered by the iron atom upon its coordination of the TCNE ligand to allow for two TCNE ligands to be bonded to the iron atom, unlike the DPPA ligand. The disubstituted compound, $[Fe_2(\mu\text{-DPPE})(NO)_4(TCNE)_2]$, **23**, revealed similar reductions as the monosubstituted compound, **25**, although, the current utilized for the reduction of **23** was double that of **25**. Furthermore, compound **19** may not demonstrate redox properties due to the nonlinearity of the FcP_2 ligand, which is a common characteristic of complexes exemplifying this phenomenon.[47] This idea of linearity of the bidentate phosphine may also be extended to the t-DPPEN ligand.

Table 6. Electrochemical Data for Iron Dinitrosyl Complexes at a Scan Rate of 300 mVs^{-1}.

Complexes	**E_{PC} (V)**		**E_{PA}(P) (V)**		**Ref.****
$[Fe_2(\mu\text{-DPPA})(NO)_4(TCNE)_2]$, **18**	-0.77	-0.80	-0.05	-0.25	
$[Fe_2(\mu\text{-}FcP_2)(NO)_4(TCNE)_2]$, **19**	-0.92		-0.38		
$[Fe_2(\mu\text{-DPPE})(NO)_4(TCNE)_2]$, **23**	-0.83		-0.73		65
$[Fe(NO)_2(TCNE)](\mu$-t-DPPEN$)[Fe(NO)_2(CO)]$, **20**	-0.88		-0.30		
$[Fe(NO)_2(TCNE)](\mu$-DPPE$)[Fe(NO)_2(CO)]$, **25**	-0.82		-0.75		65

** All compounds were characterized in this thesis, unless otherwise stated.

Figure 2-7. Cyclic Voltammogram of Complex **18**.

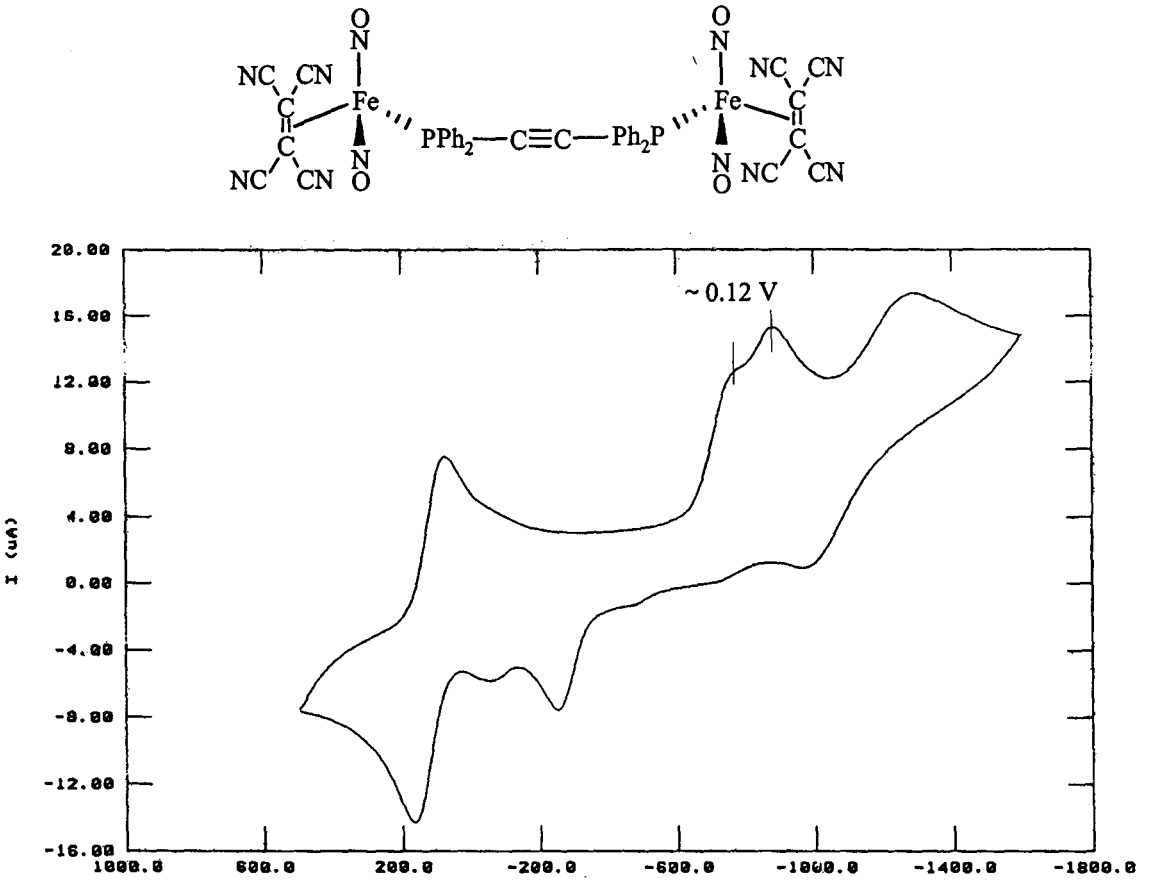

Summary

To conclude, we have demonstrated that the syntheses of both dimeric and cyclic dinitrosyliron complexes have been achieved by the use of bidentate phosphine ligands and $Fe(NO)_2(CO)_2$. The compounds have been identified through the use of several spectroscopic techniques, including ^1H, ^{13}C and ^{31}P NMR, and infrared. The structures of the four compounds, **10**, **11**, **16**, and **17** were confirmed from crystallographic data. Interestingly, **11** and **17** are the first structurally characterized compounds containing a dinitrosyliron DPPA fragment. The coordination of the TCNE ligand to the $(ON)_2FeP{\sim}PFe(NO)_2$ motif allowed the molecule to be studied by electrochemical methods to examine its potential redox properties. Of the three TCNE adducts synthesized, only the compound with an acetylene group tethered by two phosphines, joined to a $Fe(NO)_2(\eta^2\text{-TCNE})$ moiety revealed communication (electron delocalization) between the two iron termini.

CHAPTER 3

INVESTIGATIONS OF THE ELECTROPHILIC NATURE OF IRON NITROSYL COMPLEXES

3.1 Background

It has been thoroughly documented in literature that iron dinitrosyl compounds undergo nucleophilic substitution reactions. In one of the very first reports, by Malatesta and Aràneo,[13] numerous examples were reported of nucleophilic substitutions by Lewis bases such as phosphines, arsines, stibines, and many others. Over the past thirty years, researchers have attempted to isolate the products from substitution reactions of iron dinitroysls and hard bases containing nitrogen atoms. It was not until very recently, that the structure of the first non-heme iron dinitroysl complex, $Fe(NO)_2(1\text{-MeIm})_2$, **26**, as shown in Figure 3-1,[71] was determined in this laboratory.

Figure 3-1. The X-ray structure of $Fe(NO)_2(1\text{-MeIm})_2$, **26**, showing the atomic numbering scheme. Anisotropic thermal displacement ellipsoids are shown at the 50% probability level.

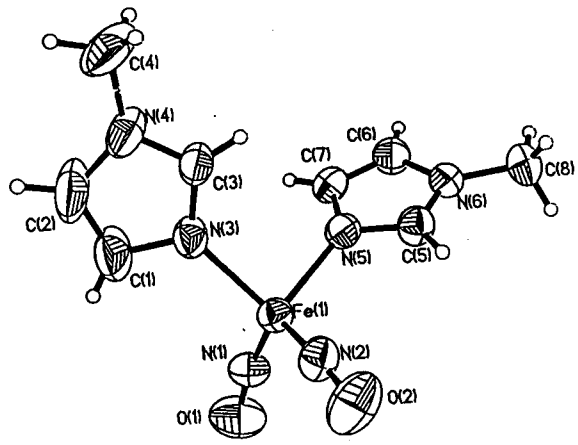

We trust that the biological importance of **26**, will lead to the isolation of other complexes in the biological system containing nitrosyl non-heme-iron and amino acids of proteins. Thus, the chemistry of iron dinitrosyls and their reactivity with nucleophiles is quite extensive. On the other hand, the nature of the iron center in various iron nitrosyls has been of interest with respect to its reactivity towards electrophiles. Since the formal oxidation state of $Fe(NO)_2(CO)_2$ is -2 (as mentioned in chapter 1), one would expect that the iron atom would be susceptible to electrophilic attack. In the late 60's, Chaudari *et al.* have examined a series of reactions of sodium tricarbonylnitrosyliron, $[Na^+][Fe(CO)_3(NO)^-]$ with a variety of alkyl halides and triphenylphosphine.[72] It is appropriate to address the issue of the anion or neutral form of iron nitrosyls with respect to their susceptibility to electrophilic attack. This chapter provides preliminary data relevant to this question.

3.2 Results and Discussion

As an extension of the reactivity of dinitrosyliron compounds, the following neutral dinitrosyliron compounds, $Fe(NO)_2(CO)_2$, **1**, $Fe(NO)_2(CO)(PPh_3)$, **21**, and $Fe(NO)_2(PPh_3)_2$, **22**, were allowed to react with a series of electrophiles including HCl, $SiMe_3Cl$, $Et_3O^+SbCl_6^-$, trifluoroacetic acid (TFA) and trifluoromethanesulfonic acid (TFSA). The reactivity of electrophiles was further extended to include iron nitrosyl anions such as $[PPN^+][Fe(CO)_3(NO)^-]$, **24** and $[N(Bu)_4^+][Fe(CO)_3(NO)^-]$, **25**. In principle, one would anticipate that the attack of the electrophile would occur on the iron

centre, which has a formal oxidation state of -2 in the compounds of interest (**1**, **21** and **22**). In the case of the iron tricarbonyl nitrosyl anion, its reactivity with alkyl halides (RX), in the presence of triphenylphosphine, yielded the product $[Fe(CO)_2(COR)(NO)(PPh_3)]$, where the alkyl cation (R^+) is bonded to the carbon of the carbonyl moiety.[72] Despite the authors' efforts, the primary product, $[Fe(CO)_3(R)(NO)]$ was not identified by any spectroscopic techniques. As in Scheme 3-1, one can envisage a route to $[Fe(CO)_2(COR)(NO)(PPh_3)]$ that proceeds *via* nucleophilic attack by the anion on the alkyl halide. Subsequent alkyl migration generates a 16-electron species whose vacant coordination site can be filled by the phosphine.

Scheme 3-1. A Synthetic Pathway to $[Fe(CO)_2(COR)(NO)(PPh_3)]$.

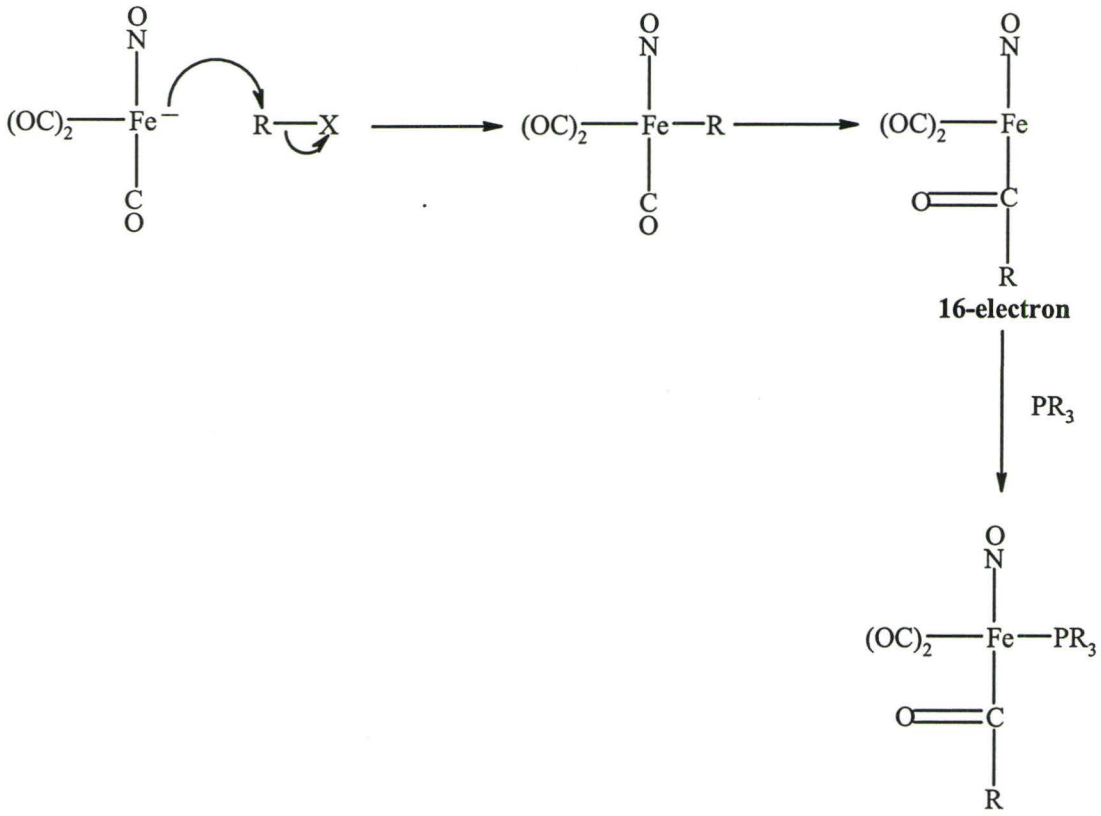

The sodium salt most commonly used in these reactions, $[Na^+][Fe(CO)_3(NO)^-]$, is extremely air-sensitive and thus difficult to work with. Other iron nitrosyl anions have been synthesized with PPN^+ and $N(Bu)_4^+$ as counterions; these cations enhance the stability of the iron tricarbonyl nitrosyl anion and facilitate its use. The synthesis of the PPN^+ salt was more efficient than the $N(Bu)_4^+$ salt. Moreover in the solid state their yields were not significantly affected by a minimal exposure to air. The chemistry of the anion has been investigated in terms of its reactivity with CH_3I and CF_3CO_2H, both in the presence of PPh_3, yielding $Fe(NO)(CO)_2(COCH_3)(PPh_3)$[72] and $FeH(CO)_3(NO)$,[39] respectively. The nitrosyl hydride $FeH(CO)_3(NO)$ was isolated and characterized by ^{31}P NMR and X-ray crystallography.

It was observed that $[PPN^+][Cr(CO)_4(NO)^-]$ acted as a nucleophile towards several reagents such as $CF_3SO_3CH_3$, CF_3SO_3H and Ph_3SnCl and its reactivity was found to be similar to that of $[Fe(CO)_3(NO)^-]$.[73] However, attempts to isolate $Cr(CO)_4(NO)(CH_3)$ and $HCr(CO)_4(NO)$ were unsuccessful.

3.2.1 Syntheses and Reactions

The neutral dinitrosyliron compounds, $Fe(NO)_2(CO)_2$, **1**, $Fe(NO)_2(CO)(PPh_3)$, **21**, and $Fe(NO)_2(PPh_3)_2$, **22**, were treated with a series of electrophiles mentioned above, at room temperature or at -78 °C. The products arising from the reaction of **1**, **21**, **22**, $[PPN^+][Fe(CO)_3(NO)^-]$, **24** and $[N(Bu)_4^+][Fe(CO)_3(NO)^-]$, **25**, with the aforementioned series of ligands are air-sensitive and undergo complete decomposition in both solution and solid states, even when stored under an atmosphere of nitrogen. The solid samples

undergo decomposition more slowly. The products produced from the series of reactions lead to decomposition or products that could not be clearly identified. A detailed description of the reaction conditions can be found in the experimental section (Chapter 5). The two tables listed below present the IR and NMR spectroscopic data for the products.

Table 7. Infrared Frequencies for Iron Nitrosyl Complexes.

Complex	ν_{CO} (cm^{-1})	ν_{NO} (cm^{-1})
$Fe(NO)_2(CO)_2$, **1**	2090	1810
	2040	1766
$Fe(NO)_2(CO)(PPh_3)$, **21**	2004	1761
		1719
$Fe(NO)_2(PPh_3)_2$, **22**		1716
		1669
$[PPN^+][Fe(CO)_3(NO)^-]$, **24**	1979	1650
	1881	
$[PPN^+][Fe(CO)_3(NO)^-]$, **25**	1979	1650
	1881	
27		1714
		1662
28		1666
		1611
32		1816
		1723
35		1785
		1724

* The values listed are those in which the sample was prepared as a KBr pellet.

Table 8. ^{31}P NMR Chemical Shifts of Compounds **21**, **22**, **32** and **35**.

Complex	^{31}P (ppm)
$Fe(NO)_2(CO)(PPh_3)$, **21**	56.7
$Fe(NO)_2(PPh_3)_2$, **22**	60.9
32	42.0
35	38.7 23.4

3.2.2 EHMO Calculations

EHMO calculations were performed on several compounds such as $Fe(NO)_2(CO)_2$, $Fe(NO)_2(CO)(PPh_3)$, $Fe(NO)_2(PPh_3)_2$, $Fe(CO)_4^-$ and $Cr(NO)_4$ to calculate the charge on the metal centre and to investigate the effects that different ligands would have on the nitrosyl moiety. These types of semi-empirical methods were used only to observe the trends in the compounds listed in Table 9 and should not be regarded as accurate values; however, the relative effects are evident. Ab initio computational methods would undoubtedly provide better data but they are beyond the scope of this paper.

Table 9. Calculated Mulliken Charges for Compounds **1**, **21**, **22**, **37** and **38**.

Compound	M	N	O	C	O	P
$Fe(NO)_2(CO)_2$, **1**	0.272	0.412	-0.642	0.740	-0.651	
$Fe(NO)_2(CO)(PPh_3)$, **21**	0.158	0.419	-0.664	0.605	-0.797	
$Fe(NO)_2(PPh_3)_2$, **22**	-0.173	0.305	-0.729			0.247
$Fe(CO)_4^{2-}$, **37**	-0.851			0.568	-0.855	
$Cr(NO)_4$, **38**	0.793	0.377	-0.575			

In compound **1**, each nitrosyl unit has a charge of -0.23 and the carbonyl unit has a charge of 0.89, while in **38** each nitrosyl unit has a charge of -0.198 suggesting that there is more backdonation from the iron atom in **1** to the nitrosyl groups than in the chromium compound. Each carbonyl unit in compound **37** has a charge of -0.287. Comparing the two iron phosphine compounds, **21** and **22**, it is evident that the iron centres possess more negative character with further substitution of the carbonyl moieties by phosphorus donor ligands. This result is expected and corroborates data from infrared and NMR spectroscopy, that the coordination of the phosphine groups results in more backdonation from the iron atom to the phosphorous atom and therefore, there is more electron density surrounding the iron atom going from compounds **1** to **21** and then to **22**. These calculations also provide evidence that assigning oxidation states to nitrosyl compounds produces inaccurate assumptions about the potential reactivity of the compounds. For example, $Fe(NO)_2(CO)_2$ is considered to have a formal oxidation state of -2, however, the actual charge as determined by EHMO calculations reveals that the iron atom is positive and the nitrosyl moiety possess a negative character. Figures 3-2 and 3-3 depict two of the highest lying occupying orbitals of $Fe(NO)_2(CO)_2$ illustrating clearly the phenomena of back-bonding from the iron atom into π^* orbitals of the CO and NO ligands, respectively. The perspectives are (a) along the C_2 axis and (b) showing the tetrahedral geometry of $Fe(NO)_2(CO)_2$.

In light of the experimental data, EHMO calculations suggest that the iron centres in $Fe(NO)_2(CO)_2$, **1**, $Fe(NO)_2(CO)(PPh_3)$, **21**, and $Fe(NO)_2(PPh_3)_2$, **22**, will not undergo

attack by an electrophile. In addition, infrared spectroscopy of these compounds provide further evidence that the iron centre does not possess a negative charge because the low nitrosyl stretching frequencies are attributed to backdonation from the iron atom to the NO groups.

Figure 3-2. A Molecular Orbital illustrating the Backbonding into the NO orbital (a) along the C_2 axis and (b) showing the tetrahedral geometry.

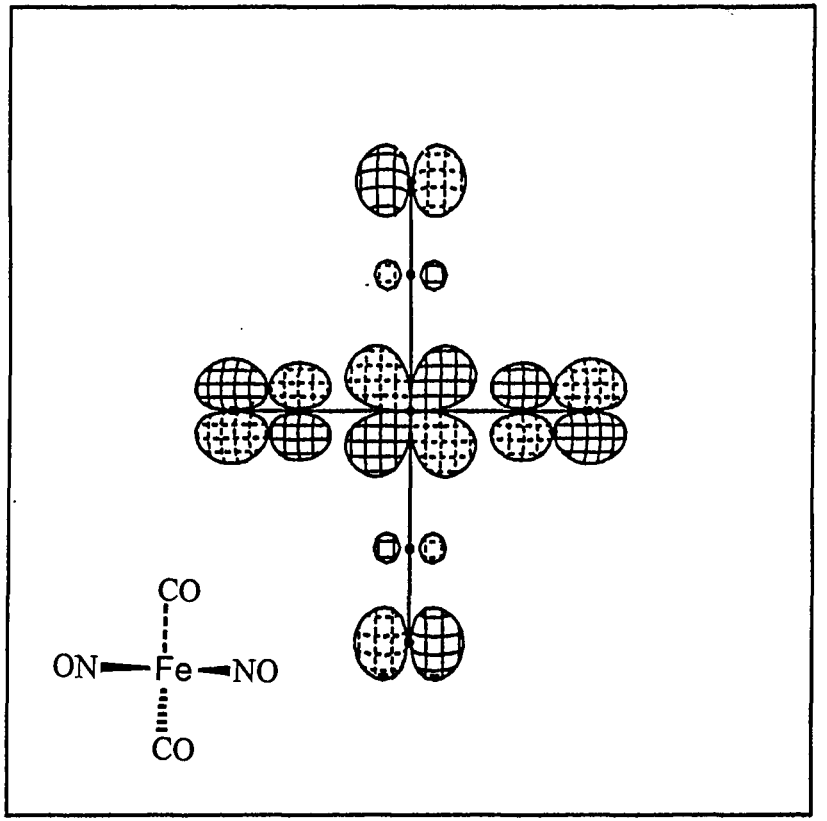

a

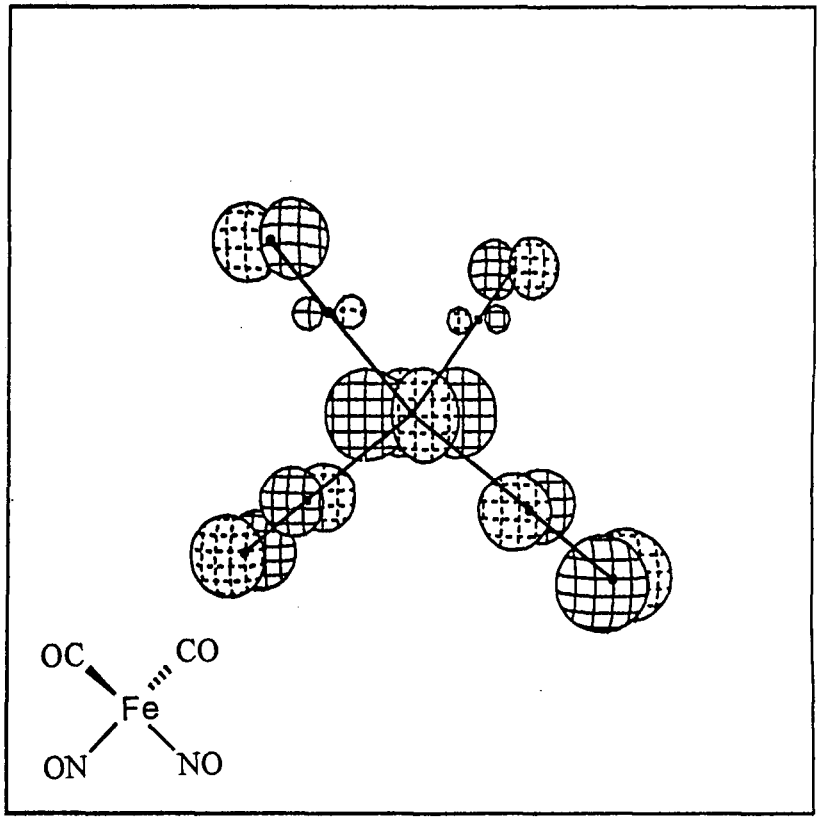

b

Figure 3-3. A Molecular Orbital illustrating the Backbonding into the CO orbital (a) along the C_2 axis and (b) showing the tetrahedral geometry.

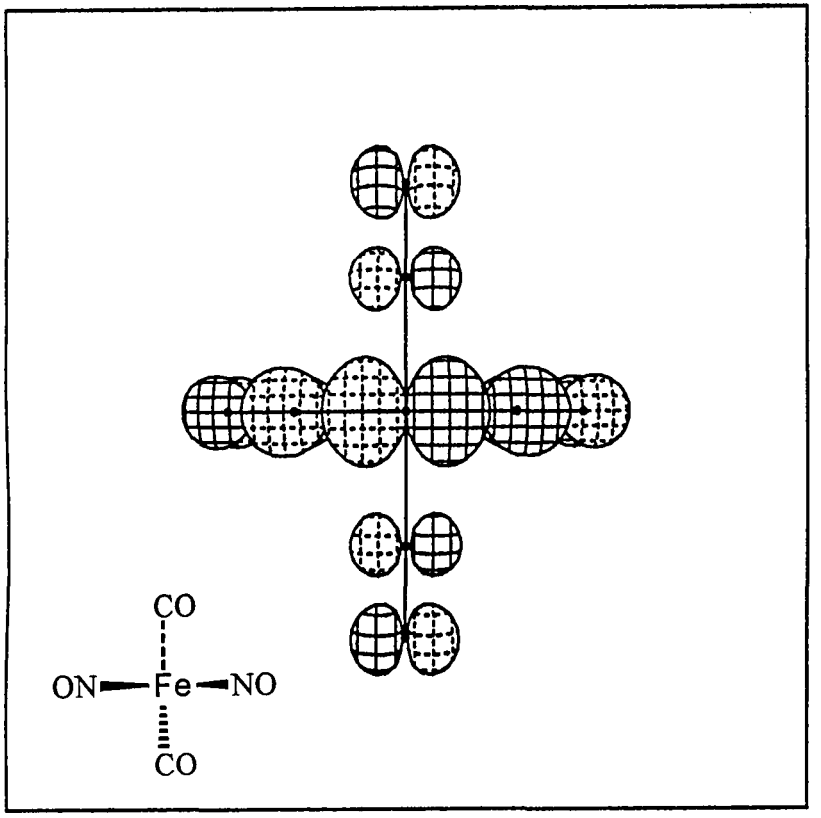

a

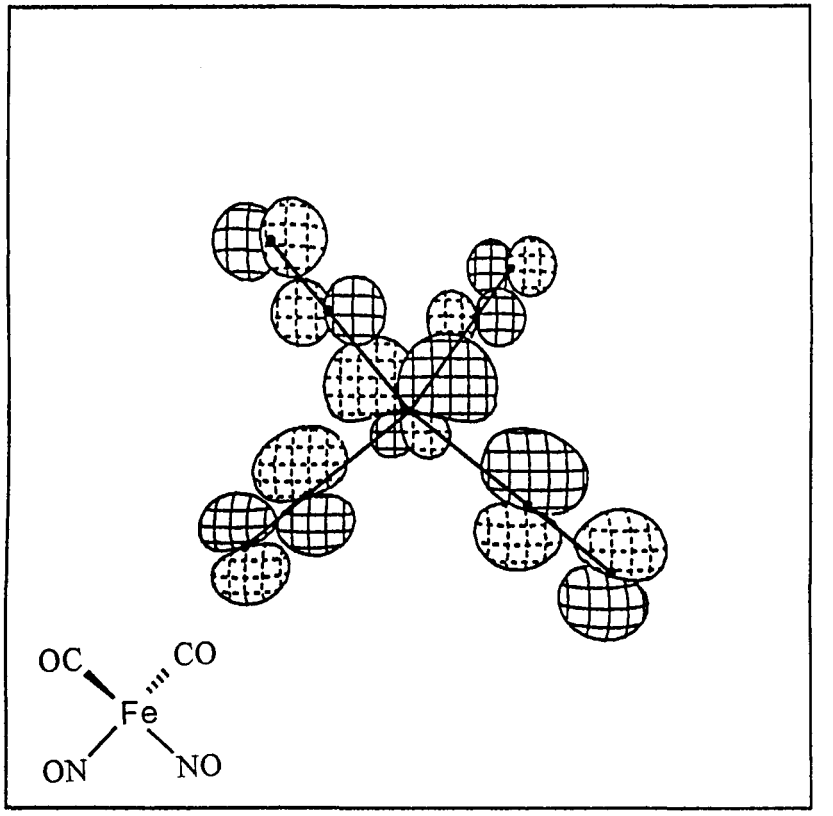

b

3.3 Summary

To conclude, the electrophilic attack of the neutral iron dinitrosyl compounds to either the iron centre or the nitrosyl moiety has not been proven. The re-investigation of the chemistry of the iron anion with several different cations did not produce any new results. Despite, these preliminary results further investigation will be beneficial in understanding the chemistry surrounding iron nitrosyl complexes.

CHAPTER 4

FUTURE WORK AND GENERAL CONCLUSIONS

4.1 Future Work

It has been clearly demonstrated that conductivity between two redox-active metal centres linked by a conjugated bidentate phosphine ligand along with coordinated TCNE ligands was achieved with compound **18**, $[Fe_2(\mu\text{-DPPA})(NO)_4(TCNE)_2]$. However, this is the only example in the iron dinitrosyl compounds that was examined in this thesis. The challenge would be to select other bidentate phosphines and investigate the effects of these ligands. One possibility could be to extend the alkyne chain within the bidentate phosphine and probe the effectiveness of the chain length to the communication between the two iron centres. Bridged species, such as –C≡C–R–C≡C–, where R = aromatic rings, disilanes, or disiloxanes have attracted attention for this very reason and are known to possess unique physical and chemical properties, such as displaying electrical conducing behaviour.[74] In light of the use of these bridged species in other systems, their incorporation into the $(ON)_2FeP\sim PFe(NO)_2$ moiety with or without the TCNE ligand may provide further insight into this chemistry, especially their electrochemical behaviour.

The ability of neutral iron dinitrosyl to be susceptible to electrophilic attack has not

been clearly concluded. It is clear that further work is needed to gain more insight and determine if there is a possibility of isolating and characterizing any products from electrophilic reactions with iron dinitrosyl complexes.

4.2 General Conclusions

We have demonstrated that both linear and cyclic complexes containing the dinitrosyliron fragments connected by a difunctional ligand can be synthesized from $Fe(NO)_2(CO)_2$ and a specific diphosphine. Indeed, the X-ray crystal structures of [Fe_2(μ-DPPM)$(NO)_4(CO)_2$], [Fe_2(μ-DPPA)$(NO)_4(CO)_2$], [Fe_2(μ-DPPM)$_2(NO)_4$] and [Fe_2(μ-DPPA)$_2(NO)_4$] confirm their existence along with the spectroscopic techniques utilized. The linear and cyclic DPPA complexes have exhibited unique properties owing to the acetylene functional group. Coordination of these $Fe(NO)_2$-containing bis(phosphine) compounds to TCNE ligands enabled us to investigate their redox properties. Of all the systems evaluated, only the DPPA complex demonstrated a communicating behaviour between the two iron centres upon reduction.

The examination of the iron dinitrosyl complexes to undergo electrophilic attack was not clearly established. The use of PPN^+ and $N(Bu)_4^+$ salts produced data similar to that of Chaudhari[72] and Pannell.[75] EHMO calculations suggest that the iron centre in dinitrosyldicarbonyliron does not possess a negative charge as expected. However, it was noted that subsitution of the carbonyls by phopshines contributes to the negative character of the iron, which may increase the possibility of being attacked an electrophile.

CHAPTER 5

EXPERIMENTAL

5.1 General Procedures

All manipulations were carried out in an atmosphere of dry nitrogen using freshly distilled and degassed solvents. Unless otherwise stated all chemicals, including bis(diphenylphosphino)methane (DPPM), trans-1,2-bis(diphenylphosphino)ethylene (t-DPPEN), 1,1'-bis(diphenylphosphino)ferrocene (FcP_2), trifluoroacetic acid (TFA), trifluoromethanesulfonic acid (TFSA), methyl iodide, triphenylphosphine, triethyloxonium hexachloroantimonate (V), sodium nitrite, bis-(triphenylphosphoranylidene)ammonium chloride (PNP)Cl, and tetracyanoethylene TCNE) were purchased from the Aldrich Chemical Company and used as supplied; bis(diphenylphosphino)acetylene (DPPA, Strem Chemicals) and 1,4-bis(diphenylphosphino)benzene (DPPB, Organometallics Inc.) were used as supplied. $Fe(NO)_2(CO)_2$ was prepared following a published procedure.[9] The ^1H, ^{13}C and ^{31}P NMR spectral data were acquired using either a Bruker AC-200 or AC-300 spectrometer in deuterated methylene chloride, unless otherwise stated. All ^{13}C and ^{31}P NMR spectra were recorded in proton-decoupled mode with phosphorus chemical shifts externally referenced relative to 85% H_3PO_4 in D_2O. Melting and decomposition points were measured using differential scanning calorimetry performed on a DSC 2910 instrument (TA instruments). IR spectra were recorded on a Bio-Rad FTS-40 single beam

spectrometer using KBr pellets, unless otherwise stated. Mass spectra were recorded on a Micromass Quattro LC instrument using positive electrospray ionization (ESI+).

5.2 X-Ray Crystallography

Crystallographic data[76] for **10**, **11**, **16** and **17**•CH_2Cl_2 were collected from suitable single crystal samples mounted on glass fibers. The instrument used for the collection of diffraction data was a Siemens P4 diffractometer equipped with a Siemens SMART 1K CCD Area Detector (using the program SMART) and a rotating anode using graphite-monochromated Mo-Kα radiation (λ = 0.71073 Å). Data processing was carried out by use of the program SAINT, while the program SADABS was utilized for the scaling of diffraction data, the application of a decay correction, and an empirical absorption correction based on redundant reflections. Structures were solved by using the direct methods procedure in the Siemens SHELXTL program library, and refined by full-matrix least squares methods on F^2. All non-hydrogen atoms, with the exception of the disordered atoms in **17**•CH_2Cl_2, were refined using anisotropic thermal parameters. Hydrogen atoms were added as fixed contributors at calculated positions, with isotropic thermal parameters based on the bonded carbon atom. Compound **11** crystallizes in the space group $P(\bar{1})$ with half a molecule per asymmetric unit; the other half of the molecule is generated by a crystallographic inversion center, resulting in the observation of only one molecule per unit cell (Z = 1). Combustion analysis previously obtained by other workers for compound **16** (similarly prepared in tetrahydrofuran) suggested the presence of a solvated tetrahydrofuran per molecule of **16** in the crystalline lattice.

However, despite the fact that the data readily allow for a complete anisotropic refinement of the target molecule, attempts to resolve atomic positions for the disordered solvate were unsuccessful, leading to rather high values for the residual electron density and the refinement statistics. In the case of **17•CH_2Cl_2**, the final refined structure involved a disordered model in which the phenyl rings containing C(20)-C(25) and C(50)-C(55) could exist in one of two orientations, resulting from rotation about the P-C(*ipso*) bond. Based on the observed thermal displacement ellipsoids, it was assumed that only these carbon atoms were significantly affected by this disorder process. The occupancies for each of the two orientations were each allowed to refine as a free variable (final ratio of approximately 55:45 for both of the phenyl units). Moreover, during the refinement of **17•CH_2Cl_2**, a disordered molecule of dichloromethane was located in the asymmetric unit. Given the magnitude, location and number of electron density difference peaks observed in the region of the solvate, the final refined structure was based on a disordered model involving two possible orientations, generated by rotation about a fixed and non-disordered (fully occupied) central methylene carbon. The occupancies for each of the two orientations were each allowed to refine as a free variable (final ratio of approximately 90:10). Hydrogen atoms for each unique component of the disordered phenyl and dichloromethane units were added at calculated positions with occupancy factors equal to the occupancy factor of the associated carbon atom. The hydrogen atoms were refined using a riding model with isotropic displacement parameters equal to 1.2 times the equivalent isotropic displacement parameter of the

attached carbon.

5.3 Electrochemsitry

Electrochemical measurements were performed on a PARC (Princeton Applied Research, Princeton, NJ) 263A potentiostat, controlled by a computer running the electrochemistry software M270. The working electrode used was a commercial gold electrode purchased from Bioanalytical Systems and the counter electrode was a platinum coil. The quasi-reference electrode was a Ag wire and the potentials were reported with respect to a ferrocinium-ferrocene standard. The CH_2Cl_2 solution containing the supporting electrolyte $(\eta\text{-}C_6H_{13})_4NPF_6$ (0.1 M) was prepared and each complex (1.0 mM) was added to the degassed solution and degassed before running CV experiments. During these experiments, the electrochemical micro-cell, containing a 10 mL solution, was kept in a Smart Stir Faraday Cage purchased from EG&G to prevent any interference from electromagnetic waves.

5.4 Molecular Orbital Calculations

Molecular orbital calculations were performed using the extended Hückel method[77] and orbital drawings were obtained by the use of the program CACAO.[78]

5.5 Compound Preparation and Spectra Data

Synthesis of Iron dinitrosyl dicarbonyl, $Fe(NO)_2(CO)_2$, 1

$Fe(NO)_2(CO)_2$ was synthesized by a modified method of Hieber and Beutner.[9] Sodium nitrite (17 g, 0.25 mol) and sodium (10 g, 0.44 mol) were added to dried methanol (450 mL), while cooling and stirring. After all the sodium had dissolved, iron pentacarbonyl

(25 mL, 0.2 mol) was slowly added to give a yellow solution. The solution was refluxed at a temperature between 75-80 °C until the distillate was no longer yellow in colour (approximately 2 hours). The methanol was distilled off at 80 °C to give rise to a yellow salt, $[Fe(CO)_3(NO)]^-$. To the salt, water (400 mL) and sodium nitrite, $NaNO_2$, (17 g, 0.25 mol) were added. A slow flow of CO_2 was bubbled through the solution, which passed through three $CaCl_2$ traps and **1** was collected in a series of three U-tubes cooled to –78 °C in dry ice/acetone bath as a brick red solid in a 60 % (15 mL) yield. The product was stored in the freezer under N_2. MW = 171.88 g mol^{-1}; ρ = 1.56 g cm^{-3}; m.p. 21.6 °C; IR (diethyl ether solution) ν/cm^{-1} 2087 (CO), 2038 (CO), 1810 (NO), 1767 (NO).

General Preparation of Compounds 9-15

Method (A): To an Erlenmeyer flask containing $Fe(NO)_2(CO)_2$ was added a suspension of the phosphine ligand in pentane at room temperature. After stirring the solution for 18 h, the precipitate generated was filtered and washed with pentane. Method (B): To an Erlenymeyer flask containing the phosphine ligand in THF, $Fe(NO)_2(CO)_2$ was added at room temperature. After stirring the solution for 18 h, the solvent was removed under reduced pressure and the remaining solid washed with pentane.

General Preparation of Compounds 16 and 17

Method (C): A solution of the reactants was filtered into a sealable tube, degassed by use of freeze-pump-thaw procedures, flame-sealed under vacuum and subsequently heated to 75 °C.

General Preparation of Compounds 18-19

Method (D): To an Erlenymeyer flask containing the iron dinitrosyl phosphine complex in diethyl ether, TCNE was added at room temperature. The initially dark red solution turned to a light yellowish-green after an hour and a precipitate was formed. After stirring the solution for 18 h, the precipitate was filtered and washed three times with diethyl ether and hexanes, and dried under vacuo.

[Fe(DPPM)(NO)$_2$(CO)] 9. Method (A): Fe(NO)$_2$(CO)$_2$ (0.05 mL, 0.45 mmol) and DPPM (170 mg, 0.44 mmol) in pentane (8 mL) produced **9** as a bright orange/red powder (70 mg, 30 %). Method (B): DPPM (170 mg, 0.44 mmol), Fe(NO)$_2$(CO)$_2$ (0.05 mL, 0.45 mmol) and THF (6 mL) produced **9** (160 mg, 69 %), m.p. 119 °C (with decomposition); IR(KBr) ν/cm^{-1} 2014 (CO), 1993 (CO), 1765 (NO), 1725 (NO); IR (THF-solution) ν/cm^{-1} 2005 (CO), 1761 (NO), 1718 (NO); ^{1}H NMR (CD_2Cl_2, 200.13 MHz) δ 3.21 (d, 2H, $^2J_{HP}$ = 8.7 Hz, CH_2), 7.27-7.49 (m, 20H, Ph); ^{13}C NMR (CD_2Cl_2, 50.03 MHz) δ 31.7 (m, CH_2), 127.9-137.6 (Ph), 221.3 (s, CO); ^{31}P NMR (CD_2Cl_2, 121.50 MHz) δ -25.0 (d, 1P, $^2J_{PP}$ = 110 Hz), 48.0 (d, 1P, $^2J_{PP}$ = 107 Hz, P-Fe).

[Fe$_2$(μ-DPPM)(NO)$_4$(CO)$_2$] 10. Method (A): Fe(NO)$_2$(CO)$_2$ (0.10 mL, 0.91 mmol) was added to a suspension of DPPM (174 mg, 0.45 mmol) in pentane (10 mL). During the course of the reaction the DPPM dissolved and a dark red/brown powder precipitated which was filtered and washed with pentane (87 mg, 29 %). Method (B): DPPM (500 mg, 1.3 mmol), Fe(NO)$_2$(CO)$_2$ (0.3 mL, 2.7 mmol) and THF (10 mL) produced **10** (700 mg, 80 %), m.p. 144 °C (with decomposition); IR(KBr) ν/cm^{-1} 2005 (CO), 1760 (NO),

1719 (shoulder) (NO), 1702 (NO); IR (THF-solution) ν/cm^{-1} 2004 (CO), 1764 (NO), 1718 (NO); ^{1}H NMR (CD_2Cl_2, 300.13 MHz) 3.76 (t, 2H, $^{2}J_{HP}$ = 9.7 Hz, CH_2), 7.41-7.44 (m, 20H, Ph); ^{13}C NMR (CD_2Cl_2, 75.47 MHz) δ 32.6 (t, $^{1}J_{CP}$ = 11.4 Hz, CH_2), 129.3 (t, J_{CP} = 5.2 Hz, C_o or C_m), 131.1 (s, C_p), 132.6 (t, J_{CP} = 6.5 Hz, C_m or C_o), 134.3 (t, J_{CP} = 22 Hz, C_i), 221.1 (s, CO); ^{31}P NMR (CD_2Cl_2, 121.50 MHz) δ 45.6 (s). Single crystals suitable for X-ray diffraction studies were grown from pentane by slow evaporation under an atmosphere of nitrogen.

[Fe_2(μ-DPPA)$(NO)_4(CO)_2$] 11. Method (B): DPPA (500 mg, 1.27 mmol), $Fe(NO)_2(CO)_2$ (0.28 mL, 2.5 mmol) and THF (15 mL) yielded **11** (484 mg, 56 %); IR(KBr) ν/cm^{-1} 2004 (CO), 1735 (NO), 1777 (NO); ^{1}H NMR (CD_2Cl_2, 300.13 MHz) δ 7.43-7.64 (m, 20H, Ph); ^{13}C NMR (CD_2Cl_2, 75.47 MHz) δ 105.0 (d, J_{CP} = 60.4 Hz, C≡C) 129.1 (d, J_{CP} = 11.5 Hz, C_o or C_m), 131.1 (s, C_p), 131.8 (d, J_{CP} = 14.4 Hz, C_m or C_o), 132.0 (d, J_{CP} = 48 Hz, C_i), 218.7 (s, CO); ^{31}P NMR (CD_2Cl_2, 121.50 MHz) δ 33.1 (s). Single crystals suitable for X-ray diffraction studies were grown from pentane by slow evaporation under an atmosphere of nitrogen.

[Fe_2(μ-DPPB)$(NO)_4(CO)_2$] 12. Method (B): DPPB (500 mg, 1.1 mmol), $Fe(NO)_2(CO)_2$ (0.27 mL, 2.5 mmol) and THF (25 mL) yielded **12** (760 mg, 94 %); m.p. 301 °C (with decomposition); IR(KBr pellet) ν/cm^{-1} 2009 (CO), 1999 (CO), 1760 (NO), 1707 (NO); ^{1}H NMR (CD_2Cl_2, 200.13 MHz) δ 7.34-7.42 (m, Ph); ^{13}C NMR (CD_2Cl_2, 50.03 MHz) δ 129.0 (d, J_{CP} = 10.8 Hz, C_o or C_m and *o*-C_6H_4), 130.8 (s, C_p), 132.3 (d, J_{CP} = 24.6 Hz, *i*-C_6H_4), 133.2 (d, J_{CP} = 13.6 Hz, C_m or C_o), 136.9 (d, J_{CP} = 38.2 Hz, C_i), 221.0 (s, CO); ^{31}P

NMR (CD_2Cl_2, 121.50 MHz) δ 57.1 (s).

$Fe_2(\mu$-t-DPPEN)$(NO)_4(CO)_2$] 13. Method (B): t-DPPEN (456 mg, 1.15 mmol), $Fe(NO)_2(CO)_2$ (0.30 mL, 2.3 mmol) and THF (10 mL) yielded **13** as a red powder (118 mg, 26 %), m.p. 128 °C (with decomposition); IR(KBr) ν/cm^{-1} 2009 (CO), 1724 (NO), 1765 (NO); ^{13}C NMR (CD_2Cl_2, 75.47 MHz) δ 129.5-133.1 (m, 24C, Ph), 141.9 (t, $^2J_{CP}$ = 18.1 Hz, HC=CH), 220.9 (s, CO); ^1H NMR (CD_2Cl_2, 300.13 MHz) δ 6.9 (t, 2H, $^2J_{CH}$ = 18.5 Hz, HC=CH), 7.7-7.1 (m, 20H, Ph); ^{31}P NMR (CD_2Cl_2, 121.50 MHz) δ 52.6 (s).

[$Fe_2(\mu$-$FcP_2)(NO)_4(CO)_2$] and [Fe (FcP_2)$(NO)_2$] 14 and **14a.** Method (B): FcP_2 (1.54 g, 2.79 mmol), $Fe(NO)_2(CO)_2$ (0.65 mL, 5.9 mmol) and THF (25 mL) yielded **14** and **14a** as a red powder (2.77 g), m.p. 272 °C (with decomposition); IR(KBr) ν/cm^{-1} 2004 (CO), 1708 (NO), 1758 (NO), 1660 (NO), 1095 (P-C); ^{13}C NMR (CD_2Cl_2, 75.47 MHz) δ 76.4-68.2 (m, 10C, C_5H_4), 136.3-128.8 (m, 34C, Ph and C_5H_4), 220.2 (s, CO); ^{31}P NMR (CD_2Cl_2, 121.50 MHz) δ 57.7 (s), 48.4 (s). IR(KBr) values ν/cm^{-1} 1708 (NO), 1660 (NO) and 1095 (P-C) are consistent with those reported in the literature **ref** for **14a** and with ^{31}P NMR (CD_2Cl_2, 121.50 MHz) δ 57.6 (s), from a previous synthesis where **14a** was the sole product.

[$Fe_2(\mu$-DPPB)$_2(NO)_4$] 15. Method (B): DPPB (1.01 mg, 2.27 mmol) and $Fe(NO)_2(CO)_2$ (0.55 mL, 4.54 mmol) in THF (20 mL) yielded **15** as a red powder (1.83 g, 30 %), m.p. °C (with decomposition); IR(KBr) ν/cm^{-1} 1721 (NO), 1677 (NO); ^{13}C NMR (CD_2Cl_2, 75.47 MHz) δ 137.8-128.6 (m, Ph and C_6H_4); ^{31}P NMR (CD_2Cl_2, 121.50 MHz) δ 80.2 (s).

[$Fe_2(\mu$-DPPM)$_2(NO)_4$] 16. Method (C): After stirring DPPM (72 mg, 0.19 mmol) and **10** (125 mg, 0.19 mmol) in THF (6 mL) for 18 h, the solution gradually turned black. After 2 days, a red crystalline product (**16**) was isolated by filtration (45 mg, 24 %); these crystals were utilized for X-ray diffraction studies. m.p. 167 °C; IR(KBr) ν/cm^{-1} 1733 (NO), 1721 (NO), 1687 (NO), 1668 (NO); the spectrum run in CH_2Cl_2 matches previously reported values. ^1H NMR (CD_2Cl_2, 200.13 MHz) δ 3.7 (t, $^2J_{HP}$ = 6.5 Hz, 2 x CH_2), 7.5-7.3 (m, Ph, 40H); ^{31}P NMR (CD_2Cl_2, 121.50 MHz) δ 43.5 (s); MS/MS (90:10 CH_2Cl_2/MeOH, m/z, (%)): 1000 (100, $[M]^+$), 970(2, $[M\text{-}NO]^+$), 500 (45, $[M/2]^+$).

[$Fe_2(\mu$-DPPA)$_2(NO)_4$] 17. Method (C): After stirring **11** (100 mg, 1.5 mmol) and DPPA (58 mg, 1.5 mmol) in THF (5 mL) for 18 h, the solution gradually turned black. After 72 h the tube was opened, the solvent removed under reduced pressure and the remaining brown solid (**17**) was washed with pentane (90 mg, 64 %). Single crystals suitable for X-ray analysis were grown from CH_2Cl_2 by slow evaporation of the solvent under an N_2 atmosphere. IR(KBr) ν/cm^{-1} 1723 (NO), 1679 (NO); ^1H NMR (CD_2Cl_2, 200.13 MHz) δ 7.51-7.09 (m, Ph, 40H); ^{13}C NMR (CD_2Cl_2, 75.47 MHz) δ 133.3-128.9 (m, Ph); ^{31}P NMR (CD_2Cl_2, 121.50 MHz) δ 38.6 (s).

[$Fe_2(\mu$-DPPA)$(NO)_4(TCNE)_2$] 18. Method (D): TCNE (182 mg, 1.42 mmol), [$Fe_2(\mu$-DPPA)$(NO)_4(CO)_2$], **11**, (484 mg, 0.71 mmol) and diethyl ether (20 mL) yielded **18** as a yellow powder (138 mg, 29 %), m.p. 134 °C (with decomposition); IR(KBr) ν/cm^{-1} 2224 (CN), 1798 (NO), 1837 (NO); ^{13}C NMR (CD_2Cl_2, 75.47 MHz) δ 102.7 (s, C≡C), 107.3 (s, C≡C), 113.0 (CN, d, J_{CP} = 53.0 Hz), 118.0 (CN, d, J_{CP} = 34.2 Hz), 124.6-134.1 (m,

Ph); ^{31}P NMR (CD_2Cl_2, 121.50 MHz) δ 24.7 (s).

$[Fe_2(\mu\text{-}FcP_2)(NO)_4(TCNE)_2]$ 19. Method (D): TCNE (862 mg, 6.73 mmol), $[Fe_2(\mu\text{-}FcP_2)(NO)_4(CO)_2]$, **14**, (2.35 g, 3.37 mmol) and diethyl ether (30 mL) yielded **19** as a brown powder (2.87 g, 83 %), m.p. 161 °C (with decomposition); IR(KBr) ν/cm^{-1} 2222 (CN), 2160 (CN), 1789 (NO), 1831 (NO), 1097 (P-C); ^{13}C NMR (CD_2Cl_2, 75.47 MHz) δ 133.2-129.3 (overlapping multiplet from Ph and C_5H_4), 113.1 (s, CN), 108.4 (s, CN), 76.8-74.5 (m, 10C, C_5H_4); ^{31}P NMR (CD_2Cl_2, 121.50 MHz) δ 41.4 (s), 25.7 (s).

$[Fe(NO)_2(TCNE)](\mu\text{-t-DPPEN})[Fe(NO)_2(CO)]$ 20. Method (D): TCNE (519 mg, 4.05 mmol), $[Fe_2(\mu\text{-t-DPPEN})(NO)_4(CO)_2]$, **13**, (1.08 g, 1.99 mmol) and diethyl ether (15 mL) yielded **20** as a yellowish-orange solid (595 mg, 38 %), m.p. 172 °C (with decomposition); IR(KBr) ν/cm^{-1} 2220 (CN), 2017 (CO), 2001 (CO shoulder), 1796 (NO), 1726 (NO shoulder), 1845 (NO); ^{13}C NMR (CD_2Cl_2, 75.47 MHz) δ 137.2 (t, J_{CP} = 15.2 Hz, HC=CH), 133.3-129.0 (m, Ph), 112.6 (s, CN); ^{31}P NMR (CD_2Cl_2, 121.50 MHz) δ 55.0 (d, J_{PP} = 29.5 Hz), 38.0 (s), 37.0 (d, J_{PP} = 29.0 Hz).

Synthesis of $Fe(NO)_2(CO)(PPh_3)$, 21.

$Fe(NO)_2(CO)(PPh_3)$ was synthesized by a modified method of McBride *et al.*[79] To an Erlenmeyer flask containing triphenyphosphine (1.11 g, 4.23 mmol) in toluene (6 mL) was added an equimolar amount of $Fe(NO)_2(CO)_2$ (0.45 mL, 4.11 mmol). After stirring the dark red solution for 18 h at room temperature, an equivolume amount of methanol (6 mL) was added to precipitate out **21** and place in an ice bath for crystallization. The brick-red powder, **21** (1.44 g, 86 %), was filtered and washed with

cold methanol IR (KBr) ν/cm^{-1} 2003 (CO), 1760 (NO), 1717 (NO); ^{31}P NMR (CD_2Cl_2, 121.50 MHz) δ 56.7 (s).

Synthesis of $Fe(NO)_2(PPh_3)_2$, 22.

$Fe(NO)_2(PPh_3)_2$ was synthesized by a modified method described by Malatesta and Aràneo.[13] To an Erlenmeyer flask containing triphenyphosphine (5.02 g, 19.1 mmol) in toluene (15 mL) was added to $Fe(NO)_2(CO)_2$ (1.05 mL, 9.57 mmol). The dark red solution was refluxed for 18 h at 85 °C and then filtered off and washed with methanol. The precipitate was a red powder, **22** (4.45 g, 73 %); IR (KBr) ν/cm^{-1} 1716 (NO), 1677 (NO); ^{31}P NMR (CD_2Cl_2, 121.50 MHz) δ 60.9 (s).

Synthesis of $PPN(NO_2)$, 23.

$PPN(NO_2)$ was synthesized as outlined by Stevens, Yanta and Gladfeter.[80] (PNP)Cl (5.02 g, 8.74 mmol) in a 500 mL round bottom was dissolved with hot distilled water (150 mL), while $NaNO_2$ was dissolved with hot distilled water (60 mL) and placed in a dropping separatory funnel. The $NaNO_2$ solution was added dropwise to the (PNP)Cl solution producing a cloudy solution. When all the $NaNO_2$ was added, the solution was cooled in an ice bath for 30 min. The product was filtered and washed with water and diethyl ether and dried overnight forming bis(triphenylphosphoranylidene)ammonium nitrite monohydrate, $PPN(NO_2)\bullet H_20$, (5.43 g, 9.02 mmol). Azeotropic distillation with benzene produced a white, air-stable solid, $PPN(NO)_2$, (0.33 g, 0.57 mmol).

Synthesis of $[PPN^+][Fe(CO)_3(NO)^-]$, 24.

The synthesis of $[PPN^+][Fe(CO)_3(NO)^-]$ was performed as outlined by Stevens

and Gladfelter.[38] The 250 mL round bottom flask containing $PPN(NO_2)$ (1.00 g, 1.72 mmol) was purged with N_2 followed by the addition of THF (120 mL) via syringe. Only a small amount of the $PPN(NO_2)$ dissolved until the addition of iron pentacarbonyl (0.24 mL, 1.83 mmol) via syringe. Immediate effervescence was observed and the solution turned yellow as $PNP(NO_2)$ dissolved. After 45 min, all of the solid $(PNP)NO_2$ dissolved producing a clear yellow solution. The solvent was removed by rotary evaporator yielding **24** as yellow crystals (1.06 g, 1.50 mmol), IR (KBr) ν/cm^{-1} 1980 (CO), 1885 (CO), 1657 (NO) consistent with the reported literature values.[38]

Synthesis of $[N(Bu)_4^+][Fe(CO)_3(NO)^-]$, 25.

$[N(Bu)_4^+][Fe(CO)_3(NO)^-]$ was synthesized by a modified method of Steel.[81] Sodium nitrite (17 g, 0.25 mol) and sodium (10 g, 0.44 mol) were added to dried methanol (400 mL), while cooling and stirring. After all the sodium had dissolved, iron pentacarbonyl (25 mL, 0.2 mol) was slowly added to give a yellow solution. The solution was refluxed at a temperature between 75-80 °C until the distillate was no longer yellow in colour (approximately 2 hours). The methanol was distilled off at 80 °C to give rise to a yellow salt, $[Fe(CO)_3(NO)]^-$. To the salt, water (400 mL) and $N(Bu)_4^+Br^-$ (60 g, 0.19 mol) were added. After stirring for an hour and a half, the solution was filtered and yielded **25** as a yellow precipitate; IR (KBr) ν/cm^{-1} 1978 (CO), 1837 (CO), 1666 (NO) consistent with the reported literature values.[81]

Reaction of $Fe(NO)_2(CO)_2$ and HCl, 26.

To a round bottom flask containing HCl (0.28 mL, 2.27 mmol) in CH_2Cl_2 (10 mL)

was added $Fe(NO)_2(CO)_2$, **1**, (0.25 mL, 2.26 mmol) at room temperature. After stirring the reaction for 18 h, the solution was green and liquid IR in CH_2Cl_2 revealed decomposition.

Reaction of $Fe(NO)_2(CO)_2$ and $SiMe_3Cl$, 27.

To a round bottom flask containing $SiMe_3Cl$ (0.14 mL, 1.135 mmol) in CH_2Cl_2 (10 mL) was added $Fe(NO)_2(CO)_2$, **1**, (0.13 mL, 1.14 mmol) at room temperature. After stirring the reaction for 18 h, the solvent was removed under pressure and yielded a yellow powder; IR(KBr) ν/cm^{-1} 1714 (NO) and 1662 (NO).

Reaction of $Fe(NO)_2(CO)_2$ and $SiMe_3Cl$, 28.

To a round bottom flask containing $SiMe_3Cl$ (0.15 mL, 1.18 mmol) in CH_2Cl_2 (4 mL) was added $Fe(NO)_2(CO)_2$, **1**, (0.12 mL, 1.01 mmol) and was cooled to -78 °C in a dry ice/isopropanol bath. After stirring the reaction for 18 h, the solution was filtered with CH_2Cl_2 and yielded a brown precipitate and IR spectrum was obtained as a KBr pellet showed decomposition.

Reaction of $Fe(NO)_2(CO)_2$ and $Et_3O^+SbCl_6^-$, 29.

To a round bottom flask containing $Et_3O^+SbCl_6^-$ (119 mg, 0.27 mmol) in CH_2Cl_2 (13 mL) was added $Fe(NO)_2(CO)_2$, **1**, (0.03 mL, 0.27 mmol) and was cooled to -78 °C in a dry ice/isopropanol bath. After stirring the reaction for 18 h, the solvent was removed under pressure and yielded a yellow powder; IR (KBr) ν/cm^{-1} 1666 (NO) and 1611 (NO).

Reaction of $Fe(NO)_2(CO)(PPh_3)$ and HCl, 30.

To a round bottom flask containing $Fe(NO)_2(CO)(PPh_3)$, **21**, (96.6 mg, 0.24

mmol) and CH_2Cl_2 (5 mL), HCl (0.03 mL, 0.25 mmol) was added dropwise at room temperature. After stirring the reaction for 18 h, the solvent was removed under pressure and yielded an orangish-brown powder, whose IR spectrum revealed that it was starting material, **21**.

Reaction of $Fe(NO)_2(CO)(PPh_3)$ and HCl, 31.

To a round bottom flask containing $Fe(NO)_2(CO)(PPh_3)$, **21**, (96.6 mg, 0.24 mmol) and diethyl ether (14 mL), HCl (0.03 mL, 0.25 mmol) was added dropwise and was cooled to -78 °C in a dry ice/isopropanol bath. After stirring the reaction for 10 h, the solvent was removed under pressure and yielded an orangish-brown powder, whose ^{31}P NMR spectrum revealed a singlet at 59.0 ppm, assigned as starting material, **21**.

Reaction of $Fe(NO)_2(CO)(PPh_3)$ and $Et_3O^+SbCl_6^-$, 32.

To a round bottom flask containing $Et_3O^+SbCl_6^-$ (306 mg, 0.70 mmol) in CH_2Cl_2 (8 mL) was added $Fe(NO)_2(CO)(PPh_3)$, **21**, (292 mg, 0.72 mmol) and was cooled to -78 °C in a dry ice/isopropanol bath. After 1 h, a dark green precipitate was observed. After stirring the reaction for 18 h, the solvent was removed under pressure and yielded a dark green powder; IR (KBr) ν/cm^{-1} 1816 (NO), 1723 (NO), 1120 (P-C); ^{31}P NMR (C_6D_6, 121.50 MHz) δ 42.0 (s).

Reaction of $Fe(NO)_2(PPh_3)_2$ and $Et_3O^+SbCl_6^-$, 33.

To a round bottom flask containing $Et_3O^+SbCl_6^-$ (354 mg, 0.81 mmol) in CH_2Cl_2 (12 mL) was added $Fe(NO)_2(PPh_3)_2$, **22**, (499 mg, 0.78 mmol) and was cooled to -78 °C in a dry ice/isopropanol bath. After 1 h, a dark black-green precipitate was observed.

After stirring the reaction for 18 h, the solvent was removed under pressure and yielded a dark green powder; IR (KBr) ν/cm^{-1} 1785 (NO), 1724 (NO), 1123 (P-C); ^{31}P NMR (CD_2Cl_2, 121.50 MHz) δ 38.7 (s) and 23.4 (s).

Low temperature ^{31}P NMR studies of the reaction of $Fe(NO)_2(CO)(PPh_3)$, 21 and TFSA, 34.

Reaction of $Fe(NO)_2(CO)(PPh_3)$ with TFSA in CD_2Cl_2 denoted as **34**, revealed a singlet a 55.9 ppm at -70 °C, upon warming the temperature to -24 °C revealed a singlet at 55.9 and a peak at 43.3 ppm. At -17 °C, the peak at 56.3 ppm is still present and the peak at 43.2 is more intense, but a broad peak is seen at 6.0 ppm. At -3 °C, only the peak at 55.9 and ~6.0 ppm are evident. Warming to room temperature had no further effect on the reaction, the same peaks were seen as at -3 °C. Crystals obtained from the solution of reaction **34**, possessed a unit cell consistent with that of $Fe(NO)_2(PPh_3)_2$ suggesting that a disproportionation reaction had occurred

Low temperature ^{31}P NMR studies of the reaction of $Fe(NO)_2(PPh_3)_2$, 22 and TFSA, 35.

The addition of TFSA to $Fe(NO)_2(PPh_3)_2$ in CD_2Cl_2 denoted as reaction **35**, revealed a singlet a 60.8 ppm characteristic of $Fe(NO)_2(PPh_3)_2$ and a very small peak at 58.6 ppm. No change occurred until T = -42 °C, where another peak appeared at ~5.6 ppm which was broad. Upon warming the solution to T = -2 °C caused the peaks at 58.6 and 5.6 to become more intense. However, at room temperature, only a broad peak at ~4.0 ppm was evident. The solution was left in the freezer, which produced crystals,

however upon mounting the crystals they decomposed.

Reaction of $[N(Bu)_4^+][Fe(CO)_3(NO)^-]$ and PPh_3 and CH_3I, 36.

To a round bottom containing **25** (3.03 g, 7.31 mmol) in methanol (60 mL) was added PPh_3 (1.92g, 7.30 mmol) in toluene (10 mL) followed by the addition of CH_3I (1.2 mL, 19.3 mmol) via syringe. After stirring the solution for 18 h, the brown precipitate, **36a**, generated was filtered and washed with hexanes. A second product was obtained when it precipitated out from the mother liquor after a few days, **36b**. The infrared spectrum of **36a** showed stretches at 1927, 1890, 1712 and 1665 cm^{-1} attributable to two carbonyls, a nitrosyl and an acyl-CO group. Similar infrared stretches were observed for the reaction involving the sodium salt.[72] Conversely, **36b** was a mixture of products, $Fe(NO)_2(CO)(PPh_3)$ and $Fe(NO)_2(PPh_3)_2$, as indicated by the infrared spectrum.

6. REFERENCES

1. Clarke, M. J; Gaul, J. B. *Structure and Bonding* **1983**, *81*, 149.

2. Feldman, P. L; Griffith, O. W.; Stuehr, D. J. *Chem. Eng. News.* **1993**, *Dec. 20*, 26.

3. Koshlan, D. E. Jr. *Science* **1992**, *268*, 1861.

4. Butler, A. *Science* **1992**, 1.

5. Konstadt, S. J. *Cardiothoracic & Vascular Anaesthesia* **1995**, *9*, 625.

6. Richter-Addo, G. B.; Legzdins, P. *Metal Nitrosyls*, Oxford University Press, New York, **1992**.

7. Mond, R. L.; Wallis, A. E. *J. Chem. Soc.* **1922**, *121*, 32.

8. Anderson, J. S.; Hieber, W. *Z. Anorg. Allgem. Chem.* **1932**, *208*, 238.

9. Hieber, W.; Beutner, H. *Z. Anorg. Allgem. Chem.* **1963**, *320*, 101.

10. Hieber, W.; Anderson, J. S. *Z. Anorg. Allgem. Chem.* **1933**, *211*, 132.

11. Bramley, R.; Figgis, B. N.; Nyholm, R. S. *Trans. Faraday Soc.* **1962**, *58*, 1893.

12. Brockway, L. O.; Anderson, J. S. *Trans. Faraday Soc.* **1937**, *33*, 1233.

13. Malatesta, L.; Aràneo, A. *J. Am. Chem. Soc.* **1957**, 3803.

14. Albano, V. G.; Aràneo, A.; Bellon, P. L.; Ciani, G.; Manassero, M. *J. Organomet. Chem.* **1964**, *67*, 413.

15. Basolo, F. *Polyhedron* **1990**, *9*, 1503.

16. (a) Thorsteinson, E. M.; Basolo, F. *J. Am. Chem. Soc.* **1966**, *88*, 3929.
    (b) Thorsteinson, E. M.; Basolo, F. *Inorg. Chem.* **1966**, *5*, 1691.

17. Tolman, C. A. *Chem. Soc. Rev.* **1972**, *1*, 337.

18. Hodgson, D. J.; Ibers, J. *Inorg. Chem.* **1969**, *8*, 1282.

19. Connelly, N. G. *Inorg. Chim. Acta.* **1972**, 47.

20. Morris, D. E.; Basolo, F. *J. Am. Chem. Soc.* **1968**, *90*, 2531.

21. Morris, D. E.; Basolo, F. *J. Am. Chem. Soc.* **1968**, *90*, 2536.

22. Li, L.; Enright, G. D.; Preston, K. F. *Organometallics* **1994**, *13*, 4686.

23. Gadd, G. E.; Poliakoff, M.; Turner, J. *Inorg. Chem.* **1986**, *25*, 3604.

24. Gadd, G. E.; Poliakoff, M.; Turner, J. *Organometallics* **1987**, *6*, 391.

25. Cardaci, G.; Foffani, A. *J. Chem. Soc., Dalton Trans.* **1974**, 1808.

26. Cardaci, G. *J. Chem. Soc., Dalton Trans.* **1984**, 815.

27. (a) Connelly, N. G.; Gilbert, M.; Orpen, A. G.; Sheridan, J. B. *J. Chem. Soc., Dalton Trans.* **1990**, 1291. (b) Connelly, N. G.; Gilbert, M. *J. Chem. Soc., Dalton Trans.* **1990**, 373.

28. Tkatchenko, I. *J. Organomet. Chem.* **1977**, *124*, C39.

29. Candlin, J. P.; Hanes, W. H. *J. Chem. Soc. C.* **1968**, 1856.

30. Ballivet-Tkatchenko, D.; Riveccie, M.; El Murr, N. *Inorg. Chim. Acta.* **1978**, *30*, L289.

31. tom Dieck, H.; Bruder, H.; Kuhl, E.; Junghans, D.; Hellfeldt, K. *New J. Chem.* **1989**, *13*, 259.

32. Haymore, B.; Huffman, J. C.; Dobson, A.; Robinson, S. D. *Inorg. Chim. Acta.* **1982**, *65*, L231.

33. La Monica, G.; Freni, M.; Cenini, S. *J. Organomet. Chem.* **1974**, *71*, 57.

34. Wilson, R. D.; Ibers, J. A. *Inorg. Chem.* **1979**, *18*, 336.

35. Dalby, F. W. *Can. J. Phys.* **1958**, *36*, 1336.

36. Sellmann, D.; Seubert, B.; Moll, M.; Knoch, F. *Angew. Chem., Int. Ed. Engl.* **1988**, *27*, 1164.

37. Grundy, K. R.; Reed, C. A.; Roper, W. R. *Chem. Commun.* **1970**, 1501.

38. Stevens, R. E.; Gladfelter, W. L. *Inorg. Chem.* **1983**, *22*, 2034.

39. Cygler, M.; Ahmed, F. R.; Forgues, A.; Roustan, J. L. A. *Inorg. Chem.* **1983**, 22, 1026.

40. Pierpont, C. G.; Eisenberg, R. *Inorg. Chem.* **1972**, 11, 1094.

41. (a) Mingos, D. M. P.; Ibers, J. A. *Inorg. Chem.* **1971**, *10*, 1479. (b) Clark, G. R.; Waters, J. M.; Whittle, K. R. *Inorg. Chem.* **1974**, *13*, 1628.

42. Casey, M.; Manning, A. R. *J. Chem. Soc. (A).* **1971**, 256.

43. King, R. B. *Inorg. Chem.* **1963**, *2*, 1275.

44. Li Kam Wah, H.; Postel, M.; Pierrot, M. *Inorg. Chim. Acta* **1989**, *165*, 215.

45. Munyejabo, V.; Guillaume, P.; Postel, M. *Inorg. Chim. Acta* **1994**, *221*, 133.

46. (a) Ballivet-Tkatchenko, D.; Riveccie, M.; El-Murr, N. *J. Am. Chem. Soc.* **1979**, *101*, 2763. (b) Ballivet-Tkatchenko, D.; Billard, C.; Revillon, A. *J. Polym. Sci.* **1981**, *19*, 1697. (c) Ballivet, D.; *J. Organomet. Chem.* **1977**, *124*, C9.

47. (a) Manners, I. *Angew. Chem., Int. Ed. Engl.* **1996**, *35*, 1602. (b) Manners, I. *Adv. Mater.* 1994, 6, 68. (c) Puddephatt, R. J. *J. Chem. Soc., Chem. Commun.* **1998**, 1055. (d) Casado, C. M.; Cuadrado, I. Morán, M.; Alonso, B.; Lobete, F.; Losada, J. *Organometallics* **1995**, *14*, 2618. (e) Altmann, M.; Enkelmann, V.; Beer, F.; Bunz, U. H. W. *Organometallics* **1996**, *15*, 394. (f) Cerveau, G. Corriu, R. J. P.; Lepeytre, C. *J. Mater. Chem.* **1995**, *5*, 793. (g) Imori, T.; Tilley, T. D. *Polyhedron* **1994**, *13*, 2231. (h) Lucht, B. L.; Mao, S. S. H.; Tilley, T. D. *J. Am. Chem. Soc.* **1998**, *120*, 4354. (i) Weng, W.; Bartik, T.; Gladysz, J. A. *Angew. Chem., Int. Ed. Engl.* **1994**, *33*, 2199. (j) Brady, M.; Weng, W.; Zhou, Y. Seyler, J. W.; Amoroso, A. J.; Arif, A. M.; Bohme, M.; Frenking, G.; Gladysz, J. A. *J. Am. Chem. Soc.* **1997**, *119*, 775. (k) Kuhnen, T.; Ruffolo, R.; Stradiotto, M.; Ulbrich, D.; McGlinchey, M. J.; Brook, M. A. *Organometallics* **1997**, *16*, 5042. (l) Kuhnen, T.; Stradiotto, M.; Ruffolo, R.; Ulbrich, D.; McGlinchey, M. J.; Brook, M. A. *Organometallics* **1997**, *16*, 5048.

48. (a) Puddephatt, R. J. *Chem. Soc. Rev.* **1983**, *12*, 99. (b) Chaudret, B.; Poiblanc, R. *Coord. Chem. Rev.* **1988**, *86*, 191. (c) Semmelmann, M.; Fenske, D.; Corrigan, J. F. *J. Chem. Soc., Dalton Trans.* **1998**, 2541. (d) Johnson, B. F. G.; Lewis, J.; Massey, A. N.; Raithby, P. R.; Wong, W. T. *J. Organomet. Chem.* **1990**, *397*, C28. (e) Orama, O. *J. Organomet. Chem.* **1986**, *314*, 273. (f) Layer, T. M.; Lewis, J.; Martin, A.; Raithby, P. R.; Wong, W.T. *J. Chem. Soc., Dalton Trans.* **1992**, 3411. (g) Adams, C. J.; Bruce, M. I.; Skelton B. W.; White,A. H. *J. Organomet. Chem.* **1993**, *447*, 91. (h) Lee, J.; Humphrey, M. G.; Hockless, D. C. R.; Skelton, B. W.; White, A. H. *Organometallics* **1993**, *12*, 3468. (j) Louattani, E.; Suades, J.; Urtiaga, K.; Arriortua, M. I.; Solans, X. *Organometallics*, **1996**, *15*, 468.

49. (a) Carty, A. J.; Efraty, A. *Can. J. Chem.* **1968**, *46*, 1598. (b) Carty, A. J.; Efraty, A. *Can. J. Chem.* **1969**, *47*, 2573. (c) Carty, A. J.; Efraty, A. *Inorg. Chem.* **1969**, *8*, 543. (d) Eaton, G. R.; Holm, R. H. *Inorg. Chem.* **1971**, *10*, 805. (e) Carty, A. J.; Efraty, A.; Ng, T. W. *Can. J. Chem.* **1969**, *47*, 1429. (f) Carty, A. J.; Ng, T. W.; Carter, W.; Palenik, G. J.; Birchall, T. *Chem. Commun.* **1969**, 1101. (g) Carty, A. J.; Ng, T. W. *Chem Commun.* **1970**, 169. (h) Hogarth, G.; Norman, T. *J. Chem. Soc., Dalton Trans.* **1996**, 1077. (i) Hogarth, G.; Pang, J. Y. *J. Organomet. Chem.* **1996**, *515*, 193. (j) Wright, M. E.; Lawson, L.; Baker, R. T.; Roe, D. C. *Polyhedron* **1992**, *11*, 323.

50. (a) Jia, G.; Puddephatt, R. J.; Scott, J.D.; Vittal, J. J. *Organometallics* **1993**, *12*, 3565. (b) Anderson, W. A.; Carty, A. J.; Efraty, A. *Can. J. Chem.* **1969**, *47*, 3361.

51. Braunstein, P.; Richert, J. *J. Chem. Soc., Dalton Trans.* **1990**, 3801.

52. Atkinson, F. L.; Blackwell, H. E.; Brown, N. C.; Connelly, N. G.; Crossley, J. G.; Orpen, A. G.; Rieger, A. L.; Rieger, P. H. *J. Chem. Soc., Dalton Trans.* **1996**, 3491.

53. Therien, M. J.; Ni, C. L.; Anson, F. C.; Osteryoung, J. G.; Trogler, W. C. *J. Am. Chem. Soc.* **1986**, *108*, 4037.

54. Griffith, W. P. *Adv. Organomet. Chem.* **1968**, *7*, 211.

55. Chong, K. S.; Rettig, S. J.; Storr, A.; Trotter, J. *Can. J. Chem.* **1979**, *57*, 3119.

56. Trumpy, V. A.; Oriskovich, T. A.; Schreiner, S. *Inorg. Chim. Acta* **1993**, *205*, 3119.

57. Harrison, W.; Trotter, J. *J. Chem. Soc. (A).* **1971**, 1542 and references cited therein.

58. Rosenblum, M.; Fish, R. W.; Bennet, C. *J. Am. Chem. Soc.* **1964**, *86*, 5166.

59. (a) Rettig, M. F.; Wing, R. W. *Inorg. Chem.* **1969**, *8*, 2685. (b) Olbrich-Deubner, B.; Grob, R.; Kaim, W. *J. Organoet. Chem.* **1989**, *366*, 155.

60. Hörsken, A.; Zheng, G.; Stradiotto, M.; McCrory, C. T. C.; Li, L. *J. of Organomet. Chem.* **1998**, *558*, 1.

61. Bradley, W. H. *Inorg. Chim. Acta* **1968**, *2*, 7.

62. Herberhold, M. *Angew. Chem. Int. Ed. Engl.* **1968**, *7*, 305.

63. Amoroso, D; Li, L. *Unpublished results.*

64. Munyeejabo, V.; Damiano, J-P.; Postel, M.; Bensimon, C.; Roustan, J. L. *J. of Organomet. Chem.* **1995**, *491*, 61.

65. Axelson, D. E.; Holloway, C. E. *J. Chem. Soc., Chem. Commun.* **1973**, 455.

66. Green, M.; Osborn, R. B. L.; Rest, A. J.; Stone, F. G. A. *Chem. Commun.* **1966**, 502.

67. Cramer, R.; Kling, J. B.; Roberts, J. D. *J. Am. Chem. Soc.* **1969**, *91*, 2519.

68. Thomas, J. T.; Robertson, J. H.; Cox, E. G. *Acta Cryst.* **1958**, *11*, 599.

69. Clark, H. C.; Ferguson, G.; Kapoor, P. N.; Parvez, M. *Inorg. Chem.* **1985**, *24*, 3924.

70. Hogarth, G.; Norman, T. *Polyhedron* **1996**, *15*, 2859.

71. McCrory, C. T .C.; Reginato, N.; Li, L. *Submitted for publication in JACS.*

72. Chaudhari, F. M.; Knox, G. R.; Pauson, P. L. *J. Chem. Soc. (C).* **1967**, 2255.

73. Mantell, D. R.; Gladfelter, W. L. *J. of Organomet. Chem.* **1988**, *347*, 333.

74. Reference 52(a) and references therein.

75. Pannell, K. H.; Chen, Y.; Belknap, K.; Wu, C. C.; Bernal, I.; Creswick, M. W.; Huang, H. N. *Inorg. Chem.* **1983**, *22*, 418.

76. (a) Sheldrick, G. M. SMART (1996), Release 4.05; Siemens Energy And Automation Inc., Madison, WI 53719. (b) Sheldrick, G. M. SAINT (1996), Release

4.05; Siemens Energy And Automation Inc., Madison, WI 53719. (c) Sheldrick, G. M. SADABS (Siemens Area Detector Absorption Corrections) (1996). (d) Sheldrick, G. M. Siemens SHELXTL (1994), Version 5.03; Siemens Crystallographic Research Systems, Madison, WI 53719.

77. (a) Hoffmann, R. *J. Chem. Phys.* **1963**, *39*, 1397. (b) Hoffmann, R.; Lipscomb, W.N. *Chem. Phys.* **1962**, *36*, 2179. (c) Hoffmann, R.; Lipscomb, W. N. *J. Chem. Phys.* **1962**, *36*, 3489. (d) Ammeter, J. H. Bürgi, H. B.; Thibeault, J. C., Hoffmann, R. *J. Am. Chem. Soc.* **1978**, *100*, 3686.

78. Mealli, C.; Proserpio, D. M. *J. Chem. Ed.* **1990**, *67*, 3399.

79. McBride, D. W.; Stafford, S. L.; Stone, F. G. A. *Inorg. Chem.* **1962**, *1*, 386.

80. Stevens, R. E.; Yanta, T. J.; Gladfelter, W. L. *Inorg. Syn.* **1983**, *22*, 163.

81. Steel, F. Z. *Anorg. Allgem. Chem.* **1952**, *269*, 40.

7. APPENDIX

Table A1. Atomic coordinates (x 10^4) and equivalent isotropic displacement parameters (A^2 x 10^3) for **10**. U(eq) is defined as one third of the trace of the orthogonalized Uij tensor.

	x	y	z	U(eq)
Fe(1)	5824(1)	5189(1)	2180(1)	45(1)
Fe(2)	7117(1)	339(1)	2824(1)	51(1)
P(1)	7768(2)	4098(2)	2838(1)	37(1)
P(2)	8652(2)	1766(2)	1957(1)	35(1)
O(1)	4827(7)	7112(7)	3177(4)	83(2)
O(2)	3198(7)	3791(6)	2183(4)	83(2)
O(3)	7598(8)	6460(6)	715(4)	76(2)
O(4)	3743(8)	1244(6)	3339(4)	76(2)
O(5)	8975(9)	-647(7)	4043(4)	98(3)
O(6)	7522(7)	-1398(6)	1728(4)	75(2)
N(1)	6901(9)	5932(7)	1319(5)	56(2)
N(2)	4316(8)	4328(6)	2206(4)	53(2)
N(3)	5151(9)	920(7)	3105(4)	56(2)
N(4)	8255(10)	-230(7)	3538(5)	68(2)
C(1)	9358(8)	3050(7)	2313(4)	40(2)
C(2)	5201(9)	6337(9)	2804(6)	51(2)
C(3)	7351(8)	-712(7)	2172(5)	39(2)
C(11)	7055(11)	3150(7)	3794(5)	49(2)
C(12)	5360(12)	3186(10)	4108(6)	74(3)
C(13)	4790(16)	2460(14)	4856(7)	109(5)
C(14)	5942(23)	1715(13)	5259(7)	115(5)
C(15)	7576(20)	1694(11)	4943(8)	101(4)
C(16)	8137(14)	2406(9)	4217(6)	70(3)
C(21)	9054(9)	5186(7)	3050(5)	42(2)
C(22)	9046(11)	5332(8)	3799(6)	68(3)
C(23)	9953(14)	6241(11)	3926(7)	98(4)
C(24)	10889(12)	6936(10)	3293(8)	84(4)
C(25)	10865(10)	6829(8)	2539(7)	70(3)
C(26)	9942(9)	5940(8)	2414(5)	57(3)
C(31)	7799(9)	2535(7)	1104(5)	38(2)
C(32)	6221(8)	2303(7)	1045(5)	39(2)
C(33)	5556(11)	2883(9)	389(6)	63(3)
C(34)	6434(13)	3688(9)	-202(6)	67(3)
C(35)	7990(12)	3933(8)	-156(5)	64(3)
C(36)	8651(10)	3339(8)	502(5)	51(2)
C(41)	10624(8)	953(7)	1543(5)	37(2)
C(42)	11765(9)	484(7)	2022(5)	45(2)
C(43)	13192(10)	-254(8)	1772(6)	56(3)
C(44)	13517(10)	-529(8)	1012(7)	65(3)
C(45)	12400(11)	-75(9)	536(6)	70(3)
C(46)	10984(10)	648(8)	791(5)	54(2)

Table A2. Complete listing of bond lengths [Å] for **10**.

Fe(1)-N(2)	1.654(6)
Fe(1)-N(1)	1.693(8)
Fe(1)-C(2)	1.782(9)
Fe(1)-P(1)	2.262(2)
Fe(2)-N(3)	1.675(8)
Fe(2)-N(4)	1.705(8)
Fe(2)-C(3)	1.745(8)
Fe(2)-P(2)	2.262(2)
P(1)-C(11)	1.813(9)
P(1)-C(21)	1.841(7)
P(1)-C(1)	1.840(7)
P(2)-C(31)	1.807(8)
P(2)-C(41)	1.829(8)
P(2)-C(1)	1.855(6)
O(1)-C(2)	1.144(8)
O(2)-N(2)	1.175(6)
O(3)-N(1)	1.171(8)
O(4)-N(3)	1.182(8)
O(5)-N(4)	1.163(8)
O(6)-C(3)	1.162(8)
C(11)-C(16)	1.370(11)
C(11)-C(12)	1.393(11)
C(12)-C(13)	1.414(14)
C(13)-C(14)	1.39(2)
C(14)-C(15)	1.35(2)
C(15)-C(16)	1.377(14)
C(21)-C(22)	1.358(10)
C(21)-C(26)	1.382(11)
C(22)-C(23)	1.404(12)
C(23)-C(24)	1.365(14)
C(24)-C(25)	1.362(13)
C(25)-C(26)	1.393(10)
C(31)-C(36)	1.365(10)
C(31)-C(32)	1.397(9)
C(32)-C(33)	1.391(10)
C(33)-C(34)	1.364(11)
C(34)-C(35)	1.377(11)
C(35)-C(36)	1.395(11)
C(41)-C(46)	1.388(10)
C(41)-C(42)	1.385(9)
C(42)-C(43)	1.380(10)
C(43)-C(44)	1.390(11)
C(44)-C(45)	1.364(11)
C(45)-C(46)	1.367(11)

Table A3. Complete listing of bond angles [deg] for **10**.

N(2)-Fe(1)-N(1)	122.1(3)
N(2)-Fe(1)-C(2)	112.6(3)
N(1)-Fe(1)-C(2)	106.0(4)
N(2)-Fe(1)-P(1)	111.7(2)
N(1)-Fe(1)-P(1)	105.2(2)
C(2)-Fe(1)-P(1)	95.9(3)
N(3)-Fe(2)-N(4)	118.1(3)

N(3)-Fe(2)-C(3)	113.7(3)
N(4)-Fe(2)-C(3)	110.5(3)
N(3)-Fe(2)-P(2)	112.2(2)
N(4)-Fe(2)-P(2)	104.6(3)
C(3)-Fe(2)-P(2)	95.0(3)
C(11)-P(1)-C(21)	104.1(4)
C(11)-P(1)-C(1)	104.4(4)
C(21)-P(1)-C(1)	101.3(3)
C(11)-P(1)-Fe(1)	117.6(3)
C(21)-P(1)-Fe(1)	109.9(3)
C(1)-P(1)-Fe(1)	117.6(2)
C(31)-P(2)-C(41)	104.3(4)
C(31)-P(2)-C(1)	104.7(3)
C(41)-P(2)-C(1)	101.7(3)
C(31)-P(2)-Fe(2)	115.9(3)
C(41)-P(2)-Fe(2)	108.3(3)
C(1)-P(2)-Fe(2)	119.9(3)
O(3)-N(1)-Fe(1)	177.8(7)
O(2)-N(2)-Fe(1)	174.8(7)
O(4)-N(3)-Fe(2)	175.0(7)
O(5)-N(4)-Fe(2)	177.1(8)
P(1)-C(1)-P(2)	117.8(3)
O(1)-C(2)-Fe(1)	177.0(9)
O(6)-C(3)-Fe(2)	178.9(7)
C(16)-C(11)-C(12)	119.2(9)
C(16)-C(11)-P(1)	121.8(8)
C(12)-C(11)-P(1)	119.0(7)
C(11)-C(12)-C(13)	119.5(11)
C(14)-C(13)-C(12)	119.0(12)
C(15)-C(14)-C(13)	120.5(14)
C(14)-C(15)-C(16)	120.7(14)
C(15)-C(16)-C(11)	121.1(11)
C(22)-C(21)-C(26)	119.9(7)
C(22)-C(21)-P(1)	122.2(7)
C(26)-C(21)-P(1)	117.7(6)
C(21)-C(22)-C(23)	120.0(9)
C(24)-C(23)-C(22)	119.3(10)
C(25)-C(24)-C(23)	121.2(9)
C(24)-C(25)-C(26)	119.2(10)
C(21)-C(26)-C(25)	120.2(8)
C(36)-C(31)-C(32)	118.1(7)
C(36)-C(31)-P(2)	122.2(5)
C(32)-C(31)-P(2)	119.7(6)
C(33)-C(32)-C(31)	120.2(8)
C(34)-C(33)-C(32)	120.4(8)
C(33)-C(34)-C(35)	120.4(8)
C(36)-C(35)-C(34)	118.8(9)
C(31)-C(36)-C(35)	122.1(7)
C(46)-C(41)-C(42)	116.8(7)
C(46)-C(41)-P(2)	123.6(6)
C(42)-C(41)-P(2)	119.3(6)
C(43)-C(42)-C(41)	122.1(8)
C(44)-C(43)-C(42)	119.4(8)
C(43)-C(44)-C(45)	119.0(8)
C(46)-C(45)-C(44)	121.2(9)
C(45)-C(46)-C(41)	121.6(8)

Table A4. Anisotropic displacement parameters ($Å^2$ x 10^3) for **10**. The anisotropic displacement factor exponent takes the form: $-2\pi^2$ [$h^2 a^{*2}$ U11 + ... + 2 h k a* b* U12]

	U11	U22	U33	U23	U13	U12
Fe(1)	39(1)	45(1)	53(1)	-7(1)	-17(1)	-4(1)
Fe(2)	49(1)	44(1)	57(1)	-1(1)	-8(1)	-11(1)
P(1)	39(1)	39(1)	34(1)	-8(1)	-10(1)	-6(1)
P(2)	35(1)	37(1)	37(1)	-10(1)	-9(1)	-6(1)
O(1)	80(5)	78(6)	99(6)	-48(5)	-17(4)	9(4)
O(2)	54(4)	74(5)	132(6)	-22(4)	-29(4)	-23(4)
O(3)	88(5)	84(6)	54(5)	-5(4)	-4(4)	-25(4)
O(4)	49(4)	99(6)	79(5)	-30(4)	2(4)	-6(4)
O(5)	136(6)	86(6)	86(6)	-20(5)	-65(5)	23(5)
O(6)	76(4)	61(5)	99(6)	-29(4)	-27(4)	-1(4)
N(1)	58(5)	58(6)	56(6)	-15(5)	-13(4)	-9(4)
N(2)	39(4)	58(5)	65(5)	-17(4)	-14(4)	0(4)
N(3)	60(5)	60(6)	47(5)	-4(4)	-6(4)	-20(4)
N(4)	86(6)	61(6)	56(6)	-9(5)	-17(5)	-3(4)
C(1)	37(4)	41(5)	48(5)	-13(4)	-11(4)	-9(4)
C(2)	38(5)	49(7)	67(7)	-18(5)	-9(5)	2(4)
C(3)	35(5)	34(6)	50(6)	-8(5)	-1(4)	-4(4)
C(11)	81(7)	32(6)	41(6)	-11(5)	-18(6)	-9(5)
C(12)	71(7)	98(9)	46(7)	-24(6)	27(6)	-27(6)
C(13)	121(11)	148(14)	55(9)	-39(9)	38(8)	-60(10)
C(14)	219(18)	86(11)	37(8)	0(7)	-14(11)	-45(12)
C(15)	182(14)	69(9)	58(10)	-1(8)	-34(9)	-17(10)
C(16)	115(8)	45(7)	47(7)	2(5)	-27(7)	0(6)
C(21)	31(5)	44(6)	55(6)	-20(5)	-13(4)	1(4)
C(22)	107(8)	52(7)	56(7)	-14(5)	-26(6)	-24(6)
C(23)	119(10)	111(11)	93(10)	-52(8)	-45(8)	-27(8)
C(24)	56(7)	73(9)	148(12)	-63(9)	-34(8)	-7(6)
C(25)	53(6)	45(7)	119(10)	-20(6)	-17(6)	-18(5)
C(26)	46(5)	60(7)	64(7)	-20(5)	3(5)	-18(5)
C(31)	40(5)	27(5)	47(6)	-15(4)	-3(4)	-3(4)
C(32)	34(5)	34(5)	48(6)	-13(4)	-4(4)	-3(4)
C(33)	67(6)	76(8)	57(7)	-18(6)	-32(6)	-4(6)
C(34)	103(8)	53(7)	52(7)	0(5)	-44(7)	5(6)
C(35)	86(7)	66(7)	40(6)	-3(5)	-8(6)	-16(6)
C(36)	55(6)	57(6)	45(6)	-16(5)	-12(5)	-9(5)
C(41)	36(5)	35(5)	39(5)	-3(4)	-12(4)	-5(4)
C(42)	43(5)	43(6)	54(6)	-14(5)	-14(5)	-6(4)
C(43)	36(5)	62(7)	74(7)	-13(6)	-15(5)	-5(5)
C(44)	40(5)	50(7)	108(9)	-37(6)	-8(6)	1(5)
C(45)	50(6)	92(8)	74(8)	-39(7)	-9(6)	8(6)
C(46)	48(6)	69(7)	48(6)	-23(5)	-8(5)	4(5)

Table A5. Hydrogen atom coordinates for **10**.

	x	y	z	U(eq)
H(1A)	10123(8)	2670(7)	2666(4)	48
H(1B)	9994(8)	3567(7)	1855(4)	48
H(12A)	4601(12)	3690(10)	3824(6)	89
H(13A)	3651(16)	2479(14)	5078(7)	131
H(14A)	5577(23)	1223(13)	5755(7)	138
H(15A)	8341(20)	1187(11)	5222(8)	121
H(16A)	9282(14)	2382(9)	4008(6)	83
H(22A)	8433(11)	4826(8)	4232(6)	82
H(23A)	9917(14)	6369(11)	4442(7)	117
H(24A)	11563(12)	7499(10)	3380(8)	101
H(25A)	11462(10)	7348(8)	2107(7)	84
H(26A)	9924(9)	5853(8)	1896(5)	68
H(32A)	5607(8)	1753(7)	1451(5)	47
H(33A)	4496(11)	2720(9)	352(6)	76
H(34A)	5974(13)	4077(9)	-643(6)	81
H(35A)	8595(12)	4491(8)	-561(5)	77
H(36A)	9718(10)	3499(8)	532(5)	61
H(42A)	11561(9)	675(7)	2534(5)	54
H(43A)	13938(10)	-569(8)	2112(6)	68
H(44A)	14492(10)	-1020(8)	830(7)	78
H(45A)	12608(11)	-263(9)	23(6)	84
H(46A)	10236(10)	946(8)	450(5)	65

Table A6. Atomic coordinates (x 10^4) and equivalent isotropic displacement parameters (A^2 x 10^3) for **16**. U(eq) is defined as one third of the trace of the orthogonalized Uij tensor.

	x	y	z	U(eq)
Fe(1)	2996(1)	-21(1)	2344(1)	33(1)
Fe(2)	2125(1)	-2482(1)	3191(1)	33(1)
P(1)	2100(1)	677(2)	2530(1)	32(1)
P(2)	3776(1)	-97(2)	3368(1)	30(1)
P(3)	1710(1)	-934(2)	3440(1)	32(1)
P(4)	3259(1)	-2279(2)	3775(1)	32(1)
O(1)	3467(6)	1586(9)	1713(5)	106(4)
O(2)	2781(5)	-1985(7)	1637(4)	71(2)
O(3)	1598(4)	-2891(7)	1841(4)	66(2)
O(4)	1766(5)	-4184(7)	3854(5)	76(3)
N(1)	3269(5)	955(8)	2003(5)	55(2)
N(2)	2848(4)	-1204(7)	1976(4)	42(2)
N(3)	1864(4)	-2629(6)	2388(4)	43(2)
N(4)	1921(4)	-3452(7)	3589(4)	48(2)
C(1)	1978(5)	429(7)	3295(4)	32(2)
C(2)	3661(5)	-928(7)	4006(4)	32(2)
C(11)	1250(5)	469(8)	1900(5)	43(3)
C(12)	697(5)	1071(10)	1911(6)	58(3)
C(13)	70(7)	985(14)	1435(8)	84(4)
C(14)	-26(8)	240(18)	956(8)	104(6)
C(15)	513(8)	-409(14)	934(7)	92(5)

C(16)	1154(6)	-271(9)	1424(5)	59(3)
C(21)	2174(5)	2155(8)	2538(5)	44(3)
C(22)	2428(6)	2763(9)	3106(7)	63(3)
C(23)	2504(7)	3885(11)	3071(11)	104(6)
C(24)	2312(8)	4392(11)	2457(11)	93(5)
C(25)	2045(10)	3772(11)	1883(9)	99(5)
C(26)	1982(10)	2682(10)	1950(7)	93(5)
C(31)	3981(4)	1230(7)	3763(4)	33(2)
C(32)	4212(6)	2033(8)	3467(5)	51(3)
C(33)	4364(6)	3058(9)	3722(6)	62(3)
C(34)	4284(6)	3321(9)	4282(6)	56(3)
C(35)	4051(6)	2542(8)	4596(5)	52(3)
C(36)	3898(5)	1504(8)	4336(5)	41(2)
C(41)	4623(5)	-527(7)	3408(4)	36(2)
C(42)	5209(5)	-265(9)	3941(5)	48(3)
C(43)	5839(5)	-589(9)	3961(5)	51(3)
C(44)	5887(6)	-1176(9)	3463(6)	51(3)
C(45)	5318(6)	-1423(9)	2942(6)	51(3)
C(46)	4687(5)	-1105(8)	2909(5)	41(2)
C(51)	784(5)	-834(9)	3058(5)	45(3)
C(52)	432(6)	-27(10)	3263(6)	61(3)
C(53)	-287(8)	18(14)	2928(9)	92(6)
C(54)	-635(7)	-708(17)	2429(8)	89(5)
C(55)	-291(7)	-1454(13)	2262(7)	82(4)
C(56)	426(5)	-1547(10)	2566(6)	58(3)
C(61)	1861(5)	-877(8)	4303(5)	37(2)
C(62)	2171(5)	-33(9)	4715(5)	45(3)
C(63)	2293(6)	-69(10)	5377(5)	57(3)
C(64)	2106(7)	-969(12)	5627(6)	70(4)
C(65)	1780(9)	-1811(10)	5215(6)	80(4)
C(66)	1671(7)	-1738(9)	4580(6)	64(3)
C(71)	3466(5)	-2882(7)	4580(4)	35(2)
C(72)	3502(6)	-3994(8)	4642(5)	60(3)
C(73)	3614(8)	-4476(10)	5222(7)	81(4)
C(74)	3707(7)	-3868(11)	5777(6)	66(3)
C(75)	3666(6)	-2757(10)	5721(5)	60(3)
C(76)	3552(6)	-2281(8)	5130(5)	48(3)
C(81)	3843(5)	-2999(7)	3486(5)	39(2)
C(82)	4523(5)	-3130(9)	3881(6)	52(3)
C(83)	4963(6)	-3663(10)	3649(6)	60(3)
C(84)	4728(7)	-4088(9)	3032(7)	63(3)
C(85)	4052(7)	-3949(9)	2645(6)	62(3)
C(86)	3601(5)	-3410(8)	2869(5)	44(3)

Table A7. Complete listing of bond lengths [Å] for **16**.

Fe(1)-N(1)	1.643(9)
Fe(1)-N(2)	1.644(8)
Fe(1)-P(2)	2.251(3)
Fe(1)-P(1)	2.268(3)
Fe(2)-N(4)	1.644(9)
Fe(2)-N(3)	1.668(9)
Fe(2)-P(3)	2.261(3)
Fe(2)-P(4)	2.273(3)
P(1)-C(21)	1.831(10)
P(1)-C(11)	1.832(10)
P(1)-C(1)	1.847(9)

P(2)-C(31)	1.832(9)
P(2)-C(2)	1.844(9)
P(2)-C(41)	1.847(9)
P(3)-C(51)	1.825(10)
P(3)-C(61)	1.827(9)
P(3)-C(1)	1.844(9)
P(4)-C(81)	1.831(10)
P(4)-C(71)	1.835(10)
P(4)-C(2)	1.853(9)
O(1)-N(1)	1.188(11)
O(2)-N(2)	1.200(10)
O(3)-N(3)	1.176(10)
O(4)-N(4)	1.192(11)
C(11)-C(16)	1.35(2)
C(11)-C(12)	1.40(2)
C(12)-C(13)	1.35(2)
C(13)-C(14)	1.36(2)
C(14)-C(15)	1.41(2)
C(15)-C(16)	1.39(2)
C(21)-C(26)	1.38(2)
C(21)-C(22)	1.39(2)
C(22)-C(23)	1.40(2)
C(23)-C(24)	1.41(2)
C(24)-C(25)	1.41(2)
C(25)-C(26)	1.37(2)
C(31)-C(32)	1.380(14)
C(31)-C(36)	1.396(13)
C(32)-C(33)	1.37(2)
C(33)-C(34)	1.36(2)
C(34)-C(35)	1.39(2)
C(35)-C(36)	1.393(14)
C(41)-C(46)	1.370(13)
C(41)-C(42)	1.391(14)
C(42)-C(43)	1.382(14)
C(43)-C(44)	1.36(2)
C(44)-C(45)	1.35(2)
C(45)-C(46)	1.371(14)
C(51)-C(56)	1.39(2)
C(51)-C(52)	1.42(2)
C(52)-C(53)	1.42(2)
C(53)-C(54)	1.40(2)
C(54)-C(55)	1.32(2)
C(55)-C(56)	1.42(2)
C(61)-C(66)	1.365(14)
C(61)-C(62)	1.380(14)
C(62)-C(63)	1.40(2)
C(63)-C(64)	1.37(2)
C(64)-C(65)	1.38(2)
C(65)-C(66)	1.35(2)
C(71)-C(72)	1.379(14)
C(71)-C(76)	1.383(14)
C(72)-C(73)	1.36(2)
C(73)-C(74)	1.39(2)
C(74)-C(75)	1.38(2)
C(75)-C(76)	1.38(2)
C(81)-C(86)	1.368(14)
C(81)-C(82)	1.384(14)

C(82)-C(83)	1.40(2)
C(83)-C(84)	1.37(2)
C(84)-C(85)	1.37(2)
C(85)-C(86)	1.41(2)

Table A8. Complete listing of bond angles [deg] for **16**.

N(1)-Fe(1)-N(2)	117.0(4)
N(1)-Fe(1)-P(2)	104.2(3)
N(2)-Fe(1)-P(2)	113.3(3)
N(1)-Fe(1)-P(1)	106.0(3)
N(2)-Fe(1)-P(1)	114.5(3)
P(2)-Fe(1)-P(1)	100.07(9)
N(4)-Fe(2)-N(3)	116.8(4)
N(4)-Fe(2)-P(3)	105.9(3)
N(3)-Fe(2)-P(3)	110.7(3)
N(4)-Fe(2)-P(4)	102.3(3)
N(3)-Fe(2)-P(4)	118.1(3)
P(3)-Fe(2)-P(4)	101.19(10)
C(21)-P(1)-C(11)	101.7(5)
C(21)-P(1)-C(1)	101.4(5)
C(11)-P(1)-C(1)	103.8(4)
C(21)-P(1)-Fe(1)	107.8(3)
C(11)-P(1)-Fe(1)	117.2(4)
C(1)-P(1)-Fe(1)	122.0(3)
C(31)-P(2)-C(2)	101.8(4)
C(31)-P(2)-C(41)	100.6(4)
C(2)-P(2)-C(41)	102.6(4)
C(31)-P(2)-Fe(1)	113.5(3)
C(2)-P(2)-Fe(1)	122.8(3)
C(41)-P(2)-Fe(1)	112.8(3)
C(51)-P(3)-C(61)	102.2(5)
C(51)-P(3)-C(1)	102.0(4)
C(61)-P(3)-C(1)	102.0(4)
C(51)-P(3)-Fe(2)	113.3(4)
C(61)-P(3)-Fe(2)	111.3(3)
C(1)-P(3)-Fe(2)	123.6(3)
C(81)-P(4)-C(71)	101.9(4)
C(81)-P(4)-C(2)	103.5(4)
C(71)-P(4)-C(2)	100.4(4)
C(81)-P(4)-Fe(2)	117.2(3)
C(71)-P(4)-Fe(2)	108.6(3)
C(2)-P(4)-Fe(2)	122.2(3)
O(1)-N(1)-Fe(1)	173.5(10)
O(2)-N(2)-Fe(1)	168.9(8)
O(3)-N(3)-Fe(2)	166.6(8)
O(4)-N(4)-Fe(2)	177.1(9)
P(3)-C(1)-P(1)	118.3(5)
P(2)-C(2)-P(4)	118.0(5)
C(16)-C(11)-C(12)	119.7(10)
C(16)-C(11)-P(1)	120.2(9)
C(12)-C(11)-P(1)	120.0(8)
C(13)-C(12)-C(11)	121.8(13)
C(12)-C(13)-C(14)	118(2)
C(13)-C(14)-C(15)	121.8(14)
C(16)-C(15)-C(14)	118(2)
C(11)-C(16)-C(15)	120.4(14)

C(26)-C(21)-C(22)	118.8(11)
C(26)-C(21)-P(1)	117.8(9)
C(22)-C(21)-P(1)	123.4(9)
C(21)-C(22)-C(23)	119.8(14)
C(22)-C(23)-C(24)	120(2)
C(23)-C(24)-C(25)	120.3(12)
C(26)-C(25)-C(24)	117.2(14)
C(25)-C(26)-C(21)	124.3(14)
C(32)-C(31)-C(36)	117.2(9)
C(32)-C(31)-P(2)	118.4(7)
C(36)-C(31)-P(2)	124.4(7)
C(33)-C(32)-C(31)	122.2(10)
C(34)-C(33)-C(32)	120.5(11)
C(33)-C(34)-C(35)	119.4(10)
C(34)-C(35)-C(36)	120.0(10)
C(35)-C(36)-C(31)	120.8(9)
C(46)-C(41)-C(42)	118.7(9)
C(46)-C(41)-P(2)	120.5(7)
C(42)-C(41)-P(2)	120.8(7)
C(43)-C(42)-C(41)	120.0(10)
C(44)-C(43)-C(42)	120.2(11)
C(45)-C(44)-C(43)	119.9(10)
C(44)-C(45)-C(46)	121.1(10)
C(45)-C(46)-C(41)	120.3(10)
C(56)-C(51)-C(52)	120.2(10)
C(56)-C(51)-P(3)	119.5(8)
C(52)-C(51)-P(3)	120.3(9)
C(53)-C(52)-C(51)	116.8(13)
C(54)-C(53)-C(52)	121.9(14)
C(55)-C(54)-C(53)	119.4(13)
C(54)-C(55)-C(56)	122(2)
C(51)-C(56)-C(55)	119.4(13)
C(66)-C(61)-C(62)	115.8(9)
C(66)-C(61)-P(3)	119.0(8)
C(62)-C(61)-P(3)	125.2(8)
C(61)-C(62)-C(63)	121.8(10)
C(64)-C(63)-C(62)	119.4(11)
C(63)-C(64)-C(65)	119.3(11)
C(66)-C(65)-C(64)	119.1(12)
C(65)-C(66)-C(61)	124.5(12)
C(72)-C(71)-C(76)	117.5(9)
C(72)-C(71)-P(4)	118.9(8)
C(76)-C(71)-P(4)	123.4(7)
C(73)-C(72)-C(71)	120.8(11)
C(72)-C(73)-C(74)	121.5(11)
C(75)-C(74)-C(73)	118.2(11)
C(76)-C(75)-C(74)	119.6(11)
C(75)-C(76)-C(71)	122.3(10)
C(86)-C(81)-C(82)	119.8(9)
C(86)-C(81)-P(4)	119.2(8)
C(82)-C(81)-P(4)	121.1(8)
C(81)-C(82)-C(83)	120.3(11)
C(84)-C(83)-C(82)	120.8(11)
C(85)-C(84)-C(83)	118.2(10)
C(84)-C(85)-C(86)	121.8(11)
C(81)-C(86)-C(85)	119.1(11)

Table A9. Anisotropic displacement parameters ($Å^2$ x 10^3) for **16**. The anisotropic displacement factor exponent takes the form: $-2\pi^2$ [$h^2 a^{*2}$ U11 + ... + 2 h k a* b* U12]

	U11	U22	U33	U23	U13	U12
Fe(1)	40(1)	34(1)	31(1)	-3(1)	18(1)	-5(1)
Fe(2)	36(1)	31(1)	34(1)	-3(1)	13(1)	-5(1)
P(1)	36(1)	29(1)	32(1)	1(1)	14(1)	-4(1)
P(2)	33(1)	29(1)	32(1)	-3(1)	16(1)	-1(1)
P(3)	31(1)	35(1)	33(1)	2(1)	13(1)	0(1)
P(4)	34(1)	28(1)	34(1)	-1(1)	15(1)	-1(1)
O(1)	123(9)	108(8)	109(8)	29(6)	69(7)	-45(7)
O(2)	99(7)	61(5)	65(6)	-29(5)	45(5)	-20(5)
O(3)	80(6)	75(6)	36(5)	-19(4)	15(4)	-18(5)
O(4)	92(7)	51(5)	101(7)	24(5)	54(6)	-11(5)
N(1)	55(6)	56(6)	59(6)	4(5)	26(5)	-13(5)
N(2)	53(5)	46(5)	33(5)	-7(4)	22(4)	-9(4)
N(3)	50(5)	40(5)	40(6)	-9(4)	17(4)	-1_(4)
N(4)	43(5)	44(5)	56(6)	-1(4)	17(4)	-7(4)
C(1)	33(5)	36(5)	33(5)	-4(4)	19(4)	1(4)
C(2)	37(5)	30(5)	29(5)	1(4)	13(4)	3(4)
C(11)	45(6)	48(6)	29(6)	11(5)	8(5)	-7(5)
C(12)	37(6)	68(8)	61(8)	12(6)	1_(6)	9(6)
C(13)	48(8)	108(12)	82(11)	23(9)	9(8)	3(8)
C(14)	59(10)	159(18)	68(11)	26(11)	-5(8)	-27(11)
C(15)	81(11)	110(13)	67(10)	-11(9)	7(8)	-35(10)
C(16)	67(8)	52(7)	42(7)	-1(6)	2(6)	-17(6)
C(21)	41(6)	33(6)	63(7)	4(5)	25(5)	1(4)
C(22)	40(6)	39(7)	85(9)	-1_(6)	-5(6)	3(5)
C(23)	51(8)	46(9)	184(19)	-43(11)	13(10)	-3(7)
C(24)	86(10)	32(8)	177(19)	19(10)	70(12)	-1(7)
C(25)	168(17)	42(8)	112(13)	23(8)	82(13)	5(9)
C(26)	184(17)	38(7)	79(10)	1(7)	76(11)	-14(8)
C(31)	31(5)	38(5)	32(5)	-2(4)	14(4)	1(4)
C(32)	76(8)	41(6)	46(7)	-15(5)	34(6)	-14(6)
C(33)	81(9)	32(6)	83(9)	-9(6)	41(7)	-21(6)
C(34)	69(8)	32(6)	62(8)	-15(5)	19(6)	-9(5)
C(35)	66(7)	48(7)	42(7)	-22(5)	19(6)	-6(5)
C(36)	44(6)	35(6)	44(6)	-1(5)	17(5)	-8(4)
C(41)	40(6)	36(5)	35(6)	-1(4)	19(5)	1(4)
C(42)	35(6)	57(7)	59(7)	-1_(6)	24(5)	8(5)
C(43)	41(6)	56(7)	55(7)	-5(6)	18(5)	2(5)
C(44)	51(7)	46(6)	67(8)	8(6)	34(6)	12(5)
C(45)	66(8)	47(7)	57(7)	-4(5)	43(7)	11(6)
C(46)	53(6)	40(6)	36(6)	-1(5)	23(5)	5(5)
C(51)	29(5)	58(7)	51(7)	22(5)	17(5)	2(5)
C(52)	47(7)	73(9)	67(8)	11(6)	25(6)	19(6)
C(53)	58(9)	125(14)	116(14)	57(11)	57(10)	41(9)
C(54)	35(8)	142(16)	84(11)	23(11)	16(8)	-4(9)
C(55)	44(8)	103(12)	78(10)	20(8)	0(7)	-20(8)
C(56)	39(6)	72(8)	56(7)	4(6)	9(6)	-12(6)
C(61)	41(6)	41(6)	33(6)	0(5)	19(4)	6(4)
C(62)	41(6)	64(7)	37(6)	5(5)	23(5)	-2(5)
C(63)	51(7)	78(9)	38(7)	-9(6)	15(5)	9(6)
C(64)	97(10)	83(10)	44(7)	28(7)	44(7)	38(8)

C(65)	159(15)	49(8)	58(9)	15(7)	71(9)	11(8)
C(66)	103(10)	44(7)	63(8)	-5(6)	51(8)	-1(6)
C(71)	33(5)	35(5)	38(6)	0(4)	14(4)	3(4)
C(72)	93(9)	33(6)	46(7)	4(5)	17(6)	9(6)
C(73)	126(13)	37(7)	75(10)	26(7)	32(9)	17(7)
C(74)	84(9)	72(9)	41(7)	17(6)	24(6)	20(7)
C(75)	81(9)	66(8)	38(7)	1(6)	28(6)	0(7)
C(76)	64(7)	37(6)	53(7)	-1(5)	33(6)	0(5)
C(81)	45(6)	25(5)	51(7)	4(5)	22(5)	1(4)
C(82)	50(7)	47(7)	57(7)	-1(5)	20(6)	1(5)
C(83)	43(6)	61(8)	73(9)	-4(6)	20(6)	17(6)
C(84)	66(9)	42(7)	97(10)	-11(6)	49(8)	6(6)
C(85)	79(9)	47(7)	74(9)	-29(6)	44(8)	-15(6)
C(86)	52(6)	38(6)	49(7)	-13(5)	29(5)	-1(5)

Table A10. Hydrogen atom coordinates for **16**.

	x	y	z	U(eq)
H(1A)	2408(5)	597(7)	3655(4)	39
H(1B)	1639(5)	948(7)	3318(4)	39
H(2A)	3386(5)	-510(7)	4190(4)	38
H(2B)	4109(5)	-1033(7)	4353(4)	38
H(12A)	763(5)	1547(10)	2259(6)	70
H(13A)	-290(7)	1428(14)	1435(8)	101
H(14A)	-464(8)	156(18)	631(8)	125
H(15A)	441(8)	-918(14)	601(7)	111
H(16A)	1522(6)	-693(9)	1424(5)	71
H(22A)	2549(6)	2422(9)	3511(7)	76
H(23A)	2681(7)	4299(11)	3453(11)	124
H(24A)	2363(8)	5146(11)	2432(11)	111
H(25A)	1916(10)	4095(11)	1471(9)	118
H(26A)	1796(10)	2263(10)	1571(7)	111
H(32A)	4267(6)	1873(8)	3077(5)	61
H(33A)	4525(6)	3582(9)	3509(6)	75
H(34A)	4385(6)	4024(9)	4454(6)	67
H(35A)	3996(6)	2715(8)	4984(5)	63
H(36A)	3736(5)	981(8)	4549(5)	49
H(42A)	5176(5)	132(9)	4288(5)	58
H(43A)	6235(5)	-405(9)	4319(5)	61
H(44A)	6315(6)	-1408(9)	3481(6)	62
H(45A)	5355(6)	-1819(9)	2597(6)	61
H(46A)	4297(5)	-1284(8)	2544(5)	49
H(52A)	664(6)	454(10)	3603(6)	74
H(53A)	-535(8)	551(14)	3045(9)	111
H(54A)	-1111(7)	-663(17)	2215(8)	107
H(55A)	-530(7)	-1943(13)	1929(7)	98
H(56A)	658(5)	-2088(10)	2435(6)	70
H(62A)	2304(5)	585(9)	4546(5)	54
H(63A)	2503(6)	519(10)	5648(5)	68
H(64A)	2197(7)	-1014(12)	6073(6)	84
H(65A)	1636(9)	-2427(10)	5377(6)	96
H(66A)	1448(7)	-2318(9)	4309(6)	77
H(72A)	3448(6)	-4425(8)	4278(5)	72

H(73A)	3630(8)	-5236(10)	5250(7)	98
H(74A)	3796(7)	-4208(11)	6179(6)	79
H(75A)	3715(6)	-2327(10)	6084(5)	72
H(76A)	3532(6)	-1521(8)	5099(5)	58
H(82A)	4689(5)	-2860(9)	4308(6)	62
H(83A)	5426(6)	-3733(10)	3917(6)	71
H(84A)	5022(7)	-4463(9)	2878(7)	75
H(85A)	3886(7)	-4222(9)	2219(6)	75
H(86A)	3139(5)	-3332(8)	2599(5)	52

Table A11. Atomic coordinates (x 10^4) and equivalent isotropic displacement parameters (A^2 x 10^3) for **11**. U(eq) is defined as one third of the trace of the orthogonalized Uij tensor.

	x	y	z	U(eq)
Fe(1)	3547(1)	1864(1)	3980(1)	48(1)
P(1)	2198(2)	2157(2)	5877(2)	35(1)
N(1)	3698(7)	3426(7)	3591(7)	49(2)
N(2)	2429(9)	123(10)	2577(10)	64(2)
O(1)	1644(8)	-1023(8)	1632(8)	83(2)
O(2)	6659(7)	1616(7)	5124(7)	72(2)
O(3)	3833(7)	4458(6)	3242(6)	66(2)
C(1)	526(7)	577(7)	5271(8)	35(2)
C(2)	5433(8)	1705(8)	4713(8)	37(2)
C(11)	1323(8)	3914(8)	6667(8)	39(2)
C(12)	1828(9)	5220(8)	6404(9)	53(2)
C(13)	1224(10)	6581(9)	7074(9)	60(2)
C(14)	165(9)	6635(10)	7979(9)	55(2)
C(15)	-335(11)	5369(10)	8254(10)	67(3)
C(16)	251(9)	4020(9)	7632(9)	57(2)
C(21)	3183(8)	2048(7)	7524(8)	35(2)
C(22)	4719(9)	2997(9)	8206(9)	49(2)
C(23)	5505(9)	2982(10)	9482(9)	56(2)
C(24)	4806(10)	2038(10)	10096(9)	58(2)
C(25)	3322(10)	1122(10)	9426(10)	59(2)
C(26)	2524(9)	1122(8)	8157(8)	45(2)

Table A12. Complete listing of bond lengths [Å] for **11**.

Fe(1)-N(1)	1.680(7)
Fe(1)-N(2)	1.734(11)
Fe(1)-C(2)	1.778(8)
Fe(1)-P(1)	2.270(5)
P(1)-C(1)	1.795(8)
P(1)-C(21)	1.818(8)
P(1)-C(11)	1.841(8)
N(2)-O(1)	1.164(9)
C(2)-O(2)	1.129(8)
N(1)-O(3)	1.169(7)
C(1)-C(1)#1	1.214(13)
C(11)-C(16)	1.393(10)
C(11)-C(12)	1.401(10)
C(12)-C(13)	1.396(11)
C(13)-C(14)	1.348(11)
C(14)-C(15)	1.372(11)

C(15)-C(16)	1.373(11)
C(21)-C(26)	1.382(9)
C(21)-C(22)	1.428(11)
C(22)-C(23)	1.384(10)
C(23)-C(24)	1.394(10)
C(24)-C(25)	1.381(12)
C(25)-C(26)	1.375(11)

Table A13. Complete listing of bond angles [deg] for **11**.

N(1)-Fe(1)-N(2)	115.6(4)
N(1)-Fe(1)-C(2)	110.3(3)
N(2)-Fe(1)-C(2)	114.6(4)
N(1)-Fe(1)-P(1)	112.1(2)
N(2)-Fe(1)-P(1)	100.3(3)
C(2)-Fe(1)-P(1)	102.7(3)
C(1)-P(1)-C(21)	100.9(3)
C(1)-P(1)-C(11)	102.8(4)
C(21)-P(1)-C(11)	103.6(3)
C(1)-P(1)-Fe(1)	110.6(3)
C(21)-P(1)-Fe(1)	118.0(3)
C(11)-P(1)-Fe(1)	118.5(2)
O(1)-N(2)-Fe(1)	178.1(7)
O(2)-C(2)-Fe(1)	176.6(6)
O(3)-N(1)-Fe(1)	175.9(6)
C(1)#1-C(1)-P(1)	172.9(8)
C(16)-C(11)-C(12)	118.9(7)
C(16)-C(11)-P(1)	120.9(5)
C(12)-C(11)-P(1)	120.0(5)
C(13)-C(12)-C(11)	119.8(7)
C(14)-C(13)-C(12)	119.8(7)
C(13)-C(14)-C(15)	121.0(8)
C(14)-C(15)-C(16)	120.7(8)
C(15)-C(16)-C(11)	119.7(7)
C(26)-C(21)-C(22)	118.6(7)
C(26)-C(21)-P(1)	123.8(6)
C(22)-C(21)-P(1)	117.5(5)
C(23)-C(22)-C(21)	119.8(7)
C(22)-C(23)-C(24)	120.2(8)
C(25)-C(24)-C(23)	119.6(7)
C(26)-C(25)-C(24)	121.0(8)
C(25)-C(26)-C(21)	120.8(7)

Table A14. Anisotropic displacement parameters ($Å^2 \times 10^3$) for **11**. The anisotropic displacement factor exponent takes the form: $-2\pi^2 [h^2 a^{*2} U11 + ... + 2 h k a^* b^* U12]$

	U11	U22	U33	U23	U13	U12
Fe(1)	65(1)	46(1)	44(1)	26(1)	21(1)	13(1)
P(1)	43(1)	33(1)	32(1)	17(1)	7(1)	4(1)
N(2)	79(5)	61(5)	77(7)	45(5)	41(5)	18(4)
O(1)	101(5)	59(4)	66(6)	11(4)	26(4)	-12(4)
C(2)	41(4)	38(4)	36(5)	15(4)	12(4)	16(4)

O(2)	65(4)	76(4)	87(5)	41(4)	21(4)	31(3)
N(1)	60(4)	47(4)	50(5)	29(4)	13(3)	7(3)
O(3)	83(4)	64(4)	73(4)	50(4)	16(3)	12(3)
C(1)	48(4)	31(4)	30(5)	16(4)	14(4)	12(3)
C(11)	42(4)	37(4)	33(5)	14(4)	2(4)	0(3)
C(12)	66(5)	43(5)	54(6)	25(5)	18(5)	9(4)
C(13)	75(6)	41(5)	68(7)	31(5)	2(5)	14(4)
C(14)	59(5)	51(5)	43(6)	12(5)	-6(5)	14(4)
C(15)	84(6)	66(6)	60(6)	26(5)	31(5)	36(5)
C(16)	62(5)	50(5)	69(6)	33(5)	17(5)	16(4)
C(21)	46(4)	26(4)	29(5)	10(4)	10(4)	6(3)
C(22)	63(5)	43(5)	39(6)	20(4)	1(4)	-3(4)
C(23)	60(5)	60(6)	41(6)	21(5)	-2(4)	11(4)
C(24)	81(6)	66(6)	34(6)	28(5)	7(5)	24(5)
C(25)	72(6)	68(6)	49(6)	37(5)	13(5)	11(5)
C(26)	53(4)	45(5)	30(5)	18(4)	-5(4)	-7(4)

Table A15. Hydrogen atom coordinates for **11**.

	x	y	z	U(eq)
H(12A)	2571(9)	5179(8)	5777(9)	63
H(13A)	1555(10)	7457(9)	6895(9)	72
H(14A)	-237(9)	7555(10)	8428(9)	66
H(15A)	-1088(11)	5425(10)	8875(10)	80
H(16A)	-69(9)	3172(9)	7855(9)	68
H(22A)	5194(9)	3629(9)	7791(9)	59
H(23A)	6514(9)	3610(10)	9936(9)	67
H(24A)	5342(10)	2025(10)	10960(9)	69
H(25A)	2851(10)	489(10)	9842(10)	71
H(26A)	1518(9)	485(8)	7716(8)	54

Table A16. Atomic coordinates (x 10^4) and equivalent isotropic displacement parameters (A^2 x 10^3) for **17**• CH_2Cl_2. U(eq) is defined as one third of the trace of the orthogonalized Uij tensor.

	x	y	z	U(eq)
Fe(1)	8539(1)	6745(1)	6151(1)	38(1)
Fe(2)	6439(1)	10660(1)	5863(1)	38(1)
P(1)	7510(1)	7055(2)	5631(2)	37(1)
P(2)	6654(1)	9606(2)	6827(2)	38(1)
P(3)	7397(1)	10806(2)	5546(2)	36(1)
P(4)	8901(1)	8273(2)	6211(2)	36(1)
O(1)	9210(4)	5920(7)	5078(5)	70(3)
O(2)	8622(4)	5747(6)	7556(5)	68(2)
O(3)	5597(4)	9821(7)	4609(6)	75(3)
O(4)	6223(5)	12454(6)	6534(6)	82(3)
N(1)	8913(4)	6271(6)	5506(5)	49(2)
N(2)	8569(4)	6212(5)	6985(6)	43(2)
N(3)	5960(4)	10125(7)	5126(5)	46(2)
N(4)	6315(4)	11701(6)	6250(5)	50(2)
C(1)	7143(5)	7859(7)	6200(6)	36(2)

C(2)	6940(5)	8497(8)	6536(6)	43(3)
C(3)	7969(5)	9863(7)	5727(5)	35(2)
C(4)	8364(5)	9249(7)	5920(6)	38(2)
C(10)	7354(5)	7677(7)	4695(6)	43(3)
C(11)	6831(6)	8250(8)	4490(7)	55(3)
C(12)	6718(7)	8723(9)	3781(7)	69(4)
C(13)	7169(8)	8615(10)	3306(8)	78(4)
C(14)	7677(8)	8053(11)	3518(8)	78(4)
C(15)	7783(6)	7564(9)	4218(6)	59(3)
C(20)	7091(11)	5931(16)	5570(11)	33(6)
C(21)	6899(11)	5397(20)	4904(13)	66(9)
C(22)	6496(11)	4692(17)	4737(14)	52(7)
C(23)	6342(13)	4306(17)	5375(14)	51(7)
C(24)	6544(13)	4647(20)	6076(17)	59(8)
C(25)	6930(13)	5460(21)	6118(18)	57(8)
C(201)	6892(10)	6092(13)	5484(9)	15(5)
C(211)	6555(16)	5781(30)	4777(14)	104(12)
C(221)	6146(18)	5008(27)	4763(24)	113(13)
C(231)	6061(12)	4543(18)	5361(13)	48(7)
C(241)	6297(20)	4883(30)	5960(27)	114(14)
C(251)	6746(21)	5699(33)	6078(32)	123(16)
C(30)	5986(5)	9245(7)	7265(6)	45(3)
C(31)	5409(5)	9694(9)	7053(7)	61(3)
C(32)	4897(6)	9446(12)	7399(9)	88(5)
C(33)	4982(7)	8787(12)	7965(9)	87(5)
C(34)	5541(7)	8304(11)	8173(8)	82(5)
C(35)	6063(6)	8539(11)	7809(8)	73(4)
C(40)	7261(5)	9958(7)	7649(6)	43(3)
C(41)	7181(8)	10803(11)	8015(9)	97(6)
C(42)	7628(9)	11125(13)	8629(11)	116(7)
C(43)	8168(8)	10613(11)	8874(8)	82(4)
C(44)	8279(6)	9810(10)	8512(7)	66(4)
C(45)	7824(5)	9501(9)	7881(7)	53(3)
C(50)	7810(10)	11817(11)	5931(14)	22(6)
C(51)	7712(13)	12764(11)	5680(13)	45(6)
C(52)	8019(14)	13550(19)	6003(13)	55(8)
C(53)	8462(12)	13436(18)	6619(16)	45(7)
C(54)	8630(12)	12534(24)	6981(18)	60(9)
C(55)	8298(16)	11719(28)	6617(23)	62(13)
C(501)	7966(15)	11796(15)	6155(20)	28(7)
C(511)	7928(16)	12683(17)	5786(17)	55(10)
C(521)	8294(17)	13461(21)	6142(19)	49(9)
C(531)	8681(13)	13209(20)	6881(16)	29(8)
C(541)	8663(14)	12316(29)	7209(25)	62(12)
C(551)	8287(14)	11635(26)	6785(21)	33(10)
C(60)	7368(5)	11028(7)	4514(6)	42(3)
C(61)	6831(5)	11384(8)	4082(6)	52(3)
C(62)	6806(6)	11594(10)	3298(8)	71(4)
C(63)	7330(7)	11396(10)	2968(8)	68(4)
C(64)	7870(6)	11057(8)	3415(7)	61(3)
C(65)	7902(6)	10851(8)	4185(7)	51(3)
C(70)	9479(5)	8426(7)	5588(6)	39(3)
C(71)	10085(5)	8040(8)	5807(7)	52(3)
C(72)	10532(6)	8088(9)	5355(8)	66(4)
C(73)	10371(6)	8544(8)	4634(7)	56(3)
C(74)	9771(6)	8915(8)	4396(7)	55(3)
C(75)	9333(5)	8868(7)	4879(6)	46(3)

C(80)	9316(4)	8744(7)	7133(6)	37(2)
C(81)	9548(5)	9681(8)	7191(7)	50(3)
C(82)	9857(5)	10035(9)	7886(8)	57(3)
C(83)	9968(5)	9458(10)	8521(8)	61(3)
C(84)	9763(6)	8533(10)	8476(7)	63(3)
C(85)	9433(5)	8178(8)	7773(6)	49(3)
C(99A)	4645(16)	2921(26)	3942(22)	90(13)
Cl(1)	5077(12)	3414(18)	3441(11)	177(8)
Cl(2)	4943(6)	2227(12)	4664(10)	131(6)
Cl(4)	4807(10)	2554(19)	4953(16)	186(8)
Cl(3)	5362(9)	3067(13)	3578(8)	132(7)

Table A17. Complete listing of bond lengths [Å] for **17**• CH_2Cl_2.

Fe(1)-N(2)	1.651(10)
Fe(1)-N(1)	1.663(10)
Fe(1)-P(4)	2.253(3)
Fe(1)-P(1)	2.254(3)
Fe(2)-N(4)	1.646(9)
Fe(2)-N(3)	1.670(10)
Fe(2)-P(2)	2.233(3)
Fe(2)-P(3)	2.242(3)
P(1)-C(1)	1.790(11)
P(1)-C(20)	1.79(2)
P(1)-C(10)	1.850(11)
P(1)-C(201)	1.86(2)
P(2)-C(2)	1.772(12)
P(2)-C(40)	1.822(11)
P(2)-C(30)	1.830(10)
P(3)-C(3)	1.776(11)
P(3)-C(50)	1.73(2)
P(3)-C(60)	1.854(11)
P(3)-C(501)	2.01(3)
P(4)-C(4)	1.784(11)
P(4)-C(80)	1.826(10)
P(4)-C(70)	1.831(9)
O(1)-N(1)	1.189(11)
O(2)-N(2)	1.190(11)
O(3)-N(3)	1.160(11)
O(4)-N(4)	1.195(11)
C(1)-C(2)	1.198(14)
C(3)-C(4)	1.203(13)
C(10)-C(11)	1.36(2)
C(10)-C(15)	1.38(2)
C(11)-C(12)	1.40(2)
C(12)-C(13)	1.41(2)
C(13)-C(14)	1.33(2)
C(14)-C(15)	1.40(2)
C(20)-C(21)	1.39
C(20)-C(25)	1.28(4)
C(21)-C(22)	1.30(3)
C(22)-C(23)	1.35(3)
C(23)-C(24)	1.33(4)
C(24)-C(25)	1.39(4)
C(201)-C(211)	1.39
C(201)-C(251)	1.28(5)
C(211)-C(221)	1.38(5)

C(221)-C(231)	1.29(4)
C(231)-C(241)	1.19(4)
C(241)-C(251)	1.47(6)
C(30)-C(35)	1.36(2)
C(30)-C(31)	1.37(2)
C(31)-C(32)	1.40(2)
C(32)-C(33)	1.35(2)
C(33)-C(34)	1.36(2)
C(34)-C(35)	1.44(2)
C(40)-C(45)	1.35(2)
C(40)-C(41)	1.37(2)
C(41)-C(42)	1.38(2)
C(42)-C(43)	1.35(2)
C(43)-C(44)	1.33(2)
C(44)-C(45)	1.40(2)
C(50)-C(51)	1.39
C(50)-C(55)	1.45(4)
C(51)-C(52)	1.34(3)
C(52)-C(53)	1.31(4)
C(53)-C(54)	1.42(4)
C(54)-C(55)	1.42(5)
C(501)-C(511)	1.39
C(501)-C(551)	1.22(6)
C(511)-C(521)	1.41(4)
C(521)-C(531)	1.45(4)
C(531)-C(541)	1.37(5)
C(541)-C(551)	1.37(5)
C(60)-C(61)	1.34(2)
C(60)-C(65)	1.40(2)
C(61)-C(62)	1.42(2)
C(62)-C(63)	1.39(2)
C(63)-C(64)	1.35(2)
C(64)-C(65)	1.39(2)
C(70)-C(75)	1.38(2)
C(70)-C(71)	1.385(14)
C(71)-C(72)	1.37(2)
C(72)-C(73)	1.41(2)
C(73)-C(74)	1.37(2)
C(74)-C(75)	1.39(2)
C(80)-C(85)	1.367(14)
C(80)-C(81)	1.389(14)
C(81)-C(82)	1.37(2)
C(82)-C(83)	1.37(2)
C(83)-C(84)	1.35(2)
C(84)-C(85)	1.40(2)
Cl(1)-C(99A)	1.56(4)
Cl(2)-C(99A)	1.63(4)
C(99B)-Cl(3)	1.79(4)
C(99B)-Cl(4)	1.84(4)

Table A18. Complete listing of bond angles [deg] for **17**• CH_2Cl_2.

N(2)-Fe(1)-N(1)	120.5(4)
N(2)-Fe(1)-P(4)	115.4(3)
N(1)-Fe(1)-P(4)	101.4(3)
N(2)-Fe(1)-P(1)	108.4(3)
N(1)-Fe(1)-P(1)	110.9(3)

P(4)-Fe(1)-P(1)	97.92(11)
N(4)-Fe(2)-N(3)	126.5(4)
N(4)-Fe(2)-P(2)	106.2(3)
N(3)-Fe(2)-P(2)	108.3(3)
N(4)-Fe(2)-P(3)	104.9(3)
N(3)-Fe(2)-P(3)	106.9(3)
P(2)-Fe(2)-P(3)	101.21(11)
C(1)-P(1)-C(20)	107.9(8)
C(1)-P(1)-C(10)	101.5(5)
C(20)-P(1)-C(10)	110.7(7)
C(1)-P(1)-C(201)	98.6(6)
C(10)-P(1)-C(201)	102.3(6)
C(1)-P(1)-Fe(1)	112.9(3)
C(20)-P(1)-Fe(1)	107.1(8)
C(10)-P(1)-Fe(1)	116.5(4)
C(201)-P(1)-Fe(1)	121.9(7)
C(2)-P(2)-C(40)	103.6(5)
C(2)-P(2)-C(30)	103.3(5)
C(40)-P(2)-C(30)	102.9(5)
C(2)-P(2)-Fe(2)	112.0(4)
C(40)-P(2)-Fe(2)	116.6(3)
C(30)-P(2)-Fe(2)	116.7(4)
C(3)-P(3)-C(50)	104.4(8)
C(3)-P(3)-C(60)	100.9(4)
C(50)-P(3)-C(60)	100.0(8)
C(3)-P(3)-C(501)	94.9(9)
C(60)-P(3)-C(501)	108.6(8)
C(3)-P(3)-Fe(2)	121.2(3)
C(50)-P(3)-Fe(2)	113.2(5)
C(60)-P(3)-Fe(2)	114.4(3)
C(501)-P(3)-Fe(2)	114.4(6)
C(4)-P(4)-C(80)	99.2(4)
C(4)-P(4)-C(70)	102.1(4)
C(80)-P(4)-C(70)	103.7(5)
C(4)-P(4)-Fe(1)	120.4(3)
C(80)-P(4)-Fe(1)	118.7(3)
C(70)-P(4)-Fe(1)	110.3(3)
O(1)-N(1)-Fe(1)	176.2(8)
O(2)-N(2)-Fe(1)	172.9(7)
O(3)-N(3)-Fe(2)	174.5(9)
O(4)-N(4)-Fe(2)	179.6(8)
C(2)-C(1)-P(1)	170.8(9)
C(1)-C(2)-P(2)	165.8(9)
C(4)-C(3)-P(3)	173.9(9)
C(3)-C(4)-P(4)	175.5(9)
C(11)-C(10)-C(15)	120.9(11)
C(11)-C(10)-P(1)	120.3(8)
C(15)-C(10)-P(1)	118.8(9)
C(10)-C(11)-C(12)	120.0(12)
C(11)-C(12)-C(13)	118.4(12)
C(14)-C(13)-C(12)	120.5(12)
C(13)-C(14)-C(15)	121.1(13)
C(10)-C(15)-C(14)	119.1(12)
C(21)-C(20)-C(25)	108(2)
C(21)-C(20)-P(1)	125(2)
C(25)-C(20)-P(1)	127(2)
C(22)-C(21)-C(20)	132(3)

C(23)-C(22)-C(21)	112(2)
C(24)-C(23)-C(22)	124(3)
C(23)-C(24)-C(25)	115(3)
C(24)-C(25)-C(20)	128(3)
C(211)-C(201)-C(251)	117(3)
C(211)-C(201)-P(1)	125(2)
C(251)-C(201)-P(1)	118(3)
C(201)-C(211)-C(221)	118(3)
C(231)-C(221)-C(211)	125(4)
C(221)-C(231)-C(241)	116(4)
C(251)-C(241)-C(231)	126(5)
C(241)-C(251)-C(201)	118(4)
C(35)-C(30)-C(31)	119.9(10)
C(35)-C(30)-P(2)	120.4(9)
C(31)-C(30)-P(2)	119.7(8)
C(30)-C(31)-C(32)	120.5(11)
C(33)-C(32)-C(31)	119.6(13)
C(32)-C(33)-C(34)	121.4(13)
C(33)-C(34)-C(35)	119.1(13)
C(30)-C(35)-C(34)	119.3(12)
C(45)-C(40)-C(41)	116.4(11)
C(45)-C(40)-P(2)	124.8(8)
C(41)-C(40)-P(2)	118.4(9)
C(40)-C(41)-C(42)	121.6(14)
C(43)-C(42)-C(41)	120.0(14)
C(44)-C(43)-C(42)	120.4(13)
C(43)-C(44)-C(45)	118.8(12)
C(40)-C(45)-C(44)	122.5(11)
C(51)-C(50)-C(55)	113(2)
C(51)-C(50)-P(3)	128(2)
C(55)-C(50)-P(3)	119(2)
C(50)-C(51)-C(52)	127(2)
C(51)-C(52)-C(53)	118(2)
C(54)-C(53)-C(52)	124(2)
C(53)-C(54)-C(55)	116(3)
C(54)-C(55)-C(50)	121(3)
C(511)-C(501)-C(551)	125(3)
C(511)-C(501)-P(3)	112(2)
C(551)-C(501)-P(3)	123(2)
C(521)-C(511)-C(501)	119(3)
C(511)-C(521)-C(531)	113(2)
C(521)-C(531)-C(541)	123(3)
C(531)-C(541)-C(551)	117(3)
C(541)-C(551)-C(501)	123(4)
C(61)-C(60)-C(65)	120.0(11)
C(61)-C(60)-P(3)	119.0(8)
C(65)-C(60)-P(3)	121.0(8)
C(60)-C(61)-C(62)	120.0(11)
C(63)-C(62)-C(61)	120.0(12)
C(64)-C(63)-C(62)	119.0(13)
C(63)-C(64)-C(65)	121.5(11)
C(64)-C(65)-C(60)	119.4(11)
C(75)-C(70)-C(71)	117.2(9)
C(75)-C(70)-P(4)	123.3(8)
C(71)-C(70)-P(4)	119.4(8)
C(72)-C(71)-C(70)	122.6(11)
C(71)-C(72)-C(73)	119.0(11)

C(74)-C(73)-C(72)	119.5(10)
C(73)-C(74)-C(75)	119.7(11)
C(70)-C(75)-C(74)	121.8(11)
C(85)-C(80)-C(81)	118.2(10)
C(85)-C(80)-P(4)	121.4(8)
C(81)-C(80)-P(4)	120.3(8)
C(82)-C(81)-C(80)	120.2(11)
C(83)-C(82)-C(81)	120.6(11)
C(84)-C(83)-C(82)	120.3(12)
C(83)-C(84)-C(85)	119.2(12)
C(80)-C(85)-C(84)	121.3(10)
Cl(1)-C(99A)-Cl(2)	122(2)
Cl(3)-C(99B)-Cl(4)	112(2)

Table A19. Anisotropic displacement parameters ($Å^2 \times 10^3$) for **17**• CH_2Cl_2. The anisotropic displacement factor exponent takes the form: $-2\pi^2 [h^2 a^{*2} U11 + ... + 2 h k a^* b^* U12]$

	U11	U22	U33	U23	U13	U12
Fe(1)	51(1)	25(1)	44(1)	1(1)	22(1)	2(1)
Fe(2)	47(1)	31(1)	43(1)	3(1)	24(1)	4(1)
P(1)	49(2)	25(1)	41(2)	-3(1)	22(1)	-2(1)
P(2)	47(2)	34(1)	39(2)	3(1)	24(1)	2(1)
P(3)	48(2)	26(1)	41(2)	1(1)	23(1)	2(1)
P(4)	43(2)	29(1)	41(2)	3(1)	22(1)	1(1)
O(1)	97(6)	75(6)	48(5)	-12(5)	35(5)	32(5)
O(2)	99(7)	45(5)	72(6)	15(5)	44(5)	5(4)
O(3)	61(6)	74(6)	89(7)	-8(6)	12(5)	-9(5)
O(4)	112(7)	52(6)	88(7)	-22(5)	37(5)	19(5)
N(1)	68(6)	33(5)	49(6)	-6(5)	14(5)	6(4)
N(2)	59(6)	15(4)	61(6)	-4(5)	28(4)	-1(4)
N(3)	43(5)	53(6)	44(5)	5(5)	15(4)	-7(4)
N(4)	59(6)	41(6)	57(6)	-8(5)	30(5)	1(4)
C(1)	48(6)	33(5)	30(6)	-3(5)	15(4)	-9(5)
C(2)	50(6)	44(6)	38(6)	2(6)	16(5)	-6(5)
C(3)	47(6)	36(6)	27(5)	5(5)	18(4)	-6(5)
C(4)	52(6)	30(6)	36(6)	0(5)	22(5)	-3(5)
C(10)	63(7)	29(5)	41(6)	-6(5)	19(5)	-17(5)
C(11)	70(8)	45(7)	48(7)	7(6)	12(6)	20(6)
C(12)	115(11)	41(7)	45(8)	3(6)	2(7)	22(7)
C(13)	143(14)	54(8)	39(8)	8(7)	20(8)	2(9)
C(14)	111(11)	78(10)	56(9)	11(8)	47(8)	-3(9)
C(15)	82(8)	61(8)	37(7)	4(6)	19(6)	7(7)
C(30)	62(7)	39(6)	44(6)	9(5)	35(5)	2(5)
C(31)	55(7)	66(8)	66(8)	33(7)	26(6)	12(6)
C(32)	64(8)	103(12)	110(12)	55(11)	51(8)	13(8)
C(33)	70(9)	104(12)	99(12)	28(11)	49(8)	2(9)
C(34)	85(10)	100(12)	70(9)	50(9)	39(7)	-4(9)
C(35)	59(8)	93(10)	77(9)	40(9)	36(6)	12(7)
C(40)	58(7)	38(6)	36(6)	-2(5)	17(5)	-5(5)
C(41)	116(13)	87(11)	76(11)	-44(9)	-11(9)	37(10)
C(42)	130(15)	92(12)	110(14)	-56(11)	-16(12)	40(11)
C(43)	105(12)	70(10)	62(9)	-10(8)	-3(8)	-13(9)
C(44)	54(7)	82(10)	61(8)	-14(8)	12(6)	4(7)
C(45)	66(8)	48(7)	55(7)	-5(6)	39(6)	-4(6)
C(60)	55(7)	29(5)	49(7)	11(5)	29(5)	3(5)
C(61)	61(7)	50(7)	53(7)	14(6)	34(6)	2(6)

C(62)	71(9)	74(9)	71(9)	31(8)	21(7)	-7(7)
C(63)	91(10)	63(8)	56(8)	11(7)	33(7)	-21(8)
C(64)	90(9)	49(7)	61(8)	9(7)	57(7)	8(7)
C(65)	68(7)	45(7)	47(7)	6(6)	29(5)	7(6)
C(70)	56(7)	29(5)	42(6)	6(5)	31(5)	0(5)
C(71)	47(7)	55(7)	58(7)	16(6)	19(5)	13(6)
C(72)	51(7)	63(8)	93(11)	-3(8)	36(7)	2(6)
C(73)	75(8)	45(7)	62(8)	-1(7)	45(6)	1(6)
C(74)	83(9)	50(7)	43(7)	2(6)	41(6)	-3(6)
C(75)	61(7)	30(5)	54(7)	0(6)	27(5)	-1(5)
C(80)	50(6)	31(6)	39(6)	3(5)	29(5)	2(5)
C(81)	65(7)	39(6)	54(7)	5(6)	30(6)	-18(6)
C(82)	62(7)	42(7)	73(9)	-17(7)	28(6)	-17(6)
C(83)	52(7)	66(9)	69(9)	-15(8)	19(6)	-8(6)
C(84)	79(9)	62(8)	49(8)	1(7)	12(6)	-1(7)
C(85)	69(7)	29(6)	53(7)	3(6)	20(6)	-5(5)

Table A20. Hydrogen atom coordinates for **17**• CH_2Cl_2.

	x	y	z	U(eq)
H(11A)	6546(6)	8329(8)	4824(7)	65
H(12A)	6352(7)	9102(9)	3626(7)	83
H(13A)	7110(8)	8943(10)	2836(8)	94
H(14A)	7970(8)	7983(11)	3193(8)	93
H(15A)	8141(6)	7163(9)	4360(6)	71
H(21A)	7097(29)	5579(155)	4500(78)	80
H(22A)	6331(11)	4476(17)	4237(14)	62
H(23A)	6075(13)	3762(17)	5317(14)	62
H(24A)	6435(13)	4362(20)	6512(17)	71
H(25A)	7093(13)	5692(21)	6614(18)	68
H(21B)	6605(38)	6087(196)	4322(42)	124
H(22B)	5914(18)	4807(27)	4285(24)	135
H(23B)	5826(12)	3968(18)	5323(13)	58
H(24B)	6189(20)	4607(30)	6399(27)	136
H(25B)	6920(21)	5925(33)	6572(32)	148
H(31A)	5356(5)	10172(9)	6673(7)	73
H(32A)	4496(6)	9738(12)	7237(9)	105
H(33A)	4647(7)	8660(12)	8222(9)	104
H(34A)	5586(7)	7822(11)	8551(8)	98
H(35A)	6453(6)	8210(11)	7943(8)	88
H(41A)	6812(8)	11171(11)	7843(9)	117
H(42A)	7558(9)	11700(13)	8878(11)	139
H(43A)	8466(8)	10825(11)	9302(8)	98
H(44A)	8656(6)	9457(10)	8678(7)	79
H(45A)	7914(5)	8955(9)	7609(7)	63
H(51A)	7398(54)	12864(29)	5237(68)	54
H(52A)	7918(14)	14165(19)	5793(13)	66
H(53A)	8683(12)	13986(18)	6837(16)	54
H(54A)	8942(12)	12480(24)	7432(18)	71
H(55A)	8397(16)	11103(28)	6827(23)	74
H(51B)	7660(67)	12763(76)	5304(100)	65
H(52B)	8289(17)	14078(21)	5924(19)	59
H(53B)	8956(13)	13677(20)	7147(16)	35
H(54B)	8899(14)	12180(29)	7702(25)	74

H(55B)	8275(14)	11014(26)	6992(21)	39
H(61A)	6472(5)	11494(8)	4300(6)	62
H(62A)	6436(6)	11866(10)	3001(8)	86
H(63A)	7308(7)	11496(10)	2441(8)	81
H(64A)	8233(6)	10958(8)	3201(7)	73
H(65A)	8278(6)	10596(8)	4484(7)	61
H(71A)	10194(5)	7733(8)	6285(7)	63
H(72A)	10940(6)	7821(9)	5522(8)	79
H(73A)	10674(6)	8592(8)	4319(7)	68
H(74A)	9656(6)	9200(8)	3910(7)	66
H(75A)	8927(5)	9143(7)	4718(6)	55
H(81A)	9493(5)	10074(8)	6753(7)	60
H(82A)	9994(5)	10680(9)	7925(8)	68
H(83A)	10188(5)	9705(10)	8992(8)	74
H(84A)	9842(6)	8135(10)	8911(7)	76
H(85A)	9288(5)	7537(8)	7741(6)	59
H(99A)	4327(16)	2538(26)	3594(22)	228
H(99B)	4411(16)	3436(26)	4142(22)	228
H(99C)	4453(16)	3504(26)	3682(22)	240
H(99D)	4394(16)	2370(26)	3706(22)	240

Figure A-1. Cyclic Voltammogram of Complex **19**.

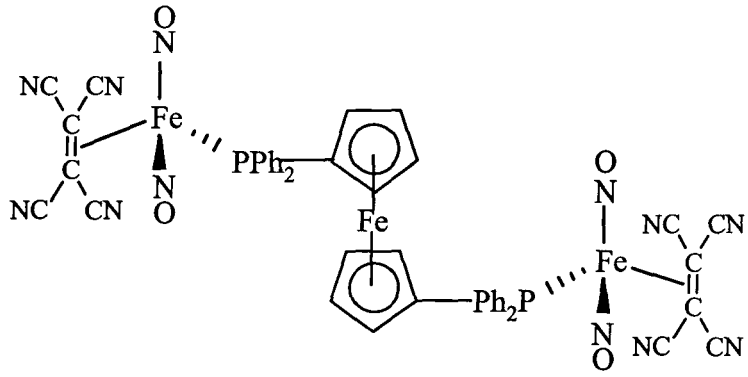

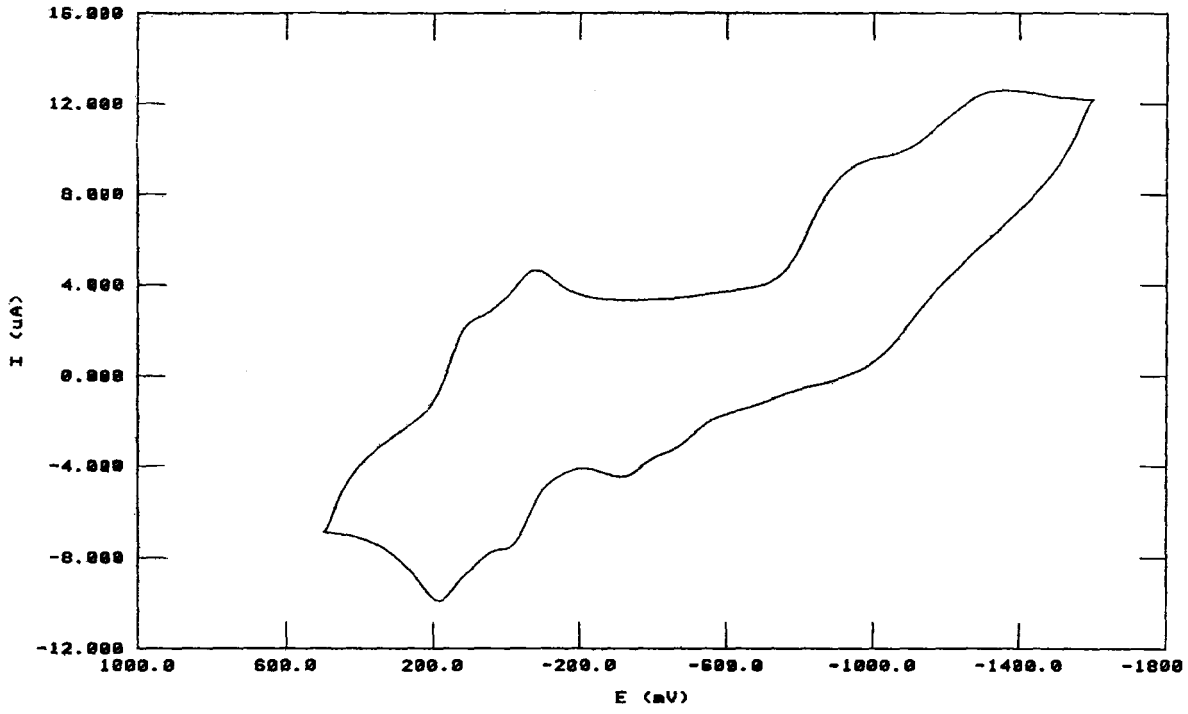

Figure A-2. Cyclic Voltammogram of Complex **20**.